A REVIEW OF RESEARCH
ON
AERONAUTICAL FATIGUE IN THE UNITED STATES

2007 - 2009

Compiled by
Dr. Ravi Chona
Air Force Research Laboratory
Wright-Patterson Air Force Base, Ohio, USA

**FOR PRESENTATION AT THE MEETING
OF THE
INTERNATIONAL COMMITTEE ON AERONAUTICAL FATIGUE**

25-29 MAY 2009

ROTTERDAM, THE NETHERLANDS

TABLE OF CONTENTS

9.1 INTRODUCTION

Leading government laboratories, universities and aerospace manufacturers were invited to contribute summaries of recent aeronautical fatigue research activities. This report contains those voluntary contributions. Inquiries regarding a particular article should be addressed to the person whose name accompanies that article. The generous contribution of each contributing organization is hereby gratefully acknowledged.

GOVERNMENT

- FAA-ATO-P, R&D
- NASA - Johnson Space Center
- United States Coast Guard
- USAF-OO-ALC
- USAF Research Laboratory - Air Vehicles Directorate
- USN - NAVAIR

ACADEMIA
- Mississippi State University
- University of Dayton
- USAF Academy
- Wright State University

INDUSTRY
- Alcoa
- Analytical Processes/Engineering Solutions, Inc.
- Computational Mechanics, Inc.
- Hill Engineering, LLC
- Jacobs ESCG
- L-3 Communications
- Lockheed Martin
- Luna Innovations, Inc.
- NDT Solutions, Inc.
- Northrop Grumman Corporation
- Sandia National Laboratories
- Southwest Research Institute
- Spirit Aerosystems, Inc.
- The Boeing Company
- TRI, Austin

References, if any, are listed at the end of each article. Figures and tables are compiled at the end of the review.

The assistance of Jim Rudd and Charlotte Burns, Universal Technology Corporation, in the preparation of this report is greatly appreciated.

One of the goals of the United States Air Force is to reduce the maintenance burden of existing and future weapon systems by eliminating programmed repair cycles. In order to achieve this goal, superior technology, infrastructure and tools are required to only bring down systems when they must be repaired or upgraded in order to preserve safety and effectiveness. This requires a condition-based-maintenance capability utilizing structural integrity concepts (CBM+SI). Knowledge is required for four emphasis areas: damage state awareness, usage, structural analysis and structural modifications (Figure 9.1-1). The following nine technology focus areas are identified to provide this knowledge: 1) non-destructive inspection/evaluation, 2) structural health monitoring, 3) structural teardown assessments, 4) loads & environment characterization, 5) characterization, modeling and testing, 6) prognostics & risk analysis, 7) life enhancement concepts, 8) repair concepts, and 9) replacement concepts. The aeronautical fatigue research activities of this report have been categorized into these nine technology focus areas.

9.2 NON-DESTRUCTIVE INSPECTION/EVALUATION

9.2.1 AUTOMATIC FLAW CLASSIFICATION SOFTWARE (AFCS)

John R. Mandeville, NDT Solutions, Inc.

There are many challenges related to ultrasonic inspection of large and complex structures. During an ultrasonic inspection process; proper data acquisition (good return signals) as well as review and analysis of the acquired data can be time consuming and subjective. The main focus of this effort is on the analysis of the acquired data using the near real time Automatic Flaw Classification Software (AFCS). The AFCS software is taught by example to discern signals from the fastener hole, geometry, corrosion, multi-layer noise, signal quality, delaminations and crack signals. When analyzing ultrasonic shear wave signals from fastener holes for crack detection the AFCS is directed to locate the fastener hole and then geometrically compare the 3-D alignment of the indication (crack) with the fastener hole focusing on spatial regions of interest. Most ultrasonic inspection systems that are used for fastener hole inspection are capable of collecting the raw ultrasound data and can present the data in A, B, and C-scan formats during the acquisition and post inspection. The data is then reviewed and evaluated by an engineer or trained evaluator. The manual review process can be very time consuming and subject to human factors. The review cycle time is reduced significantly by using the AFCS because it classifies the fastener and its surrounding 3-D area looking for clusters of return signals in the proper location in space with respect to the fastener hole location (Figure 9.2-1). AFCS also provides feed back to the inspector on the quality of the fastener hole signal(s) before moving to the next area to be inspected. This near real time feedback feature will improve the quality of the acquired data and reduce the need for the inspector to reexamine the fastener hole at a later time. Reducing the time for the overall process is always a key objective in any man power application; AFCS reduces the time for reexamination of poor signals and a significant time reduction in data review cycle (based solely on an examiner reviewing the data). After the fastener holes have been classified by a configured AFCS, a trained examiner will analyze the fastener hole data to verify the defect indication, this would reduce the amount of false calls.

This same AFCS technology (tools) is applied to longitudinal ultrasonic composite inspection. AFCS will determine ROI delaminations, inclusions, lack of bonding, impact damage, back wall plotting and statics for loss of signal due to excessive signal attenuation due to scattering and absorption that is sometimes caused by porosity and ply wrinkles (Figure 9.2-2).

9.3 STRUCTURAL HEALTH MONITORING

9.3.1 DEVELOPMENT AND USE OF STANDARD ENVIRONMENTAL EXPOSURE SPECTRA FOR VALIDATION OF HEALTH MONITORING

David Forsyth, TRI/Austin

Standard load spectra for fatigue have been used for many years in the design and test of airframe and engine components. There are many benefits of standard load spectra, including the ability to compare results between laboratories, between materials and designs, and to provide a common base of engineering information for designers.

Standard environmental exposure spectra would provide similar benefits, but there is no widely accepted standard in this domain that the authors are aware of. TRI/Austin has worked on developing accelerated life testing (ALT) protocols for a range of activities, including recent efforts to develop and validate and ALT for simulation of corrosion damage on airframes. These ALT protocols can serve as the basis for standard environmental exposure spectra.

In this effort, the TRI/Austin ALT is described, including methods and results of validation tests. The key elements of the ALT include: salt fog, elevated temperature and humidity, corrosive gas exposure, ultraviolet exposure, and temperature cycling (Table 9.3-1). The ALT is exercised as part of the validation of sensors proposed as part of a system for health monitoring for corrosion damage. The results of the sensor trials and validation before, during, and after the ALT exposure are presented.

Commercially available and experimental corrosion sensors were tested on bare coupons, under primer, and under both primer and sealant (Figure 9.3-1). Some coupons had artificial damage to the coatings. Sensor outputs were monitored continuously during the various elements of the ALT. Corrosion damage was monitored optically during the ALT, and coupons were removed for metallographic examination at different levels of visible damage.

Corrosion damage on the coupons from the ALT was compared to in-service corrosion damage to validate the ALT. Metrics of the corrosion damage were chosen based on their significance to structural integrity.

The outcome of the program will be the validation of the ability of sensors to measure corrosion damage at levels where it is structurally significant, and to provide useful inputs to corrosion structural effects models.

9.3.2 TEST BED DEVELOPMENT FOR STRUCTURAL HEALTH MONITORING: A SENSORS VALIDATION

Molly R. Walters, Cindy L. Klahn and Scott A. Fawaz, United States Air Force Academy (CAStLE)

Structural health monitoring (SHM) by sensors is becoming increasingly important for the US Air Force. If non-destructive inspection (NDI) were performed during flight, damage could be monitored while in flight to better estimate required maintenance. Rather than all NDI and maintenance being done during the depot cycle, the aircraft could have fewer procedures done on the ground, which could increase aircraft availability.

In order for SHM to work properly, the complicated failure modes found in the field must be detectable. In general, it is quite difficult to install developmental technology on in-service USAF aircraft; thus, technology development must occur in the laboratory and when the technology is mature it can be transitioned to operational aircraft. For this reason, emerging SHM sensors will be installed on laboratory test specimens that are representative of aircraft structure in terms of geometry and loading to detect damage morphologies typically found in the field. The damage morphologies of interest here are fatigue cracking and stress-corrosion cracking (SCC).

A thorough literature review[1-6] of US Air Force and Federal Aviation Administration teardown programs was done to find areas susceptible to damage and their associated failure modes. Information was compiled from C-5A, C-130 Center Wing Box, KC-135 and T-37 and other smaller scale teardown analysis efforts. Once compiled, this data was weighed by structural significance, damage severity, and difficulty of inspection. These results were then presented to AFRL/RXL who gave final approval on specimen configuration and loading. Four samples were developed from three types of structures: fittings, which were defined as having complicated load paths in 3-D structures; stiffened panels, which are built-up of a flat sheet and multiple stiffening elements; and lugs, which are heavily loaded and easily modeled as two-dimensional. (Figure 9.3-2)

REFERENCES:

[1] Destructive Evaluation and Extended Fatigue Testing of Retired Transport Aircraft, Volume 4: Extended Fatigue Testing, DOT/FAA
[2] Laboratory Inspection Results- EC-135H 61-0291 Disassembly and Hidden Corrosion Program, Boeing
[3] C-130 Center Wing Box Structural Teardown Analysis Final Report, CAStLE
[4] CAStLE Metallurgical Evaluation Request Report Summary: C-5A Structural Risk and Model Revalidation Program, CAStLE
[5] FY06 T-37B[1] Wing and Carry-Through Structure Teardown Analysis Program Final Report, CAStLE
[6] FY07 T-37B Destructive Teardown and Failure Analysis, CAStLE

9.4 STRUCTURAL TEARDOWN ASSESSMENTS

9.4.1 DAMAGE MAPPING FOR STRUCTURAL ANALYSIS - CASE STUDY OF THE T-38 DAMAGE DATABASE

Zachary Whitman, Southwest Research Institute

Aircraft structural analyses require fleet data of many types and forms. Nondestructive inspection (NDI) findings, maintenance actions, and various repairs all need to be documented and readily available. The methods described in this paper detail the process and approach taken by the T-38 Aircraft Structural Integrity Program (ASIP) to document and utilize this information on a daily basis. The first T-38 was fielded in 1961 with in-service damage following shortly thereafter. Even the initial findings of the 1960s are relevant since early block aircraft may still have the same configuration. It is important to clearly display this information to reveal the 'whole' picture. The accuracy of analyses can suffer without a thorough understanding of the current structural condition and damage history.

The historical data available within the T-38 community has varying levels of detail and fidelity over multiple decades. Some data exists only on paper tucked away in folders while others are electronically stored. One database entry may have crack length, orientation, shape and a metallurgical analysis; while another may only state the type of damage. Mapping damage locations to their nearest known location provides an easily searchable format that can be readily displayed (Figure 9.4-1).

It will be shown that when a large variety of data sources are combined, a clearer picture of the structural history can be observed. However, once a database is populated, it can be difficult to retrieve and understand the information. Thousands of individual records in a table can be obtuse and unreadable, while the plotting methods used in the T-38 database can easily reveal the history and current condition of the structure. Plots can be of a single aircraft, the entire fleet, or various subsets such as aircraft usage severity. Immediately obvious is that specific areas are prone to certain types of damage and that the frequency of damage occurrence can vary with both time and the particular subset of the fleet (Figure 9.4-2). The spatial definition of damage has another benefit for the user. If multi-site damage exists in three layers of structure at a single fastener, then a search of the area in question in the spatially defined database will show three co-located pieces of damage on three separate pieces of structure. If the data is stored based on part alone, a search may yield three crack entries on the skin, spar, and rib separately leaving the analyst with little indication that they are all common to a single fastener.

This database is commonly used to provide both an aircraft and component history when an engineering disposition is required. The aircraft history may indicate that a wing has seen significant prior damage possibly leading to it being condemned based on the total extent of damage. A search for component damage on other aircraft might indicate a systemic issue. This database satisfies the MIL-STD-1530C structural maintenance database requirement to gather and store repair and damage information. The ease of use and value it provides has made it a frequently used tool in the T-38.

9.4.2 PROCEDURES FOR AIRCRAFT STRUCTURAL TEARDOWN: BEST PRACTICES HANDBOOK DEVELOPMENT

Gregory Shoales, Center for Aircraft Structural Life Extension

Safely sustaining the ever increasing numbers of aging aircraft in the United States Air Force (USAF) has brought a correspondingly increasing demand to determine the true condition of service-aged aircraft structural components. The only means available to precisely determine the damage state of a given structure is by what is commonly referred to as a "teardown inspection" of that structure. A very large number of these teardown programs have been executed in recent years. These include: A-10, AV-8B, B-2, B-52, B-727, C-5, C-17, C-130, C-141, EC 135, F-15, F 16, F-22, F-111, KC-130, P-3, T-37, T-38, VC-10 and numerous general aviation aircraft. Unfortunately, there is little to no cross talk between organizations performing teardown programs. The lack of communication limits the sharing of lessons learned and best practices developed during the course of each program.

Efforts in the past, such as the handbook published by The Technical Cooperation Program (TTCP), have summarized policy decisions and other programmatic issues associated with teardown programs as they applied to the international military and civil community. However, the procedures and requirements to be considered during each task of a teardown program have not been documented in great detail in any published work. Because of their extensive experience in all aspects of teardown program planning and execution, the USAF Academy's Center for Aircraft Structural Life Extension (CAStLE) was tasked by 77th Aeronautical System Wing, Wright Patterson AFB, Ohio to prepare just such a document. This best practices handbook would document the task by task procedures for planning and executing an aircraft structural teardown program. CAStLE was further tasked, wherever possible, to capture lessons learned from past programs. As a result of this effort, the handbook titled "Procedures for Aircraft Structural Teardown Analysis" was published in early 2008. The handbook chapters address all teardown tasks from setting program goals and requirements through the analysis of the resulting teardown program data. This work details the handbook development effort and presents a brief summary of each chapter.

9.4.3 T-37B DESTRUCTIVE TEARDOWN AND FAILURE ANALYSIS

Molly R. Walters, Sandeep R. Shah and Gregory Shoales, United States Air Force Academy (CAStLE)

A structural teardown analysis program was executed by the USAF Academy's Center for Aircraft Structural Life Extension for the T-37/T-38 Program Office, 506th Aircraft Sustainment Squadron (506 ACSS/GFLA), located at Hill Air Force Base (AFB), Utah. This was a follow-on effort from the FY06 teardown analysis program performed by CAStLE[1].

The current program examined all critical structure in two aircraft. These 32 critical areas are in the forward fuselage, wing, wing to fuselage carry-thru structure, and empennage. Each major structural element was fully inspected per the applicable paragraphs of Technical Order (TO) 1T-37B-36 [2] prior to disassembly. After disassembly and cleaning of the parts in the 32 critical areas, shown in the highlighted areas in Figure 9.4-3, all individual structural parts were again thoroughly inspected via a variety of NDI methods. These part level inspections resulted in 110 NDI indications. Each NDI indication was evaluated by failure analysis methods to determine the root cause of the indication. Failure analysis evaluation findings include fatigue cracks, corrosion, other cracks, and a material defect, below, at right. The material defect was the only damage found at any of the prescribed fatigue critical locations. Damage evaluation reports include evaluation methodology, all pertinent dimensions, detailed micrographic photo documentation and, for corrosion findings, complete elemental analysis.

All NDI indications and evaluation data was provided to the T-37B ASIP Manager and Chief Engineer incrementally throughout the program's duration. This final report also includes a fully searchable database archive and all raw data used to achieve findings. These data can be used to corroborate findings from previous teardown programs as well as damage data received from USAF T-37B operators. Findings from this program have justified the aft spar corrosion damage inspection implemented by the T-37B ASIP Manager based upon the FY06 teardown findings. This technical report details the FY07 T-37B teardown analysis program and the data obtained during its execution.

REFERENCE:

[1] FY06 T-37B Wing and Carry-Through Structure Teardown Analysis Program Final Report. Gregory A. Shoales, Sandeep R. Shah and Daniel C. Laufersweiler, Center for Aircraft Structural Life Extension USAFA TR 2007-09

9.5 LOADS & ENVIRONMENT CHARACTERIZATION

9.5.1 VERIFICATION OF IAT PROGRAM MODELS

Pete Caruso, Lockheed Martin Aeronautics Company

Managing safety and fleet readiness depends on reliable IAT models. IAT models track life shortfall locations discovered during F-22 airframe development, test interpretation, and current usage evaluation. F-22 maintenance actions are grouped at convenient flight hour intervals in Planned Maintenance Packages (PMPs) and adjusted by IAT predictions. IAT durability and damage tolerance models utilize parametric time-history data from the air vehicle integrated flight data recorder. Periodic IAT reports predict incremental crack growth or fatigue damage, and forecast maintenance interval requirements for force management decisions.

There are some important challenges in ensuring a reliable IAT model:

- Significant amount of data analysis steps that potentially introduce errors (data collection, processing, IAT regression, life tracking software)
- Development of accurate L/ESS equations
- Managing IAT requirements to maintain fleet safety allow flexibility in maintenance scheduling

The F-22 program has found a good solution to these issues by using the following procedure:

- Perform error checking at critical process steps
- Develop a friendly graphical process to rapidly evaluate L/ESS & IAT model predictions
- Apply parametric time-history spectra to evaluate IAT equation error
- Verify IAT equation accuracy to flight strain measurements
- Evaluate limited overfly of IAT requirements with risk analysis

Results on the F-22 show that robust IAT models allow limited overfly of IAT requirements while maintaining safety and optimizing fleet readiness.

9.5.2 ANALYSIS OF ENVIRONMENTAL SEVERITY INDEX

Sarah E. Galyon, Gregory A. Shoales and Scott A. Fawaz, United States Air Force Academy (CAStLE)

The structural health of an aircraft is affected by many factors, such as flight hours, service history and basing location. Basing location, for example, can affect the damage an airframe incurs over time as some bases have environments highly-conducive to corrosion. There is interest within the damage tolerant community in comparing the environments an aircraft experiences at different basing locations. The environmental severity index (ESI) is a scale designed to allow comparison of the environmental effects of one base to that of another in terms of corrosion damage. Recently the question was posed as to whether or not ESI could be used as a structural damage criterion for selecting aircraft for a structural teardown.

To determine to usefulness of ESI in this role, it is important to understand how the raw data used to calculate ESI was collected and analyzed. Such a study of the ESI data was completed at the USAF Academy's Center for Aircraft Structural Life Extension (CAStLE). It was noted that multiple sets of raw data were in circulation, that there was no standard practice for calculation of an ESI value and that ESI is alloy specific. The raw data and ESI were examined with multiple graphical methods to determine the trends associated with the ESI value for each base. Figure 9.5-1 shows one of the graphical methods used to analyze the ESI data available. From Figure 9.5-1 it can be noted that there is most likely a seasonal effect in ESI values.

Based on the graphical analysis it was determined that ESI should not be used as a primary selection criteria. Individual ESI values should not be used for a direct comparison between aircraft damage, except when ESI values vary grossly. Also the ESI does not account for the health of the aircraft coatings or the progress of the aircraft through its depot cycle. It was determined that ESI can be employed as a broad, secondary criterion for aircraft selection; thus, in the absence of other variances, aircraft at bases with similar ESI values would likely have similar levels of damage while aircraft at bases with grossly different ESI would not.

9.5.3 IMPACT OF FLIGHT DATA ACQUISITION ON FLEET MANAGEMENT DECISIONS

James M. Greer, Jr. and Gregory A. Shoales, United States Air Force Academy (CAStLE) and Randal A. Hartnett, United States Coast Guard

In the summer of 2005, a U.S. Coast Guard HC-130H aircraft was instrumented for the purposes of monitoring the loading and environmental conditions affecting the Center Wing Box (CWB) structure. The primary instrumentation consists of accelerometers (N_z) and strain gages (43 channels, uniaxial and rosette). Sensors for cabin and pressure altitude, temperature, and humidity were also installed. Other aircraft parameters, such as true airspeed, weight-on-wheels, ramp door position, and flap position are also collected by the monitoring system. Collecting aircraft parameters facilitates matching loads and environmental information to different phases of flight and flight conditions. A simple but novel method [1] of obtaining height above terrain was also developed for this program.

Prior to this effort, usage and flight severity data were primarily inferred through surveys of aircrew and fleet managers. However, with over 2000 hours of flight data now in hand, survey data have been supplemented with actual usage data. These data are being used by the U.S. Coast Guard to make fleet management decisions for the HC-130H.

An in-depth review of the system was presented at the 2007 Aging Aircraft conference [2], in which the data were summarized. An even more detailed system description is now available in a limited distribution CAStLE report [3]. The flight data have raised the level of confidence in determining the Equivalent Baseline Hours (EBH) of the aircraft in the fleet. This has had the effect of eliminating some of the (understandable) conservatism built into the usage survey data. The actual flight data have shown that the operating environment is less severe than originally thought (Figures 9.5-2 and 9.5-3). Initial projections indicate a 20% increase in life for the youngest 16 of the Coast Guard's 26 HC-130H aircraft may be possible.

REFERENCES:

[1] J.M. Greer and G.A. Shoales, "Using a NOAA Database, GPS, and/or Pressure Altitude Measurements to Determine Height above Terrain," in *The 2008 Society of Flight Test Engineers (SFTE) International Symposium* Fort Worth, TX, November 2008.

[2] J.M. Greer, G.A. Shoales, P.J. Christiansen, R.A. Hartnett and E.B. Sheppard, Jr., "HC-130H Center Wing Box Monitoring System Update," in *Proceedings of the 10th Joint FAA/DOD/NASA Conference on Aging Aircraft*, Palm Springs, CA, 2007.

[3] J.M.Greer, Jr. and G.A. Shoales, "HC-130H Center wing Flight Data Acquisition: System Installation and First Year, " Center for Aircraft Structural Life Extension (CAStLE), USAF Academy, CO, Technical Report USAFA-TF-2008-01, October 2007.

9.5.4 CHARACTERIZATION OF ROTORCRAFT RECORDED MANEUVER/REGIME USAGE VARIABILITY

Dr. Suresh Moon, L-3 Communications and Nam Phan, NAVAIR

The rotary wing aircraft usage spectrum consists of maneuver durations and occurrences per 100 flight hours. These are derived from broad mission requirements and typical usage spectrums provided in Aeronautical Requirements 56. Over the years, the U.S. Navy (USN) has fielded Structural Usage Monitoring (SUM) systems on AH-1W, H-46, H-3, H-60, V-22, and H-53 to record maneuvers onboard or by post processing using a regime recognition algorithm. Significant variations in maneuver usage from aircraft to aircraft were observed. The variability in different maneuvers such as level flight, hover, turns, climb, descent, dive, pull-up, etc., was modeled with Weibull distributions, and Weibull parameters were determined. The Weibull distribution characteristic value and slope vary from rotorcraft to rotorcraft for identical maneuvers and is dependent on the rotorcraft mission. The Kolmogorov-Smirnov goodness of fit test was conducted to confirm the distribution fit. The Weibull cumulative distributions of different regimes were used to investigate the effect of usage variation on reliability required to implement Condition Based Maintenance (CBM). (See Figure 9.5-4)

9.6 CHARACTERIZATION, MODELING AND TESTING

9.6.1 DAMAGE TOLERANCE TESTING OF COMPOSITE HONEYCOMB FUSELAGE PANELS

John Bakuckas, FAA

Rising operating costs are driving aircraft manufacturers to reduce weight and improve efficiency by using more composite materials in aircraft design. Composite honeycomb sandwich fuselage designs have been used quite successfully in general aviation and commuter aircraft. Advantages compared to conventional structure include weight savings, an increase in bending rigidity and in-plane strength and stiffness, and improved stability. A technical challenge in airplane composite sandwich design is to adequately predict residual strength of a damaged structure.

Classical damage tolerance philosophy, which has long been used in the design of conventional metallic airplane structure, cannot be directly applied to composite sandwiched structure for several reasons. First, damage in composite structure is seldom representative of a single dominant crack needed to apply continuum facture mechanics principles. Due to the heterogeneous nature, damage in composite- sandwiched structure is much more complex than in conventional metallic materials. It can be quite extensive, yet nonvisual, and can pose difficulties with regards to inspections. In addition, there was a general lack of understanding of failure mechanisms and their interaction in the overall structural response. Linear engineering models typically are not equipped to handle complex nonlinear behavior exhibited by composite-sandwiched structure and have limited predictive capability. Empirical approaches based on experimental data from coupon, subcomponent, and full-scale tests are time-consuming and very costly. The Federal Aviation Administration (FAA) has performed several programs to develop models to predict the structural response, damage progression, and residual strength. Methodologies have been developed and validated in a building block approach at the coupon and subelement levels.

This study investigated the damage tolerance characteristics and failure mechanisms of honeycomb sandwich composite curved fuselage panels. The objective is to determine the effects of various damage scenarios, such as holes and notches, on the residual strength of composite panels that reflect typical honeycomb sandwich fuselage structure subjected to combined loading. Six panels were tested with an internal radius of 74″, a length of 125″ and a width of 73″, containing a variety of artificial damage configurations, Figure 9.6-1.

The sandwich test articles were fabricated using a Toray Composites T700SC-12K-50C/#2510 plain weave carbon fabric prepreg of 0.0085″ thickness in the facesheets and a Plascore PN2-3/16-3.0 Nomex honeycomb of 0.75″ thickness for the core. The lay-up for the test section of the sandwich is [45/0/45/Core/45/0/45].

The panels were subjected to quasi-static pressurization and axial loading using the Full-Scale Aircraft Structural Test Evaluation and Research (FASTER) facility located at the FAA William J. Hughes Technical Center, Atlantic City International Airport, NJ, Figure 9.6-2a. The test articles were instrumented with strain gages near the damage and in the far-field regions for strain surveys, Figure 9.6-2b. A digital image correlation (DIC) method was used to obtain full-field displacement and strain measurements at equal load intervals and after any visible surface damage was observed, Figure 9.6-2c. The acoustic emission (AE) method was used to monitor damage growth in real-time and served as an early warning for imminent failure, Figure 9.6-2c. Several nondestructive inspection methods were also used to scan for nonvisual damage, including pulsed thermography.

Panels were loaded quasi-statically to failure to record the structural response, damage evolution, and residual strength. The DIC method was effective in providing full-field displacement and strain measurements up to failure, as shown in Figure 9.6-3a and 9.6-3b. Visual damage occurred at high load levels where the subsequent final failures occurred quite rapidly. The AE method was effective in providing early warning for imminent failure. Results shown in Figure 9.6-3c and 9.6-3d indicate that the AE method could detect and locate damage formation that occurred from the notch tips.

Data generated during this test program will validate test data and predictions from earlier coupon and element-scale research and provide an accurate assessment of sandwich damage tolerance and design principles for use in aircraft.

9.6.2 CHARACTERIZATION OF FATIGUE CRACK THRESHOLD IN HIGH-CYCLE FATIGUE APPLICATIONS

John Bakuckas and Cu Nyugen, FAA

Aircraft propeller blades operate in a high-cycle fatigue (HCF) environment, accumulating a large number of fatigue cycles in a short period of time. Due to HCF, stable fatigue crack growth is of relatively short duration. For practical damage tolerance applications, it is desirable to operate propeller blades below the threshold region of fatigue crack growth. Traditional damage tolerance analysis uses near-threshold fatigue crack growth data from large cracks obtained mostly from compact and middle tension test specimens. However, in the case of aircraft propeller blades, the primary concern is the damage tolerance of small surface flaws. Therefore, this research program focuses on near-threshold fatigue crack growth of small, thumbnail-like, surface flaws in 7075-T7351 aluminum used in aircraft propeller blades. Of interest is the effect of compressive residual stresses at the outer surface of the specimens, introduced by shot-peening, on the near threshold fatigue crack growth behavior of small surface flaws.

The tests were conducted using dog bone specimens, as shown in Figure 9.6-4a, using the Material Characterization Laboratory located at the FAA William J. Hughes Technical Center, Atlantic City International Airport, New Jersey. A closed-loop, servo-hydraulic axial test stand with a 50-kip maximum capacity was used under load control mode, in accordance with ASTM E 647. To simulate the effect of small surface flaws (such as initial manufacturing flaw, in-service mechanical damage, and in-service corrosion damage), small 0.015-inch-radius semicircular surface flaws were introduced using a relatively new laser-machining technique, Figure 9.6-4b. The Direct Current Potential Difference method was used to monitor the subsequent fatigue crack growth (FCG). Initial and fatigue crack front profiles were measured using a stereomicroscope, optical microscope, and scanning electron microscope, at the end of the test.

The results are summarized in Figure 9.6-5a-c for the as-received 7075-T7351 aluminum specimens tested using R-ratios of 0.1 and 0.7. The fatigue precracking and subsequent load-shedding test procedures were successfully applied to obtain near-threshold FCG region and the arrest threshold stress-intensity factor range for the as-received specimens, Figure 9.6-5a. The final shape of the fatigue crack profile at the end of the cyclic loading was nearly semicircular, as shown in Figure 9.6-5b and 9.6-5c for R = 0.1 and 0.7, respectively. In general, the fatigue crack front progressed concentrically from the initial semicircular laser-machined flaw.

For the shot-peened 7075-T7351 aluminum specimens, crack initiation from the laser-machined flaws was not accomplished during fatigue precracking. Consequently, the shot-peened specimens failed outside the gage section during the fatigue tests, Figure 9.6-6a. The depth of the compressive stress region from the shot peening was greater than the depth of the surface flaw and effectively prevented crack initiation, as indicated in Figure 9.6-6b. This was further verified using the electron backscatter diffraction (EBSD) technique, which provided a two-dimensional orientation map of the material's microstructure; i.e., the grain orientation and shape, Figure 9.6-6c. However, compared to the as-received specimens, the applied load in the shot-peened specimens was more than twice as high. This suggests that crack initiation threshold values in the shot-peened specimens would be a least double that of the as-received specimens.

9.6.3 IMPROVING FATIGUE PREDICTABILITY OF LUGS WITH HIGHER ORDER GEOMETRY RATIOS

Rob Chase and Mark Ofsthun, Spirit AeroSystems, Inc.

Dimensionless geometry factors are typically used when predicting lug fatigue strength. Higher order factors can emphasize more important geometry effects while deemphasizing less important geometry. Lug fatigue predictability was improved when higher order factors were used. Using random optimization, higher order factors for aluminium were found to be different then higher order factors for titanium.

A lug is a joint that transfers load through a single pin. Lugs may be single load path critical structure and are often used to carry large loads. For this reason it is important to design them properly to ensure the lugs meet fatigue strength requirements. A lug consists of the basic geometry shown in Figure 9.6-7.

Though lugs are very simple structures, the variation in their dimensions makes predicting lug fatigue performance challenging. Lugs are a very geometry sensitive structure. Some common dimensionless geometry ratios and what they relate to are as follows (Reference):

$\frac{D}{w}$	Kt Sensitivity
$\frac{t}{D}$	Pin Bending
$\frac{c}{t}$	Aspect Ratio

These factors have traditionally been used because they provide some level of correlation between changes in lug geometry and the ability to predict fatigue life. However, dimensionless factors that use higher order parameters have the potential to emphasize certain characteristics while deemphasizing other characteristics. This extra degree of freedom can improve the correlation between a factor and the fatigue predictability. An example of the improvement in predictability is shown in Figure 9.6-8. In Figure 9.6-8, the common ratios $\frac{D}{w}$, $\frac{t}{D}$ and $\frac{c}{t}$ were used in the left plot and the ratios $\frac{c^4 \cdot w^2 \cdot t}{D^7}$, $\frac{w}{t}$ and $\frac{t^6}{c^5 \cdot D}$ were used on the right. In both plots each data point represents a characteristic life of a group of fatigue specimens. Data points close to the line represent good correlation between the prediction and the characteristic lives. Data points far from the line represent poor correlation between the prediction and the characteristic life. The higher order factors out performed the traditional factors.

The higher order factors were randomly generated by a computer. Then the baseline S-N curve was modified by a correction factor so the predicted life matched the characteristic life. This was done for each group of fatigue data. The randomly generated factor was then plotted along the x-axis and the correction factors were plotted on the y-axis. The least squares method was then used to find a best fit second order polynomial. The coefficient of determination, which measures correlation, was used as a fitness value for the randomly generated factor. This process was repeated and fitness values were compared until an optimum factor was chosen.

Figure 9.6-9 shows the improvement for titanium lugs. For this material, a different set of optimum factors were chosen. These factors are $\frac{D^2 \cdot c}{w^3}$, $\frac{D^3 \cdot c^2}{w^4 \cdot t}$ and $\frac{t^4 \cdot c}{D^2 \cdot w^3}$.

Higher order factors used to modify S-N curves were found to improve fatigue predictability in both aluminum and titanium lug structure. The higher order factors allowed for the deemphasing of some geometric effects while emphasizing others. Aluminum and titanium were better represented by different sets of higher order factors.

9.6.4 GREEN'S FUNCTION FOR THE COMPACT TEST SPECIMEN

James Newman, Jr., Mississippi State University and Mark McKenna, Luna Innovations, Inc

In the aerospace industry, structural components machined from forgings may have internal residual stresses from the manufacturing process. The linear superposition method is used herein to calculate the influence of an arbitrary residual-stress distribution on the stress-intensity factors for a compact C(T) specimen, shown in Figure 9.6-10a. C(T) specimens are used to generate the baseline fatigue-crack-growth (FCG) rate properties for a material. Of concern are the residual stresses that may be present in the material from either machining and/or the manufacturing process. The presence of these unknown residual stresses may inadvertently influence the baseline properties and should be accounted for in crack-growth analyses.

The Green's function for the compact specimen was obtained by conducting stress analyses of the C(T) specimen subjected to a pair of concentrated forces per unit thickness, Q, applied along the crack surface at location b, as shown in Figure 9.6-10b. The stress-intensity factor is

$$K_Q = 2Q/\sqrt{(2\pi b)}\ F(a/w,\ b/w') \tag{1}$$

for $0.2 \le a/w \le 0.9$ and $0 \le b/d \le 1$, where w' is the distance from the force to the back face of the specimen ($w' = 1.25\ w + b - d$). The leading term in equation (1) is the exact solution for a pair of forces applied to a semi-infinite crack surface in an infinite body. The function F is the boundary-correction factor that accounts for the influence of the crack length and external boundaries on the stress-intensity factor, such as the crack length, width, height and pin holes.

In 1983, Mall and Newman conducted a boundary-collocation analysis and developed a Green's function equation for the standard C(T) specimen. In the original analysis, however, the location of the concentrated force was restricted to $b \le a$. Herein, several stress analyses were conducted to develop additional stress-intensity factors and to improve the Green's function equation for the specimen shown in Figure 9.6-10b. The FRANC2DL, finite-element code, and the FADD2D, boundary-element code, were used to calculate stress-intensity factors for a wide range in crack configurations (a/w) and in concentrated force locations.

Figure 9.6-11 shows a comparison among the various boundary-correction factors calculated for the C(T) specimen subjected to a pair of concentrated forces. The normalized boundary-correction factor, $F\ (1-\Delta)^{3/2}$, is plotted against Δ. The dashed curves in Figure 2 are the original Green's function equation for various a/w ratios, which shows how the original equation over estimates the boundary-correction factors for a/w ratios less than about 0.4. The closed and open symbols are the recent results from FRANC2DL finite-element code; and the diamond symbols are the recent results from FADD2D boundary-element code for a pair of forces applied at the crack mouth. The solid curves show the improved equation for the normalized boundary-correction factor. The equation for the correction factor, F, is

$$F(\alpha,\Delta) = (1 + A_1\ \Delta + A_2\ \Delta^2)\ [1 - 1.05\ (1 - \alpha)^9\ (\Delta/\Delta_o)^3]\ /\ (1 - \Delta)^{3/2} \tag{2}$$

$$A_1 = 3.6 + 12.5\ (1 - \alpha)^8$$

$$A_2 = 5.1 - 15.32\ \alpha + 16.58\ \alpha^2 - 5.97\ \alpha^3$$

$$\Delta_o = 0.8\ \alpha + 0.2$$

where $\alpha = a/w$, $\Delta = b/w'$, $0 \le \Delta \le \Delta_o$, and $0.2 \le \alpha \le 0.9$. Equation (2) is within ±1 percent for $\alpha > 0.4$ and within about 1.3 percent for $0.2 \le \alpha \le 0.4$.

9.6.5 COMPRESSION PRECRACKING THRESHOLD TESTING ON ROTOCRAFT MATERIALS

James Newman, Jr., Mississippi State University

Accurate representation of fatigue-crack-growth thresholds is extremely important for many structural applications. Presently, in the United States, the threshold regime is experimentally defined by the ASTM E-647 load-reduction (LR) test procedure. Tests have shown a rise in the crack-closure levels as the threshold conditions are approached using the LR method. This behavior was attributed to roughness- and/or fretting-debris-induced crack-closure effects. Analyses have also shown a rise in the crack-closure level using strip-yield and finite-element models, which showed that the test method exhibited anomalies due to load-history effects.

To generate fatigue-crack-growth-rate data in the threshold and near-threshold regimes, without appreciable load-history effects, compression precracking (CP) methods, developed over the years by a number of investigators, such as Pippan et al and Newman et al, was used. Using CP threshold test methods, environmental effects, such as oxide and/or fretting-debris-induced closure, crack-surface roughness, and plasticity effects would *naturally* develop under constant-amplitude (CA) loading conditions. A crack grown under CP loading, as shown in Figure 9.6-12a, is fully open at the start of CA loading. The crack is growing partly because of tensile residual stresses induced by compressive yielding at the crack-starter notch. Currently, trial-and-error procedures are required to select the initial CA loading magnitudes near the unknown threshold value. If a tensile load range is selected that would produce a stress-intensity factor range below threshold, then the crack may initially grow, but become a non-propagating crack; however, if the load is high enough, then the crack will grow. The crack must be grown *several* compressive plastic-zone sizes before the effects of the tensile residual stresses have decayed and the crack-opening stresses have stabilized under CA loading conditions. This method is called the CPCA threshold test method. A second method is CP, followed by CA loading, and then LR following current ASTM E-647 procedures, except that the initial stress-intensity-factor range and crack-growth rate at the start of LR test is much less than the maximum allowed in the current standard. This method is referred to as CPLR threshold testing and the loading is depicted in Figure 9.6-12b

Compact C(T) specimens made of a Ti-6Al-4V β-STOA alloy were machined from a forging in the SL-orientation. Tests were conducted with CPCA, CPLR and the ASTM LR test methods. The latter tests were designed to use the "maximum allowed rate" (10^{-8} m/cycle) in the E-647 standard. Figure 9.6-13 shows a comparison of these data at an R-value of 0.4. For the ASTM LR tests (open symbols), the crack was grown from the crack-starter notch to a crack length, which gave a rate of about 10^{-8} m/cycle and then the LR test was conducted. These results produced an average threshold (ΔK_{th}) of about 5.8 MPa-m$^{1/2}$. For the CP tests (solid symbols), only data that satisfied the crack-extension criterion ($\Delta c \geq 3\ (1 - R)\ \rho_c$) is shown, where ρ_c is the compressive plastic-zone size. The square symbols show the CPLR test results, which produced a threshold value of about 4 MPa-m$^{1/2}$. The CPCA and CPLR tests produced higher rates than the LR method over a significant portion of the ΔK-rate curve. The β-STOA alloy has a very large grain structure, which caused very rough crack surfaces with meandering and bifurcating cracks.

Of the five materials tested in the FAA-sponsored work using the three threshold test methods (CPCA, CPLR and ASTM LR), two of the materials (7075-T651 and 4340 steel) showed very little difference, while the other three materials (7075-T7351, Ti-6Al-4V β-STOA, and Inconel-718) showed significant differences, with the CPCA and CPLR methods producing lower thresholds and faster rates in the near-threshold regime. The former two materials exhibited very flat and straight crack surfaces, while the latter three materials exhibited either very roughness crack-surface profiles or produced fretting-debris along the crack surfaces.

9.6.6 FURTHER DEVELOPMENT OF THE NASGRO SOFTWARE FOR FRACTURE MECHANICS AND FATIGUE CRACK GROWTH ANALYSIS

Craig McClung and Joseph Cardinal, Southwest Research Institute; Joachim Beek and Royce Forman, NASA Johnson Space Center; and Venkataraman Shivakumar, Randall Christian, Yajun Guo, Ben Nguyen and Feng Yeh, Jacobs ESCG

The NASGRO® software for fracture mechanics and fatigue crack growth analysis continued to be actively developed and widely used during 2007 and 2008. NASGRO is the standard fracture control software for all NASA Centers and is also used extensively by NASA contractors, the European Space Agency (ESA) and ESA contractors, and FAA Designated Engineering Representatives certified for damage tolerance analysis, as well as many aerospace companies worldwide. NASGRO has been jointly developed by NASA and Southwest Research Institute since 2001, with substantial financial support from NASA, the NASGRO Consortium, and the Federal Aviation Administration (FAA). The NASGRO Consortium began its third three-year cycle in 2007, and the international participants included Airbus, AgustaWestland, Boeing, Bombardier Aerospace, Embraer, Hamilton Sundstrand, Honeywell Aerospace, Israel Aerospace Industries, Lockheed Martin, Mitsubishi Heavy Industries, Siemens Power Generation, Sikorsky, Spirit AeroSystems, and Volvo Aero. In addition to Consortium members and other site licenses, eighty single-seat commercial NASGRO licenses were issued in 2007-2008.

Two new production versions of NASGRO were released in 2007 and 2008. Version 5.1 was released in May 2007, and Version 5.2 was released in January 2008. The primary technical advances in these versions were the development of new stress intensity factor (SIF) solutions (see Figure 9.6-14) and related computational capabilities. NASGRO 5.1 contained three new SIF solutions. TC14 is an edge through crack with remotely imposed displacement gradients. TC15 is an edge through crack in a plate of varying thickness with a univariant stress gradient on the crack plane. SC19 is an off-center surface crack in a plate with a bivariant stress gradient on the crack plane. The crack aspect ratio a/c for SC19 and its univariant counterpart SC17 can be as large as 8 and as small as 0.1 (0 for SC17). NASGRO 5.2 contained two additional new SIF solutions. CC11 is a corner crack in a plate with a univariant stress gradient on the crack plane. TC16 is a through crack in a pressurized cylinder (curved panel) with bulging effects and optional stiffeners.

Many other enhancements in SIF solutions were added in 5.1 and 5.2. The most commonly used univariant and bivariant weight function solutions now accept direct input of static residual stress fields and employ enhanced point-spacing algorithms for all stress fields. Generalized tabular compounding is now available for all through crack solutions. New or enhanced net section yield solutions were added for most crack cases. Residual strength diagram capabilities are now available for all through, corner, surface, and embedded cracks, and one-dimensional data tables. Other improvements include additional crack transitioning, new visualization and plotting options, new spectrum editing features, new material property calculation features, and an improved module to calculate critical crack size.

The Alpha and Beta development versions of NASGRO 6.0 were released for evaluation in 2008, with production release of 6.0 targeted for early 2009. New SIF solutions (see again Figure 9.6-14) included CC12, a corner crack spanning a small chamfer in a bivariant stress field, and EC04 and EC05, an offset elliptical embedded crack in a plate with a bivariant (EC04) or univariant (EC05) stress gradient on the crack plane. Weight function solutions for one crack at a hole were generalized to permit two symmetric cracks at the hole. Other enhancements include new flexibility to specify toughness values at different locations, a new threshold crack size module, and new features in the material property module to accept test data from surface crack specimens and K-gradient load histories.

Further information about NASGRO is available at www.nasgro.swri.org.

9.6.7 THREE DIMENSIONAL CRACK GROWTH PREDICTION

Sarah E. Galyon, R.A. Saravanan, James Greer and Scott A. Fawaz, United States Air Force Academy (CAStLE)

In complex aircraft structure, crack growth rarely propagates in the idealized fashion assumed in durability and damage tolerance analyses (DADTA). Usually the applied loading is not perpendicular to the crack nucleating feature and subsequent crack propagation. This situation is known as mixed mode crack growth or in more general terms, three dimensional crack growth. Most DADTA's conducted assume mode I only; thus, engineering judgment is used to estimate the amount of error present in the idealized models. The Center for Aircraft Structural Life Extension (CAStLE) at the United States Air Force (USAF) Academy completed a project to generate three dimensional (3D) crack growth data and predict the measured crack growth rate, crack trajectory and residual strength using state-of-the-art stress analysis and life prediction tools.

Specifically, we generated the 3D fatigue crack growth test data using 1.6 mm (0.063 inch) thick aluminum alloy (AA) 2024-T351 ARCAN specimens in an ARCAN test fixture. The ARCAN test fixture allows the ARCAN sample to be rotated to produce different mixtures of mode I and mode II loading (with 0° being pure tension/compression (mode I) and 90° pure shear (mode II)). ARCAN specimens were tested at angles of 0°, 30°, 60° and 75° under constant amplitude loading and a stress ratio (R) of 0.1. The stress amplitude was adjusted to control the crack growth rate and plastic zone size. A grid on the surface of the sample was used to optically track crack trajectory and crack growth rate. While mechanical testing was being completed, we also developed a crack prediction model of the ARCAN specimen using FRANC3D/NG, a solid modeling, mesh generation and fracture mechanics code from Cornell University Fracture Group. FRANC3D/NG should be able to predict the cracking behavior observed in the ARCAN tests. A parallel effort was also undertaken to develop an engineering model of mixed mode crack growth where contributions to mode I and mode II growth were accounted for using K_I and K_{II} and the appropriate baseline crack growth data. For both the FRANC3D/NG and engineering model analysis, crack growth rate data is required and was produced per ATSM E647 using 15.24 cm (6 inch) wide, 1.6 mm thick AA 2024-T351 M(T) specimen in both the LT and TL orientations under constant amplitude loading and an R of 0.1.

The fatigue crack growth trajectory prediction for the ARCAN specimens was assessed with three different measures. The first was the point-wise comparison of the measured and predicted crack angle for each of the test conditions. The second was a block comparison of the measured and predicted crack angle. A block is defined as a discrete amount of crack growth, so the crack growth was compared at ¼, ½ and ¾ the total crack length. Figure 9.6-15 shows the crack trajectory for LT samples loaded at 0°, 30°, 60° and 75°. Figure 9.6-16 shows the crack trajectories for samples loaded at 60° with TL and LT material orientations. The third was examining the effect of cracking angle on the residual strength or critical crack size of the specimen. Comparisons were also made of the predicted and observed fatigue life, number of cycles at the end of the test and crack growth rate. The success of the prediction model is based on how the correlation of the model affects the ability to predict the measured fatigue and fracture performance based on the mechanical testing.

9.6.8 PREDICTING STRESS CONCENTRATION FACTORS FROM CORRODED SURFACE TOPOGRAPHY

Tom Curtin, Computational Mechanics Inc.

A computational tool was developed to accurately predict stress concentration factors (SCF) for corroded surface topography typically found in pitted aircraft skin. This work was completed under subcontract RSC05040 for University of Dayton Research Institute (UDRI) with support from NAVAIR's Aircraft Division. Following algorithm development the software was validated using laser profilimetry data obtained for a corroded test specimen (Figure 9.6-17).

Stress analysis of a corroded surface requires solving a computer model with a very large number of degrees of freedom. As such a special methodology was developed to address the complexities inherent in modelling a typical corroded surface topology. Based on St. Venant's principle an individual pit has a limited field of influence over the stress in the surrounding area. This fact motivated the development of a submodeling technique where a corroded test specimen could be analyzed at different levels of resolution by assembling a series of sub-models with appropriate boundary conditions (Figure 9.6-18).

Given the difficulty associated with meshing a highly irregular topography a surface mesh approach based on the boundary element method was determined to be most suitable for this analysis. The solution method uses a Structured Uniform Grid to represent the corroded surface topology determined from laser profilimetry. The actual corroded surface is partitioned into a series of submodels. Each submodel is initially defeatured slightly and solved independently to determine SCFs and associated geometrical error. The geometrical error is defined as the distance between the experimental data point and the computer model mesh of the corroded surface. Following completion of the solve phase an iterative assembly scheme is started in which the results of individual submodels are combined into a unique data set representing the full test specimen.

The solution process is then repeated using an adaptive mesh refinement scheme in zones indicating high SCF or large geometrical error. In essence increased geometric detail is added only to submodels located in areas of high initial SCF.

Figure 9.6-19 shows the change in SCF for various levels of mesh refinement and submodel size. The adaptive mesh refinement process is repeated until the SCF values converge. Using this technique the SCF at various risk points in the specimen can be accurately determined without creating a computationally prohibitive computer model (Figure 9.6-20).

The computer simulation methodology described could potentially be used to randomly generate corroded surface models and solve for the associated SCFs. The computer solution not only provides the SCF but the full stress tensor on the corroded surface as well. This data could be used as input to strain life based fatigue equations. The benefit of this process would be the reduced need to laboratory corrode and fatigue test specimens in order to develop new methods to assess the impact of corrosion pitting on aircraft structural integrity.

REFERENCE:

[1] Perrata A. and Brebbia C., "SubModeling boundary element approach for stress concentration in samples exposed to pitting corrosion", 2nd Int. Conference on Simulation of Electrochemical Processes, pp 277-286, 2007, WITPress.

9.6.9 FRETTING FATIGUE CRACK GROWTH SIMULATION

Tom Curtin, Computational Mechanics Inc.

Computational Mechanics and our partner Nextgen Aeronautics recently completed a NAVAIR sponsored Phase II SBIR Contract and were successful in demonstrating the feasibility of using advanced modeling techniques and software to accurately assess failure progression rates in aircraft engine system components. The failure of a dovetail fretting fatigue specimen (Figure 9.6-21) was analyzed using a new 3D crack growth simulation tool. The analytical results were compared to existing laboratory test data published by the Air Force Research Lab (AFRL). The crack growth simulation methodology directly accounts for the impact of the high edge of contact stress gradients on the crack growth behavior. Because the actual component is modeled, with the crack automatically inserted, geometry corrections do not need to be applied to the predicted SIF data. The crack growth simulation includes the capability to solve multiple load cases with frictional contact making it a useful tool for investigating the impact of load history. The boundary element contact simulation also predicts the final stress state and it is not necessary to use multiple analytical approaches to separately calculate the bulk stress and contact stress field.

The BEASY crack growth methodology provides the capability to couple the contact analysis with a fatigue crack growth (FCG) simulation. This capability provides an added degree of accuracy in terms of analyzing fretting fatigue type problems since the presence of a crack at the edge of contact may alter the contact solution. It is likely that the compliance of the component will change once a crack begins to propagate and this will impact the contact length and contact stress state. This effect is not accounted for using existing fracture mechanics approaches such as generalized weight functions or the method of distributed displacement discontinuities. The coupled contact and FCG methodology used in the BEASY fracture analysis automatically accounts for the interrelationship between the contact stress state and increasing component compliance.

The BEASY contact solution provides two significant advantages as a method for solving contact mechanics type problems. Firstly, the primary variables of interest such as contact stress and relative tangential displacement are direct independent variables in the boundary element formulation. Secondly, the process of mesh refinement in the area of contact is simplified since only a surface mesh is required to model the two contacting bodies. The method is demonstrated using a flat rounded contact model where the predicted contact stress (Figure 9.6-22a-b) is in good agreement with a related analytical solution [2]. The method can also accurately predict the high edge of contact stresses that are typically associated with fretting fatigue damage and crack initiation (Figure 9.6-22c).

As part of the SBIR contract a new capability to model crack closure and sliding was also developed. Predicting the behaviour of cracks under compressive loading provides an important analytical component and is helpful in understanding the fretting fatigue behaviour of fracture critical components. We have leveraged existing experience using boundary element based solutions for contact mechanics and developed the methodology to directly apply contact boundary conditions on crack surfaces in 3D models. The contact condition applied to the crack surface is currently based on a Coulomb friction criterion, as an approximation, to simulating the shear resistance on a crack surface.

REFERENCES:

[1] Golden P.J. and Calcaterra, J.R., A fracture mechanics life prediction methodology applied to dovetail fretting, Tribology, V39, 1172-1180 (2006).

[2] Ciavarella M. and Macina G., New results for the fretting induced stress concentration on Hertzian and flat rounded contacts, Int. Jour. of Mech. Science, 45, (2003), 449-467.

9.6.10 FATIGUE LIFE PREDICTION OF CORROSION DAMAGED HIGH-STRENGTH STEEL USING AN EQUIVALENT STRESS RISER (ESR) MODEL

David Rusk, NAVAIRSYSCOM and Wally Hoppe, University of Dayton Research Institute

The fatigue life of metallic aircraft structural components can be significantly reduced by environmentally induced corrosion. However, there have historically been no analytical methods to quantify the specific fatigue life reduction of individual unfailed corroded components with any reasonable degree of confidence. As part of a NAVAIR High Strength Steel Corrosion-Fatigue Assessment Program, methods were studied to predict the impact that corrosion-induced surface roughness has on the fatigue life of high strength steel aircraft components. The steels of interest produce general corrosion in patches rather than localized pitting or other types of corrosion. In addition, this type of corrosion has characteristic features over a wide range of scales (Figure 9.6-23). Consequently, traditional finite element analysis approaches are not well suited to this problem, since the mesh required to accurately reflect the fine details distributed over the entire corrosion patch make computation unrealistic. Therefore, approximate elasticity methods (Figure 9.6-24) were developed using Fast Fourier Transforms that allow localized regions of interest of high stress to be identified (Figure 9.6-25). Subsequently, a simple notch metric formula is employed to approximate the stress riser in these regions of interest. Finally, an extension of Peterson's fatigue notch sensitivity theory is applied to these small "notches" that has the result of suppressing the effect of smaller notches compared to larger notches in the prediction of life. Each region of interest is assigned a probability of crack initiation as a function of fatigue cycles, based on a probabilistic strain-life analysis using the predicted notch factor. The net life (to crack initiation) for the component is then the product of the survivabilities of all of the individual regions of interest on the component surface. Tests on AF1410 steel corroded fatigue specimens have been conducted to both calibrate the parameters in the Peterson model as well as to test the life prediction capability of the approach. Predictions from the resulting model have demonstrated that an empirical approach to corrosion surface damage that builds on traditional notched-based fatigue analysis methods can be utilized to generate probabilistic life predictions that have substantial engineering value in assessing the residual fatigue life of corroded AF1410 steel components. The modeling technique has also been shown to capture the significant corrosion features that cause fatigue cracking in most cases, especially for more severely corroded surfaces.

REFERENCE:

[1] Rusk, D.T., Hoppe, W., Braisted, W., Powar, N., "Corrosion-Fatigue Life Prediction Using an Equivalent Stress Riser Model," 11th Joint NASA/FAA/DoD Conference on Aging Aircraft, Phoenix, AZ, 21-24 Apr. 2008.

9.6.11 FATIGUE EVALUATION OF VARIOUS SINGLE SIDE INSTALLED FASTENERS IN TITANIUM 6AL-4V & 7075-T7351

Bryan Woods and Mark Ofsthan, Spirit AeroSystems, Inc.

Single Side Installed (SSI) fasteners have traditionally been highly restricted in its uses in aerospace manufacturing. Because of low clamp-up and / or poor hole fill they do not perform well in high stress or high vibration structure. However, in the past decade fastener manufactures have made great strides in the design of SSI fasteners that may be considered "structurally rated". This paper compares the joint fatigue strength of these new SSI fasteners versus a standard aerospace fastener (steel Hi-Lok). In an effort to reduce weight and manufacturing time on aircraft the performance of Ergo-Tech®, Ti OSI®, and Monogram Mechani-Lok (MLA®) were compared to the steel Hi-Lok in a double lap joint fatigue study. The fastener diameters were 4.762 mm and 6.350 mm and tested in Titanium 6Al-4V and 7075- T7351 double lap joints. It was found that the Ti OSI® fastener outperformed the other fasteners. The Ergo-Tech® fastener and the Monogram MLA® met the baseline fatigue limit in some configurations, but fell short in others.

Recently Spirit AeroSystems conducted a head-to-head high load transfer fatigue joint test program comparing new Single Side Installation (SSI) fasteners of the Titanium OSI®, Monogram MLA® and Ergo-Tech® to a baseline of steel Hi-Loks. The fatigue testing of these fasteners was completed to evaluate the fasteners to determine if these fasteners are suitable for structural applications. Fasteners were installed in Aluminum 7075- T7351 and Titanium 6Al- 4V joints using 4.762 mm and 6.350 mm diameter fasteners.

Figure 9.6-26 shows the high load transfer specimen used for this test program. Shown in Figure 9.6-27 is the Ti OSI® fastener. This fastener has high desirability due to its ability to be installed from only one side. While backside inspection is still necessary, the OSI® eliminates the need for a second operator to put the nut on the backside of the bolt like traditional fasteners. The steel version of the OSI® has been used in structure for over a decade with high reliability. OSI's ® are also note for very high pre-load.

In Figure 9.6-28, the Mechani-Lok (MLA®) fastener is shown. Upon installation the tail of the body forms a large blind side upset against the tail side panel surface to mechanically lock the assembly to the structure. Preload is retained because the core bolt is set by torsion, avoiding the recoil of pull-type blind bolts (Reference 1). Figure 9.6-29 shows the Ergo-Tech fastener. This fastener uses a rotating driver that engages a splined pintail. The anti-rotation tool component then self engages the recess pattern on the sleeve head. Rotation of the core bolt starts bulbing of the sleeve, and continued rotation completes bulb formation. Lastly, the pintail is twisted off flush with the sleeve head and discarded (Reference 2).

Fatigue testing was completed with a stress ratio (R) of -0.20 and a max stress of 137.9 MPa for the aluminum specimens. The titanium specimens were tested with a R value of -0.20, and a max stress of 193.1 MPa. Aluminum and titanium specimens were drilled and reamed with a 12.7 μ clearance. Holes were then countersunk, and deburred.

Figure 9.6-30 shows the fatigue analysis for the titanium specimens. The Ti OSI® joints outperformed the other fasteners. The Ergo-Tech® fasteners performed fairly well, and only has a slight knockdown from the steel Hi-Lok fasteners. The Monogram MLA fasteners did not perform well in the titanium joint. Most notably was the MLA's severe knockdown in the 4.762 mm joint size. The Ergo-Tech specimens showed good durability in the comparison to the Hi-Lok and Ti OSI fasteners; however, the 6.350 mm titanium joint specimen showed a slightly lower Relative Fatigue Life (RFL) compared to the baseline Hi Lok specimens.

Figure 9.6-31 shows the fatigue analysis for the aluminum specimens. Ti OSI's outperformed the other fasteners in the 4.762 mm aluminum material, and hit the baseline results in the 6.350 mm thick joint. However, the aluminum specimens with a 6.350 mm diameter fastener had a consistent RFL amongst the different fasteners tested.
The largest disparity in RFL was shown in the smaller diameter fastener and was evident in both the aluminum and titanium joint. The larger diameter fasteners had consistent RFL's in both joint materials. In both tests the Ti OSI's fatigue performance outperformed both the Ergo-Tech and Hi-Lok fasteners, with the 4.762 mm aluminum joint specimen showing the best durability. However, it was decided the combination of the Ergo-Tech fastener's weight savings and fatigue performance met all expectations, and was also suitable to be used on aircraft. The Monogram (MLA ®) performed adequately in both the aluminum joint, and in the larger diameter titanium joint; however, the MLA® fastener performed poorly in the 4.762 mm diameter joint test. The SSI has been a true success, as it has been used in productions now for structural applications for over a decade.

REFERENCES:

[1] New Products: Mechani-Lok™. Monogram Aerospace 2009. http://www.monogramaerospace.com/home
[2] Ergo-Tech. Alcoa. 2007. http://www.alcoa.com/fastening_systems/aerospace/en/pdf/Ergo-Tech_Flyer_5_05.pdf

9.6.12 FATIGUE EVALUATION OF HI-LOK AND SINGLE-SIDE INSTALLED FASTENERS IN ONE-UP ASSEMBLY

Bryan Woods and Mark Ofsthan, Spirit AeroSystems, Inc.

When automated drilling and fastening equipment is used to increase productivity, the step of separating the parts for the removal of burrs at the hole interface or exits is often eliminated. The elimination of this assembly process is called 'One-Up Assembly'. The fatigue performance of Hi-Lok and single-side installed (SSI) fasteners with diameters from 4.762 mm to 9.525 mm in stack-ups of both composite to titanium and composite to aluminum was evaluated. Both the Hi-Lok and SSI fasteners exceeded the baseline fatigue life; however, it was noticed in the specimens that the larger the diameter the lower the relative fatigue life.

When automated drilling and fastening equipment is used to increase productivity, the step of separating the parts for the removal of burrs at the hole interface or exits is often eliminated. Eliminating this step can leave burrs in the assembly thus potentially reducing the fatigue performance of the joint. The elimination of this assembly process is called 'One-Up Assembly'.

Fatigue testing conducted in this test program was comprised solely of double shear joint specimens (Figure 9.6-32). Fasteners were installed by automated drilling and fastening machines; however, to obtain baseline specimens hand installed fasteners were installed in a few specimen groups. Tolerances on the holes were given either 12.7 μ or 50.8 μ clearance, or had a 25.4 μ interference fit. Total thickness of the specimens was 12.7 mm to a total stack-up thickness of 25.4 mm. The 'One-Up Assembly' process was evaluated for both titanium and aluminum specimens. The stress ratio for the titanium specimens was -0.2 and was tested at a frequency of 5 Hz with a maximum stress of 241.3 MPa. The stress ratio for the aluminum specimens was -0.2 and was tested at a frequency of 5 Hz; with a maximum stress of 137.9 MPa.

Two different machines were used for the test. The first machine is a two sided clamping machine and installs 4.762 mm to 7.938 mm diameter Hi-Lok fasteners. The second machine installs 4.762 mm to 7.938 mm diameter Single-Sided Installed (SSI) fasteners. Since the machine only clamps from the outside and is designated to install only SSI fasteners, this can create larger burrs in the assembly and can potentially decrease the fatigue life more than the two sided clamping machine.

Fatigue joint tests resulted in a reduction in the overall fatigue performance as a result of the burrs as compared to fully deburred tension head hi-loks. Figure 9.6-33 shows the titanium assembled specimens. Each group was compared to a predicted fatigue strength to generate factors to account for burrs. All failures occurred in the metal grip plate of the high load transfer specimens. The graphs shown plot each fastener size and the relative fatigue life of each group. Shown in Figure 9.6-34 is the aluminum assembled specimens. The aluminum specimens showed almost no difference between the interference fit and the 50.8 μ clearance specimens.

The trend in the titanium and aluminum data generated on the two sided installation machine generally indicated that the larger diameter fastener a specimen had, the lower the fatigue performance. 6.350 mm diameter fastener specimens easily outperformed the 7.938 mm and 9.525 mm diameter specimens, while the 7.938 mm diameter specimens only showed a slight improvement in fatigue life over the 9.525 mm diameter specimens. In most cases on the two sided installation machine, interference fit holes outperformed clearance fit holes in these fatigue tests. Also, there is no clear trend on whether the 12.7 μ clearance or the 50.8 μ inch clearance specimens had an advantage over the other.

Shown in Figures 9.6-35 and 9.6-36 are the titanium and aluminum specimen results from the single-side installation machine. In general the 50.8 μ clearance specimens outperformed the 12.7 μ specimens, and as noticed in the two sided installation specimens, the smaller diameter fasteners outperformed the larger diameter specimens. It can also be seen comparing the two sided installation results (Figures 9.6-33 and 9.6-34) and the single side installation machine results (Figures 9.6-35 and 9.6-36) that the relative fatigue life is nearly 30% higher in the 6.350 mm specimens. These results are to be expected due to the fact the SSI fasteners leave the burrs in the assembly, lower the fatigue life of the specimen. It should be noted that although the SSI fasteners have lower relative fatigue lives than the Hi-Lok's, the SSI fasteners easily exceeded the required value by nearly 50%.

In conclusion, the two-sided clamping machine specimens (Figures 9.6-33 and 9.6-34) were more robust than the single side installed specimens (Figures 9.6-35 and 9.6-36). Also, it was noticed that the larger diameter specimens had a lower fatigue life than the smaller diameter specimens. Also, in most cases for the two sided installation specimens, the interference holes outperformed clearance holes in the fatigue tests.

9.6.13 EFFECTS OF HOLE MISMATCH ON JOINT DURABILITY

Eric Ekle and Mark Ofsthan, Spirit AeroSystems, Inc.

A typical manufacturing procedure is to stack drill parts, then separate and deburr their hole edges. Alternatively, determinate assembly can be used, in which holes are drilled to full size at the detail level. However, hole misalignment with possible mismatch becomes a concern with determinate assembly. Because of this, a study was performed to evaluate the effect of hole mismatch on the fatigue properties of joints of various materials. Results proved that depending on the materials involved, small mismatches may not have an adverse effect on the fatigue performance of the structure.

Typical manufacturing procedures involve stacking mating parts of a joint for drilling, then de-stacking the parts to deburr hole edges, and finally installing fasteners. The process of separating the parts for deburr costs manufacturing flow time, as does the drilling of pilot holes during detail machining of the individual parts. An alternative process known as determinate assembly is to drill holes to full size during detail machining of each part. This saves vital manufacturing time, but what are the consequences with the alternate process, if any?

The major topic of discussion with determinate assembly is getting the accuracy desired in terms of relative hole position between parts. Modern digital machining systems can be very precise when locating a spot for hole drilling, but inevitably there will be some amount of mismatch based on the hole tolerance. Spirit AeroSystems, Inc. performed a fatigue test program to evaluate the effects of mismatch on structural joints made from aluminium, titanium, and steel. Static properties of a joint would be minutely affected with mating holes that are mismatched, but the durability of the joint is subject to concern. Because of this, extensive fatigue testing was performed to quantify the relationship of measured hole mismatch to reduction in fatigue life.

Results from Research & Development studies showed a high confidence that CNC machines could provide .076 mm or less of mismatch between mating holes. High load transfer joints with this amount of mismatch were fabricated. Several baseline specimens with no mismatch were made; other specimens had either .076 mm of mismatch in the loading direction or transverse to the loading direction. Also, a group of specimens was made in which there was combined mismatch (both in the loading and in the transverse direction). See Figure 9.6-37 for an illustration of the mismatch.

After part fabrication, the amount of hole mismatch was confirmed by using tooling pins. Fasteners were installed in all holes except 2 & 4, then if a pin .075 mm smaller than the fastener in diameter could fit in holes 2 and 4 but a pin .076 mm smaller would not, it was known that there was .076 mm of mismatch between the grip and splice parts.

Three materials were tested in this evaluation: a 2219-T851 aluminium alloy plate, Ti-6Al-4V alloy plate, and 15-5PH corrosion resistant steel plate. All specimens in this study were tested at a high stress level at constant amplitude with a negative stress ratio. Specimens were tested to complete fracture of a part.

Tests results showed no decrease in relative fatigue life for any material tested when the mismatch was only in the direction transverse to loading (Y) or with combined X+Y direction mismatch. For the aluminium alloy tested, no fatigue degradation was observed for .076 mm mismatch in any direction. However, relative fatigue life was reduced in titanium alloy and steel with .076 mm mismatch in the loading (X) direction. Figure 9.6-38 gives the relationship between mismatch, hole fit, and relative fatigue life.

The fatigue tests indicate that determinate assembly can be performed without degrading the fatigue quality of the structural detail. However, the process must be proven to be reliable (accurate location of holes to limit mismatch, repeatable (consistent from part to part), and stable (qualified with a good hole drilling process).

9.6.14 THE FATIGUE EFFECT OF SHALLOW LASER DAMAGE IN THIN ALUMINUM SHEET

Rob Chase and Mark Ofsthan, Spirit AeroSystems, Inc.

Laser scribe line damage was found on aluminium airplane skin in the context of a maskant removal operation before chemically milling the skin. Similar laser scribe damage was imprinted into the surface of open hole and Kt specimens and later a skin panel to find out if there was a fatigue life reduction. No statistically significant effect was found by laser scribe line damage to a depth of 0.0051 mm.

Scribe lines or scratches in metallic structure can cause local stress risers resulting in a shortened fatigue life. Scribe damage such as is shown in Figure 9.6-39 is notorious for degenerating fatigue performance. For a number of years it was thought that as long as scratches did not penetrate the clad layer, in thin clad aluminum, that there would not be an adverse effect on fatigue. However, this is not always the case. Scratches that were shallower then the clad layer have been observed in coupons, full scale tests and fleet fatigue cracks. At some point scribe line damage can be shallow enough that any reduction in fatigue performance is negligible.

In the context of chemically milling aluminum airplane skin to save weight, maskant is used to cover regions of the skin where a reduction in thickness is undesirable. Once the maskant is applied to the skin, Spirit AeroSystems uses a laser to cut the maskant in areas on the skin where cutouts are required to form chemically milled pockets. Then the maskant is removed. Within this process, laser damage was observed on the skin after the maskant cutout was removed. Accompanying the laser damage was a heat affected zone of unknown thickness.

To establish if a statistically significant fatigue knockdown existed, Kt and open hole fatigue specimens of clad sheet material similar to the production skin were blanked out etched by the laser and then finished and fatigue tested (See Figure 9.6-40). After this phase was completed, panels in production were observed to have deeper laser scribe lines. Consequently, Kt specimens were fabricated from a production skin panel that reflected this greater scribe line depth. The results of the phase 1 and phase 2 testing along with non-etched specimens from the same sheet of material and production skin are shown in Figure 9.6-41.

The Kt and open hole results clearly indicate in head to head testing (laser scribe damaged versus non-damaged) that the amount of degradation to the sheet from a 0.0051 mm deep laser scribe is insignificant. The specimens taken from the production skin had a similar result in that the laser scribe damage specimens were statically insignificant.

Crack origins were identified on the specimens and there was no clear interaction between the laser damage and the crack origin. Cracks in Figure 9.6-42, started too far from the scribe line to be attributed to the laser damage. Cracks in Figure 9.6-43, started near the scribe and are close enough they may have been caused by the laser scribe line. However, the fatigue tests did not result in fatigue life reduction as a result of the laser scribe damage.

No statistically significant effect was found by laser scribe line damage to a depth of 0.0051 mm. This conclusion was considred valid for 1.016 mm thick clad two-thousand seris aluminum.

9.6.15 THREE-DIMENSIONAL FINITE-ELEMENT ANALYSES OF COLD-WORKED AND REAMED HOLES

James Newman, Jr. and Steve Daniewicz, Mississippi State University

Cold-working (CW) fastener holes in aluminum and titanium alloys is a widely used technique in the aerospace industry for improving the fatigue performance of structures. The compressive hoop stress introduced in the material during the CW process reduces the natural tendency of the material to crack at the holes under cyclic tensile loading. One of the objectives of the FAA-sponsored work is to calculate the cold-working residual stresses during a typical CW and reaming process to compare with measurements and to be used in fatigue-crack-growth analyses.

Three-dimensional (3D), elastic-plastic, finite-element analyses of the cold working and reaming process were performed with ANSYS on a rectangular plate made of 7075-T6 aluminum alloy with a central hole, which simulated specimens that will be tested later in the FAA program. The interference amount was 3%, since this was the amount used to cold work the specimens prepared at Sikorsky Aircraft. The split in the sleeve was aligned at the 12 o'clock position. The cold-work simulation was performed by pulling a tapered rigid mandrel through the hole with the split sleeve. Frictionless conditions were assumed between the mandrel and the sleeve, since this had no effect on the final residual stress solution. But the friction coefficient (μ) at the sleeve-hole interface was set to 0.2. The hoop residual stress contours after the cold-work simulation is shown in Figure 9.6-44a. The reaming process was simulated by deactivating layers of elements at the hole surface to match the reaming diameter and these results are shown in Figure 9.6-44b.

Because of symmetry, only half of the plate was modeled. Two different external boundary conditions were considered in this analysis. In Case (a), the plate was constrained in the out-of-plane direction (mandrel movement direction) at all outer edges, while in Case (b), only the top and bottom edges of the plate was constrained. Case (b) should be the best representation of the boundary conditions applied during the cold expansion of the specimens at Sikorsky. On the other hand, Case (a) may correspond more closely to the constraints of a real (large) structure.

Figure 9.6-45 shows the tangential (or hoop) residual stresses produced from cold-work and reaming simulations for Case (b). The residual stresses vary through the plate thickness as well as around the circumference of the hole. Normalized hoop residual stress curves ($\sigma_{\theta\theta}/Y$) are plotted against the normalized distance from the hole center (x/r) at the entrance, mid-plane, and exit faces of the plate. It was observed that the residual-stress magnitudes prior to reaming had large variations between these two cases (a and b) with a maximum of 20% difference at the hole edge of the entrance face. Results after reaming, however, do not have as much variations; the largest difference between the results from Case (a) and (b) at the plate entrance face was about 5%. In practice, if cracking does occur at the CW and reamed hole, the entrance face would be the most likely location because of the slight reduction in the compressive residual stresses.

9.7 PROGNOSTICS & RISK ANALYSIS

9.7.1 PROBABILITY OF FRACTURE NOMOGRAPHS FOR QUICK RISK ASSESSMENTS

Eric Tuegel, Air Force Research Laboratory

Structural integrity engineers need to rapidly determine the probability of fracture for cracked structural details to support fleet maintenance decisions. The current paradigm in which the probability of fracture is calculated on a case-by-case basis does not facilitate the rapid decisions needed to support flight operations. Probability distributions for the major parameters are seldom on hand, nor is the data necessary to develop these distributions. The expertise to calculate the probability of fracture might also need to be developed.

A new paradigm for determining the probability of fracture that enables faster decisions is demonstrated for stiffened panels. The probability of fracture as a function of crack size for a range of stiffened panel geometries under a particular loading distribution is presented in a nomograph. Using the nomograph, a stiffened panel can be designed to a specified probability of fracture for a given crack size, e.g., a 2-bay crack, or the probability of fracture assessed for a cracked panel in service (Figure 9.7-1a-b). The nomograph is broadly applicable because it is developed using normalized loading and fracture toughness distributions, and the stress intensity factors for a stiffened panel are functions of ratios of geometric parameters (Figure 9.7-2a). The nomograph, or a series of nomographs for different loadings, can be constructed by experts in probabilistic analysis prior to any need to calculate the probability of fracture (Figure 9.7-2b). Later, a structural integrity engineer can rapidly determine the probability of fracture of a cracked stiffened panel using the appropriate nomograph (Figure 9.7-3). Many aerospace and naval structures are made of stiffened panels making this procedure widely applicable.

9.8 LIFE ENHANCEMENT CONCEPTS

9.8.1 EXPERIMENTALLY DERIVED BETA (β) CORRECTIONS TO PREDICT/MODEL THE FATIGUE CRACK GROWTH BEHAVIOR AT COLD EXPANDED HOLES IN 2024 AND 7075 ALUMINUM ALLOYS

Scott Carlson and Robert Pilarczykm, U.S. Air Force

Fastener holes represent one of the most common fatigue details found in airframe structures. In order to minimize the impact fastener holes have on the fatigue behavior of critical aircraft components, many are processed by cold expansion. Cold expansion imposes a residual compressive stress field around a hole that retards fatigue crack growth and increases the fatigue life of the processed component.

The purpose of this research was to determine the feasibility of using a fracture mechanics based beta (β) correction to modify the standard fatigue crack growth model to more closely match the fatigue crack growth characteristics through the three-dimensional stress field caused by the cold expansion process. This method would provide an analytical approach that could be used by sustainment engineers to more accurately calculate the fatigue life at cold expanded holes in aircraft structures.

Fatigue testing was performed on two aerospace grade aluminum alloys, 2024-T351 and 7075-T651 to determine the effects of the cold expansion process on the fatigue crack growth behavior of the material. Marker banding was used to develop an accurate map of the fatigue crack front shape as it progressed through the material. Finite element analysis was used to calculate accurate stress intensities (K_I) for the given geometry, loading and crack front shape observed during testing. This method is shown in Figure 9.8-1.

With the stress intensity (K_I) known for both the baseline non cold expanded and cold expanded configuration it was possible to calculate the β correction which represented the effect of the cold expansion process on the fatigue crack growth characteristics. The fracture mechanics based similitude principle was used to calculate the residual stress β correction. The similitude principle states that if two specimens are geometrically identical and manufactured from the same material then at the same crack growth rate or da/dN the same ΔK should be seen in both specimens. If there was a difference in the ΔK seen between the cold expanded and non cold expanded specimens then this difference would be directly related to the residual stress state imposed on the material due to the cold expansion process. To calculate the scalar β correction it was required to plot the da/dN versus ΔK characteristics for both cold and non cold expanded configurations and then ratio the ΔK for both configurations. This would provide a scalar number which could be used as a β correction to modify the analytical model from the non cold expanded prediction to the cold expanded prediction. From this method each β correction would be a function of a specific crack length. Figure 9.8-2 is a plot of β correction versus crack length for both the 2024 and 7075 alloys.

From this plot it is shown that at its maximum impact the residual stress field from the cold expansion process reduces the crack driving force by approximately 80%. It can also be seen that in general both the 2024 and the 7075 alloys have similar shapes, peaks and valley in their curves. Also contained within this plot are specimens that were tested at various stresses. The specimens tested at these different stresses also show very similar trends. This data may provide insight into a new understanding of materials that have been cold expanded. It is possible that the effects of cold expansion are somewhat independent of material and far field stress. This could have a significant impact on how the effects of residual stresses are modeled in the future and the method used to account for them.

9.8.2 EFFECTS OF BARE STEEL FASTENERS IN INTERFERENCE FIT TITANIUM HOLES

Eric Ekle and Mark Ofsthun, Spirit AeroSystems, Inc.

In order to provide a lightning strike current return path on commercial aircraft, uncoated steel fasteners may be required in composite-to-metal joints. Some of these holes may result in interference fit holes in titanium parts. A concern arose about the effect of galling or fretting that may occur with these fastener installations. Tests were performed which compared these fastener installations to coated fastener installation in interference fit, as well as to bare fasteners in clearance fit. Larger diameter fasteners seemed to have a significant reduction in fatigue life for uncoated fasteners in interference fit, while smaller diameters did not show a significant effect on fatigue life.

Because of the need for an electro-mechanical path on a commercial fleet, uncoated steel fasteners were installed in titanium in interference fit holes. This raised concern about whether galling may occur, and an evaluation was completed to quantify the effect on joint properties.

The first study in this evaluation was an installation test to determine the difficulty of installing uncoated versus coated fasteners. Fastener installations were performed under four different conditions. Bare steel solid shank fasteners were installed in .0005 inch (.013 mm) interference fit and .0015 inch (.038 mm) interference fit holes. Also, aluminum pigment coated titanium fasteners were installed in the same two hole fits. Figure 9.8-3 shows the results of the installation test. All fasteners were pushed in with a 50 kip (220 kN) static testing machine so the installation force could be measured. In both hole fits, the force used to install the bare fasteners was much greater in magnitude than the force required to install the coated fasteners. This suggested there would be a much higher possibility of galling with the uncoated fasteners in interference holes than the coated fasteners, so it was decided to perform fatigue testing on the bare fasteners.

In the second study in this evaluation, three diameters of fasteners were tested in high-load transfer joints, with stack-ups of approximately 3 times the fastener diameter. Baseline specimens of coated fasteners in interference fit holes were tested against specimens with bare fasteners in interference fit. Also, specimens with bare fasteners in clearance fit were tested. Figure 9.8-4 shows the results of this fatigue testing. From the first 4 columns on the graph, it can be seen that there is no specific trend of bare fastener specimens performing better or worse than the coated fastener specimens, for diameters at or below 6.4 mm (1/4 in.). However, for the larger diameter tested (7.9 mm or 5/16 inch), results show that there was a significant reduction in life for bare fasteners in interference fit holes as compared to coated fasteners in interference fit holes. Another discovery of interest was that for the larger diameter bare fasteners, the interference fit specimens performed with a typical fatigue life much worse than the bare fastener clearance fit specimens. This was surprising for the fact that interference fit specimens usually perform better than clearance specimens because the hole fill results in extra rigidity of the joint. To further investigate the trend in data, a metallurgical lab evaluation was performed on the 5/16 inch (7.9 mm) diameter specimens. This evaluation was inconclusive as both the bare fastener interference fit specimens and the coated interference specimens had galling inside the fastener holes. However, the study showed that for the larger diameter fasteners, coated fasteners give a definite benefit to joint durability.

In conclusion, there is a galling threshold at which fatigue performance of joints will be significantly decreased. To optimize fatigue performance, larger fasteners (≥5/16 inch or 7.9 mm diameter) should be installed with clearance fit when using uncoated fasteners.

9.8.3 FATIGUE-CRACK CLOSURE UNDER HIGH STRESS RATIO (R) CONDITIONS

James Newman, Jr., Mississippi State University

In the past, the crack-closure concept has not been able to correlate fatigue-crack-growth (FCG) rate data in the threshold regime, either from load-reduction tests at constant R or constant K_{max} tests. Variations in the threshold and near-threshold behavior with stress ratio cannot be explained from plasticity-induced crack closure (PICC) alone, but roughness-induced crack closure (RICC) and/or debris-induced crack closure (DICC) mechanisms may be needed. The constant K_{max} test procedure also produces what has been referred to as the "K_{max} effect", in that, lower thresholds are obtained using higher K_{max} values. One advantage of the K_{max} test method is that it is commonly considered to produce crack-closure-free data ($R \geq 0.7$).

To generate constant R data in the threshold and near-threshold regimes, ASTM E-647 proposes the load-reduction (LR) test method. But the ASTM LR method has been shown to produce higher thresholds and lower rates in the near-threshold regime than constant-amplitude (CA) data on a wide variety of materials. Thus, the ASTM LR test method does not, in general, produce constant-amplitude data. In order to produce steady-state CA data, compression pre-cracking (CP) methods have been proposed in the literature. One of the methods is called compression pre-cracking constant-amplitude (CPCA) threshold testing. Another method is to grow the crack at a low ΔK value, after CP loading, and then use the standard LR test method. CP allows the initial ΔK value or rate, before load reduction, to be much lower than would be needed or allowed (1.0E-8 m/cycle) in the ASTM standard LR test method. This method is called the compression pre-cracking load-reduction (CPLR) threshold test method and was used herein. (The development of the CP threshold test methods and testing on a variety of materials were conducted under FAA- and ONR-sponsored research.)

FCG tests were conducted on compact C(T) specimens made of a 2324-T39 aluminum alloy to study the behavior over a wide range in stress ratios ($0.1 \leq R \leq 0.9$) and a constant K_{max} test condition from threshold to near fracture conditions. During the tests at load ratios of 0.1, 0.7, and 0.9, strain gages were placed near and ahead of the crack tip to measure crack-opening loads from local load-strain records during crack growth. In addition, a back-face strain (BFS) gage was also used to monitor crack lengths and to measure remote load-strain records during the same test. Based on the load-strain measurements (BFS and local), crack-opening loads were determined and crack-closure-free FCG data, ΔK_{eff}, were calculated and compared.

Comparisons have been made between crack-opening loads determined from both the local and remote strain gages. Elber's reduced-displacement (or strain) method was used in all cases. For R = 0.1, the local and remote gages produced essentially the same crack-opening loads, but the local values were slightly higher than those from the remote gage. However, for high R (0.7, 0.9 and K_{max}) tests, the remote gage gave no indication of crack closure, but the local gage produced consistent indications of crack closure. Typical crack-opening load evaluations for the K_{max} test are shown in Figure 9.8-5. The shape knees (opening-load values) were located by inspection.

Figure 9.8-6 shows the ΔK against rate data (open symbols) generated at R = 0.1, 0.7, 0.9 and the K_{max} test. The CPLR test method was used and, after CP, the LR procedure was applied at rates from 1 to 2.5E-9 m/cycle for R = 0.9 to 0.1, respectively. After reaching threshold conditions, CA loading was applied to generate the upper portions of the rate curves. The solid symbols show the ΔK_{eff} against rate relation determined from the measured crack-opening load values. The data fell into fairly narrow bounds from threshold to the upper plateau region. Thus, high R and K_{max} test may not be crack-closure free as suspected from the vast amount of results from the literature. The 2324-T39 alloy produces a very rough crack surface and, thus, all three major crack-shielding mechanisms (plasticity, roughness and fretting-debris) may be active in the threshold regime. Further study is needed on other materials to see if high R closure exists.

9.9 REPAIR CONCEPTS

9.9.1 DURABILITY AND DAMAGE TOLERANCE OF BONDED REPAIRS TO METALLIC FUSELAGE STRUCTURE

John Bakuckas, Federal Aviation Administration and Keith McIver, The Boeing Company, Phantom Works

Adhesive bonding technology, using composite and metallic patches, offers an efficient and cost-effective approach to airplane structural repairs. Compared to conventional, mechanically fastened metallic repairs, bonded repairs have no stress concentrations due to holes, are less damaging to the parent material since no drilling or machining are required, and are more aerodynamically and structurally efficient. The application of bonded repairs has been studied primarily in the military sector where durability and damage tolerance aspects have been demonstrated. However, several technical challenges need to be addressed before bonded repair technology will be generally accepted and implemented in both military and commercial primary structural applications. Currently, credit is typically not provided in certification programs of bonded repairs for slowing crack growth or restoring residual strength. Of primary concern is the ability to predict the fatigue behavior and ensuring the durability of bonded repairs.

In an effort to gain a better understanding of the durability and damage tolerance aspects of bonded repair technology, the Federal Aviation Administration (FAA) and The Boeing Company partnered in a 3-year Cooperative Research and Development Agreement in October 2007. A phased approach is being undertaken where the initial study will focus on the test and analysis of bonded repairs on a B727 fuselage structure using the FAA Full-Scale Aircraft Structural Test Evaluation and Research facility. The program objectives are to characterize the long-term durability of bonded repairs under simulated flight load conditions up to one typical design service goal and then determine if the repair patches meet damage tolerance requirements in a residual strength test.

In the initial phase, bonded repairs to two damage scenarios are being considered, namely, a mid-bay through-the-thickness crack (fatigue presharpened) and a lap joint scribe, as shown in Figure 9.9-1a. Both boron/epoxy, Figure 9.9-1b, and aluminum patches, Figure 9.9-1c, were used to repair this damage.

Methods used to monitor for damage development are illustrated in Figure 9.9-2a-d. A digital image correlation (DIC) method is being used to obtain full-field displacement and strain measurements at the patch regions, Figure 9.9-2b and 9.9-2c. The acoustic emission (AE) method is being used to monitor for damage growth in real time and serve as an early warning for imminent failure, Figure 9.9-2c. Several nondestructive inspection (NDI) methods are being used, including flash thermography and computer-aided tap techniques to scan for patch disbonds and eddy current to monitor crack growth, Figure 9.9-2d.

Results to date are summarized in Figure 9.9-3a-c for the repairs subjected to 40,000 cycles. There were no indications of damage development in the form of crack growth or disbonding for the lap joint scribe line repair patches. Although no patch disbonding was observed, slow crack growth was measured under the mid-bay boron/epoxy patch, Figure 9.9-3a. A detailed finite element analysis (FEA) revealed that the patch installation resulted in eccentric loading and inward deformation of the mid-bay region, Figure 9.9-3b. As shown in Figure 9.9-3c, this resulted in higher tensile stresses on the inner skin surface and compressive stresses on the outer skin surface. The tensile stresses at the skin inner surface were high enough to cause the observed slow crack growth.

This study will be provided data to validate analytical predictions of bonded repair patch durability and residual strength, an assessment of several NDI methods in detecting disbonds and fatigue cracks, and lessons learned that will help identify safety and structural integrity issues of bonded repairs.

9.9.2 FULL SCALE TESTING OF A WELD REPAIRED ROTOCRAFT BLADE SECTION

Justin W. Rausch, Yi Lai Xu and Scott A . Fawaz, United States Air Force Academy (CAStLE)

The objective of this test program is to design a full scale test article complete with grips to evaluate the welded repair of a main rotor beam (MRB) for a heavy lift helicopter. With small production runs some of the more specialized aircraft can have a high cost of maintenance. A fatigue issue developed while in service between two countersunk attach points. Since the production run is small, fabricating more spares is cost prohibited for such a small and specialized fleet. Since the local loads in the beam are low a welded repair is desired by the manufacturer. While a repair is possible, a full scale article must be tested in order to comply with regulations for repair certification. A few challenges needed to be overcome in order to achieve a successful test. One hurdle was the actual geometry of the test article itself. Contoured shapes of actual flight structure are harder to grip and induce load into than the idealized testing of coupons. The MRB in this testing is no exception. The D-shaped cross-section makes it difficult to tie the specimen into the hydraulic test frame for proper loading. Second the existing attachment holes in the rotor beam are located such that they interfere with the placement of the holes by which the specimen is gripped and subsequently loaded. These holes then required that fewer than the optimal number of holes required for load introduction be used. The solution was to design a fixture that would generate enough clamping force around these bolt holes on the rotor beam to reduce the bearing load and prevent fatigue from initiating where the load is introduced into the specimen (Figure 9.9-4). This design challenge coupled with the high number of cycles (on the order of 10^7) the test article could endure makes this a challenging problem. There are two parts to the testing of the MRB (Figure 9.9-5). Part one is creating an S-N curve for the validation of the repair. A second part is to gather crack growth data for the repair if a crack does grow. Testing for these cases will consist of constant amplitude tensile as well as compressive loading for the S-N testing, and then a change to spectrum loading based on mission profiles for crack growth testing. The bending experienced during flight was taken into account with the magnitude of the axial loading and will not be replicated during testing. Instrumentation of the MRB was required to verify proper loading. This instrumentation consisted of strain gages and crack propagation gages. Since one of the goals of the program is to conduct a fatigue crack growth test, crack length gages will be used as a failsafe to catch any cracks that might jeopardize the second part of the testing. AFGROW fatigue crack growth software was also used as a tool to help predict specimen life as it pertains to the determination of inspection intervals.

9.9.3 SURVEY OF REPAIRS, ALTERATIONS AND MODIFICATIONS FOR WIDESPREAD FATIGUE DAMAGE

John Bakuckas and Walter Sippel, FAA ; and Mike Bode, Sandia National Laboratories

Structural fatigue has long been recognized as a significant threat to the continued airworthiness of airplanes. This is because even small fatigue cracks can significantly reduce the strength of airplane structure. A phenomenon referred to as widespread fatigue damage (WFD) is identified as a severe degraded condition that threatens the continued airworthiness of airplanes, is theoretically inevitable, and will be reached at some point in the life of a structure. The Federal Aviation Administration (FAA) has defined WFD as the simultaneous presence of cracks at multiple structural locations that are of sufficient size and density such that the structure will no longer maintain its residual strength.

A major concern of WFD is that fatigue cracks are initially so small they cannot be reliably detected with existing inspection methods. The small undetectable cracks then “link up” and grow together. This growth may be very rapid and may result in catastrophic structural failure of an airplane. To address this safety concern, the FAA issued a Notice of Proposed Rulemaking (NPRM) on WFD in April 2006. The WFD NPRM proposed that design approval holders establish for certain transport category airplanes the period of time for which it is demonstrated that the maintenance program is sufficient to preclude WFD in baseline airplane structure as well as in certain repairs, alterations, and modifications (RAMs). Comments to the NPRM suggested that inclusion of RAMs in WFD assessments should be deferred until additional information is gathered. Although there is a technical possibility that certain RAMs may pose a risk of developing WFD, there are no recorded accidents attributed to WFD occurring in properly designed and installed RAMs. Based on this, the FAA determined that there is a lower risk of WFD occurring in RAMs compared to baseline structure. In addition, there are limited resources in terms of manpower, funding, and knowledge to undertake assessments to meet the requirements. Another factor is RAM structure that may be susceptible to WFD may be limited to only one airplane or a few airplanes, whereas baseline structure typically exists on each airplane. For these reasons, the FAA determined that the focus should be on establishing the period of time for which it is demonstrated that the maintenance program is sufficient to preclude WFD in baseline airplane structure.

In taking a proactive role, the FAA teamed with Sandia National Laboratories in December 2007 in a two-year effort to further assess the need for addressing RAMs for WFD. The goal of this effort is to provide data to gain a better understanding of the risks that RAMs may pose for developing WFD and to help determine whether further rulemaking is necessary for RAMs. Existing data in the form of airworthiness directives and the Service Difficulty Database are being examined for trends that may indicate WFD occurrence in RAMs. Over 420,000 records have been screened, with a large subset of those being selected for further trend analysis. Surveys are being conducted on retired airplanes at aircraft salvage locations and on in-service airplanes at the operator's heavy maintenance locations. Additionally, RAM specimens from retired airplanes are being acquired and in-depth teardown inspections performed to look for the presence of damage indicative of WFD. The end product of this effort will be an engineering database that the FAA will use to help it determine whether further rulemaking on RAMs is necessary.

To date, this project has performed surveys on 17 retired airplanes at aircraft salvage locations and approximately 15 high-time, in-service airplanes at base maintenance locations. Figure 9.9-6a-c shows examples of models and operators from a broad cross section of the industry.

Several RAMs are being removed from retired, high-time airplanes with documented maintenance records for more in-depth teardown and damage characterization studies. As shown in Figure 9.9-7a-d, an established procedure is used to determine the structural condition of the RAMs. First, the RAMs are cataloged, Figure 9.9-7a, then a variety of nondestructive inspection (NDI) methods are used while the structure is intact to inspect for cracks. The structure is then disassembled by removing the fasteners, and layers are separated and cleaned, Figure 9.9-7c. Bolt hole eddy current is used to inspect for cracked holes, and any damage that is found is characterized to document crack sizes, shapes, and distributions, Figure 9.9-7d.

The data collected from this survey includes a matrix of information designed to provide quantitative information on the numbers, locations, condition, and engineering background of each RAM. A database of this information is being compiled with the intent of providing a rapid query capability to end users at the FAA to help identify trends that may indicate the occurrence of WFD associated with RAMs. Major expected outcomes from data generated and compiled in this study include:

- Number of RAMs per airplane
- Size(s) of RAMs
- Age of RAMs relative to design service goal
- Location of RAMs (relative to fatigue sensitivity)
- Source of RAM data (Structural Repair Manual, Designated Engineering Representative, or Engineering Completion Order)
- Reason for each RAM (i.e., the causal factor)
- Subsequent damage (especially fatigue cracking)

9.9.4 C-141 BONDED BORON PATCH REPAIR EVALUATION

Lawrence M. Butkus, James A. Gaskin, James M. Greer, Jr., Cornelis B. Guijt, Nicholas J. Jacobs, David F. Kelly and James J. Mazza, United States Air Force ; and Jui T. Huang, Surendra R. Shah, Donald J. Shelton and H. Lewis Zion, Lockheed Martin Aeronautics Company

A comprehensive evaluation was performed on the residual strength of service-aged boron/epoxy bonded repairs to the C-141 aircraft. The evaluation included 1) Nondestructive evaluation (NDE) of bonded boron patch repairs obtained from retired C-141 aircraft at the Aerospace Maintenance and Regeneration Center (AMARC), 2) a limited comparison of these NDE records to initial installation NDE records (generated at the time of repair), 3) selection of bonded repairs to be cut from the retired aircraft, 4) follow-on laboratory NDE of cutout repairs, 5) preparation of test specimens from cutout repairs, 6) preparation of test specimens from cutout sections to be tested without repairs, 7) bonding of new repairs to cutout sections that do not currently have bonded repairs, 8) preparation of test specimens from cutout sections with newly installed repairs, 9) prediction of test failure loads (residual strengths), 10) residual strength testing of all types of specimens, 11) analysis of test results, 12) success criterion for the residual strength testing, and 13) development of new USAF Aircraft Structural Integrity Program (ASIP) guidance regarding bonded repairs. The overarching goal of the effort outlined above was to provide information that would enable USAF engineering authorities (ASC/EN and the individual aircraft engineering offices) to have the confidence in adhesively bonded repair technology necessary to use this repair approach, when and where appropriate. Specifically, based on the results of this test program, it is expected that a change will be made to the current USAF approach to inspecting repaired safety-of-flight-critical components as if no bonded repair were present. In other words, it is desired to have engineering authorities allow "credit" for properly designed and applied bonded repairs rather than requiring repaired structures to be fail-safe without the presence of the bonded repair. It is anticipated that such a change will permit future inspection intervals for bonded repairs to be extended.

To achieve this goal, the subject program evaluated the effectiveness and long-term durability of bonded repairs applied to USAF C-141 aircraft during the 1990s. This program included efforts to validate the design, analysis, materials, processes, nondestructive evaluation techniques, and related items associated with bonded composite repairs applied to the C-141 aircraft, primarily to address residual strength. Practices that led to long-term durable repairs were identified. Shortcomings or requirements for further research were also highlighted. The effort was comprehensively reported [1-3]. (Figures 9.9-8 and 9.9-9)

REFERENCES:

[1] L.M. Butkus, J.A. Gaskin, J.M. Greer, C.B. Guijt, N.J. Jacobs, D.F. Kelly, J.J. Mazza, J.T. Huang, S.R. Shah, D.J. Shelton and H.L. Zion, "Bonded Boron Patch Repair Evaluation: Final Report," U.S. Air Force Academy, Technical Report USAFA-TR-2007-06, May 2007.

[2] N.J. Jacobs, "Quick Reaction Evaluation of Materials and Processes, Delivery Order 0010: Bonded Boron Patch Repair Evaluation," University of Dayton Research Institute, Dayton, OH, Technical Report AFRL-ML-WP-TR-2007-4145, September 2006.

[3] C.B. Guijt, "The Effects of In-Service Conditions and Aging on the Fatigue Performance of Bonded Composite Repairs," Center for Aircraft Structural Life Extension, United States Air Force Academy, Technical Report USAFA-TR-2007-07, May 2007

9.10 REPLACEMENT CONCEPTS

9.10.1 RESIDUAL STRESS EFFECTS IN AIRCRAFT STRUCTURAL DESIGN

Dale Ball, Lockheed Martin Aeronautics Company

The increasing utilization of advanced materials and structural concepts in aircraft design is generating the need for new design tools capable of formally addressing complex material behavior, complex geometry, and the presence of inherent, process induced residual stresses in localized, but critical areas. One example of this circumstance is the unitization of lugs and fittings with primary bulkheads in order to reduce part count and to alleviate the necessity for large numbers of fasteners and the associated hole preparation/mating requirements (Figure 9.10-1). Such unitization can be achieved through the use of large forgings, which experience has shown, may have significant residual stresses in localized areas, even after final machining. Since flight certification generally requires that primary and/or flight critical structural elements meet damage tolerance requirements (among others), the residual strength and fatigue crack growth analysis tools used to generate design allowable stresses for these parts must address the complexities cited above.

In this paper, we describe current research directed toward the formal inclusion of residual stress effects in the design of aircraft primary structure. This effort has four focus areas. The first is the extraction of confounding residual stress effects during the characterization of the fundamental fatigue crack growth rate behavior of a critical aluminum alloy (Figure 9.10-2). The second is the quantification, both by analysis and by test, of the location, spatial magnitude and stress magnitude of the residual stress fields in a candidate forged/machined part (Figure 9.10-3). The third is the development of improved fatigue crack growth analysis methods which selectively account for the presence of residual stresses (Figure 9.10-4). And the fourth is the development of a new design analysis approach (Figure 9.10-5). Each of the first three focus areas provides a critical ingredient to the proposed design analysis method in which components are analyzed using intrinsic (residual stress free) material data with residual stresses then explicitly introduced only in those areas where they are expected to exist. The discussion includes the results of a trade study on a critical bulkhead showing potential optimization, both in terms of weight savings in over-designed areas, and service life/damage tolerance enhancement in under-designed areas.

9.10.2 STRUCTURAL EVALUATION OF 7050-T7452 FORGING FROM 7050-T7451 PLATE

Mark Ofsthun and Kelby Umbehr, Spirit Aerosystems, Inc.

A production method was needed to fabricate a monolithic door surround fixture. 7050-T7451 plate was hot formed to a certain fuselage curvature; heat treated, and was to meet the specifications of 7050-T7452 hand forging properties. The tests included static, fatigue, and damage tolerance testing.

Monolithic design is used to reduce the part count, fabrication flow time, and costs of manufacturing structure. The topic of this study was in lieu of building up door surround structure for a commercial airplane, a monolithic design was considered. This new design would involve high temperature forming of a plate to the required curvature, then heat treat and machining of the part. The part machined out of a plate without forming would have needed to have been 15” (381mm) thick, which is not available. Alternatively, using a die forging was not considered because of the time flow to get parts to production.

Therefore 7050-T7451 3-inch (76.2mm) plate was hot formed to meet the required fuselage curvature of a 5ft radius (1.52m) and was to meet the specifications of 7050-T7452 hand forging. Forging from plate is not disallowed per any forging specification but the process is new to Spirit AeroSystems. This hot forming is similar to a die forging, which typically have larger residual stresses than hand forgings and plates. These residual stresses tend to lead to a decrease in fatigue and crack growth properties. Testing was conducted on this hot forming process and this paper describes the results. The static, fatigue, and crack growth results are shown in this document.

Figure 9.10-6 shows the final fixture used. Before the 7050-T7451 plate was formed and fabricated, a small section was removed and was used as the baseline. The main portion of the plate was hot formed to a certain curvature. A small section was removed from the hot formed plate to be used to obtain test specimens. These hot formed specimens were fabricated from the prolong, as identified in Figure 9.10-6.

The test static results for the 7050 forging made from 7050-T7451 plate revealed a slight drop off in tension yield properties when comparing the 7050 forged plate to the 7050-T7451 baseline plate. The forged plate had slightly higher properties in tension ultimate, compression yield, shear ultimate, and bearing ultimate than the baseline plate. When the tested 7050 forged plate was compared to the 7050-T7452 allowables, the 7050 forged plate was found to have equivalent or better allowables in tension, compression, shear, and bearing. Thus the published 7050-T7452 allowables may be conservatively used for this process. The typical comparisons are shown in Figure 9.10-7.

The fatigue test results are shown in Figures 9.10-8 and 9.10-9. As can be seen, the 7050 forged plate specimens have equal or higher characteristic lives than the baseline 7050-T7451 plate specimens. The fatigue properties of the forged plate clearly outperformed the baseline 7050-T7451 plate properties in the L direction. This is rare, as the forming process normally causes a decrease in fatigue life due to the larger grain size.

Figure 9.10-10 shows the crack growth results for the baseline and hot formed specimens in the L-T direction. As can be seen, there is no significant difference in crack growth between any of the specimens. Crack growth rate seems to have been unaffected from the hot forming process in the L-T and the T-L directions.

Most of the data from the 7050-T7451 hot formed plate was equal to or exceeded the values of 7050-T7452 hand forging. The hot forming process done to the 7050-T7451 plate seemed to have had a positive impact on the fatigue properties without decreasing the crack growth or static properties. For these reasons, 7050-T7451, using the hot forming process done to the plate, could be engineered using 7050-T7452 allowables.

9.11 FIGURES/TABLES

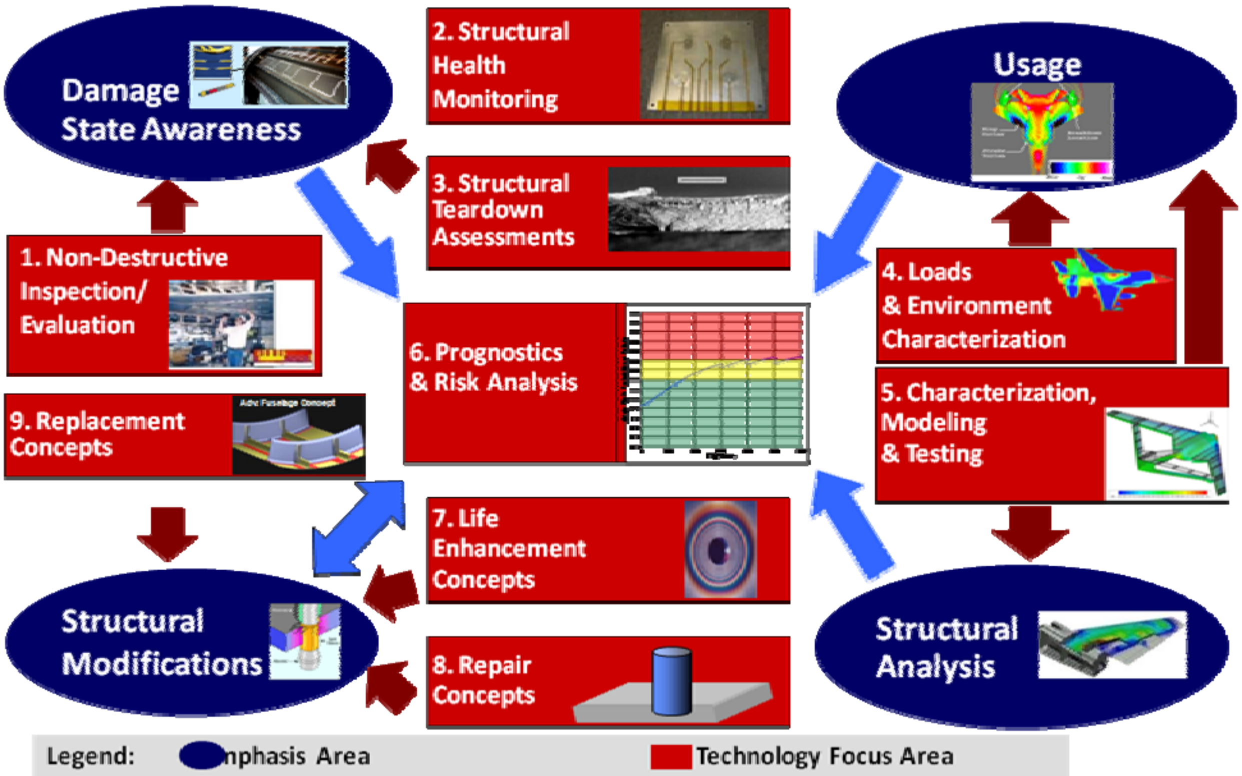

Figure 9.1-1 Condition Based Maintenance + Structural Integrity (CBM+SI)

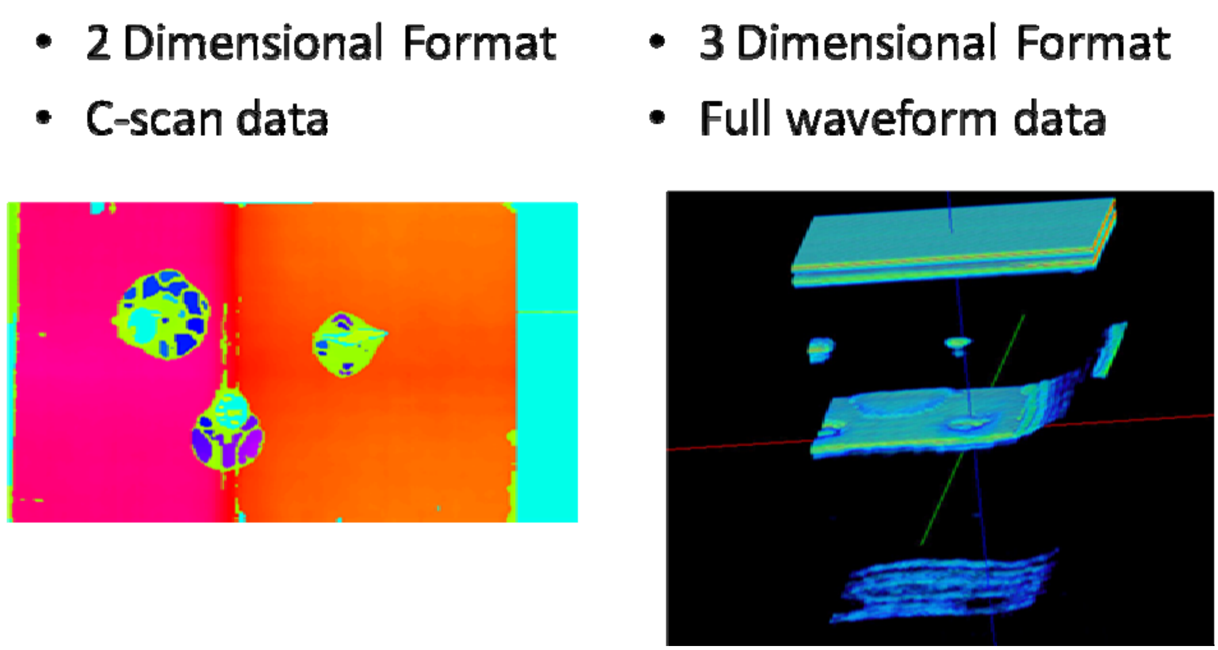

Figure 9.2-1 Versatile Analysis Tool

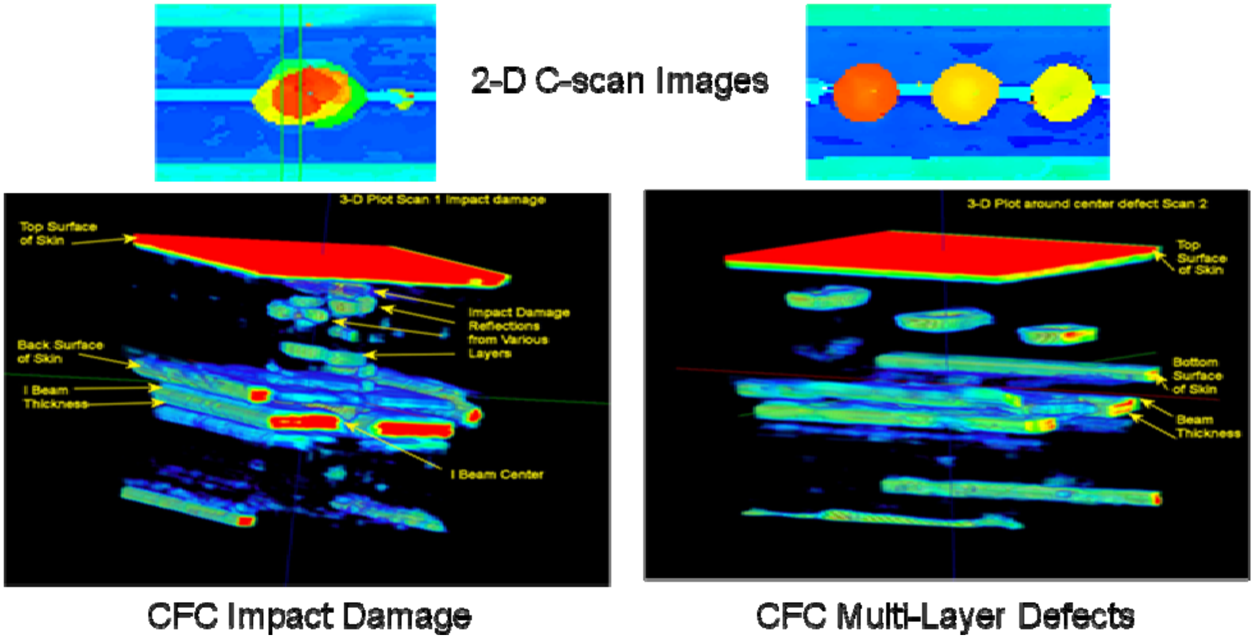

Figure 9.2-2 3-D Image of Composite Defect Areas

ALT Exposure	Hours	Exposure Level
Elevated Temperature Air	6.65	70°C
Relative Humidity	19.5	70% RH @ 70°C
Salt Fog Exposure	6.5	
Corrosive Gas	34.90	Level B @ 50°C
Dry Thermal Cycling	13.00	Cycles @ 100°C ΔT (Min. T = -45°C)
Lab Hours Required per EY	111.3	
Acceleration Factor	78.8	**~ 6 Equivalent years aging per month of exposure**

Table 9.3-1 Standard Environment Spectrum (ALT)

- Electrochemical Impedance Spectroscopy
- Galvanic
- Witness Coupons
- Linear Polarization Resistance
- TRI's Embedded Environment & Loads Sensor

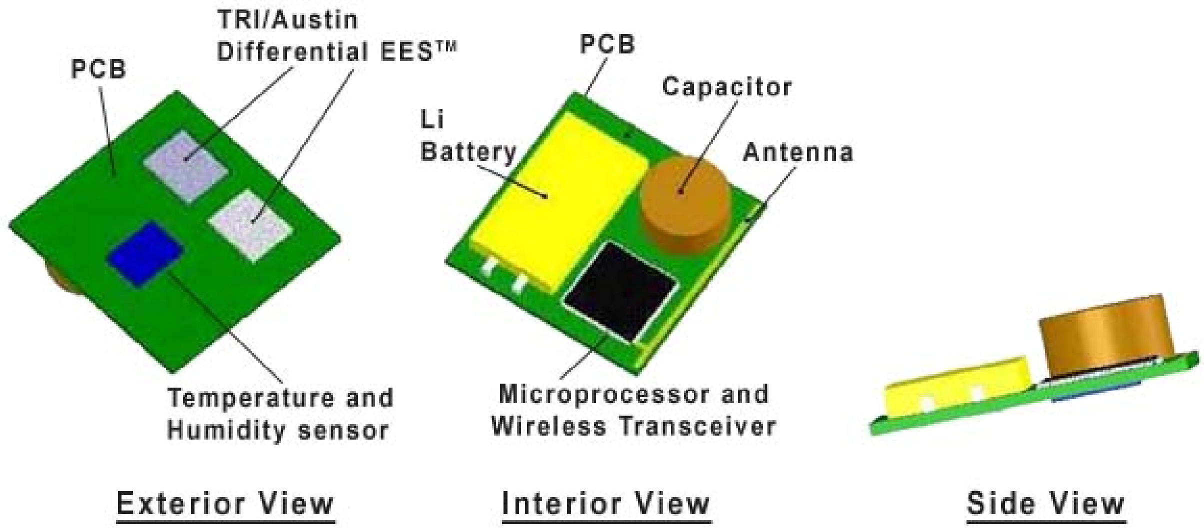

Figure 9.3-1 Candidate Sensors

Figure 9.3-2 Specimen Configuration

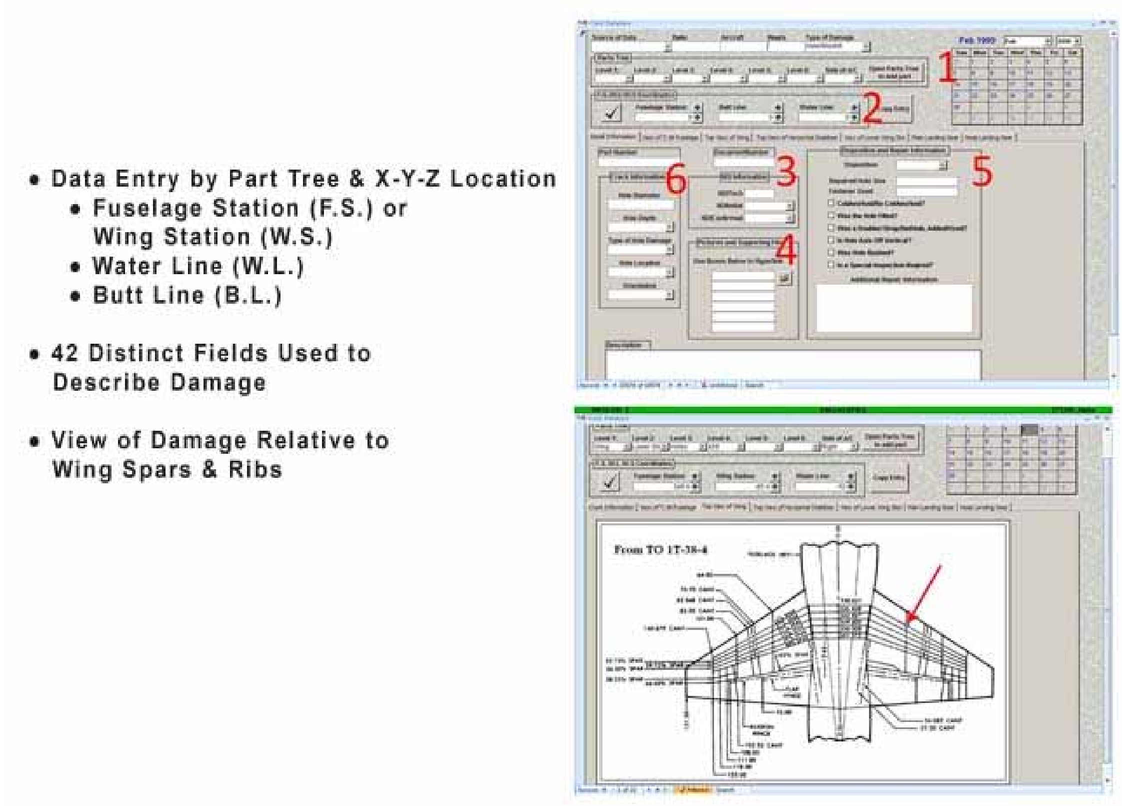

Figure 9.4-1 Data Entry and View of Damage

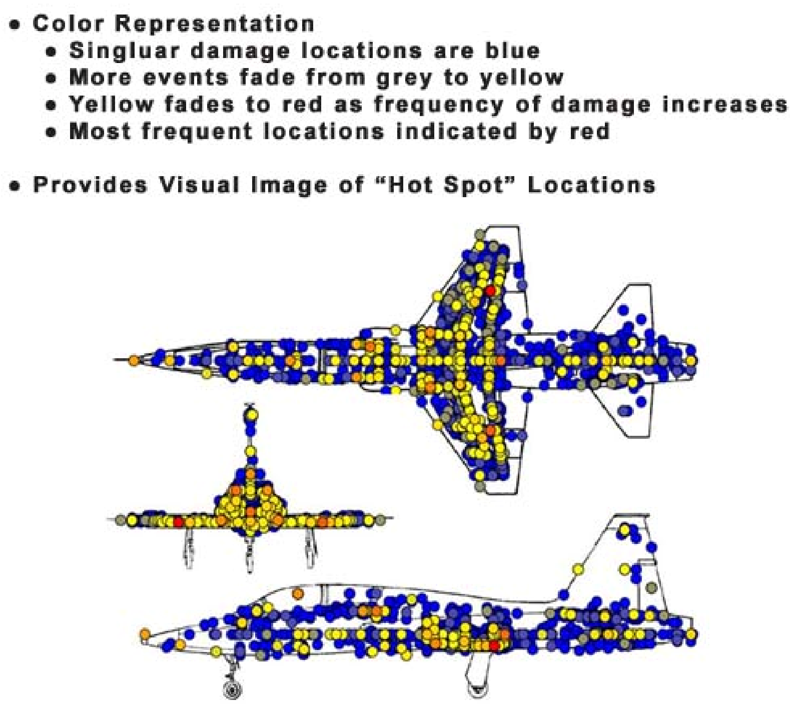

Figure 9.4-2 Frequency of Cracking

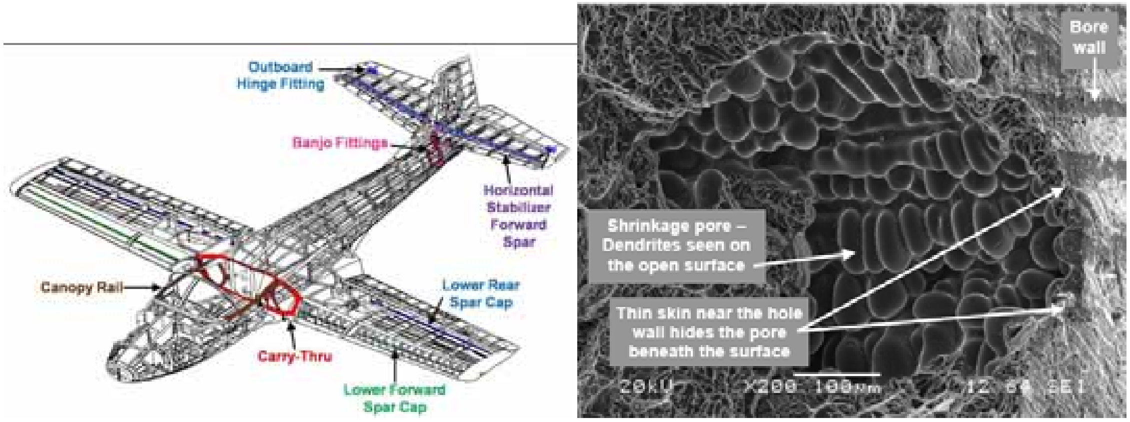

Figure 9.4-3 Location of Critical Areas

Figure 9.5-1 Trends Associated with Environmental Severity Index (ESI) (This figure shows the wide variation in weight loss data at different exposure times. The error bars show the maximum and minimum weight loss recorded at each measurement interval for each ESI value. The larger error bars suggest there is some seasonal effect to ESI.)

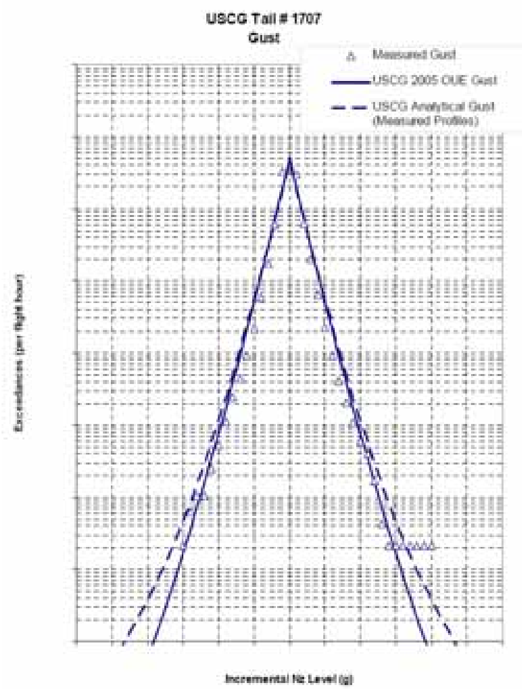

Figure 9.5-2 Indication of Reduced Severity of Measured Gust Profile vs. Previous Metrics

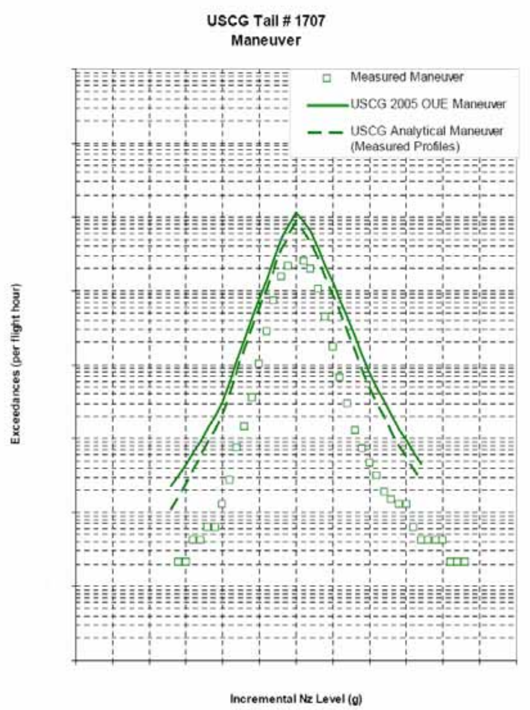

Figure 9.5-3 Indication of Reduced Severity of Measured Maneuver Profile vs. Previous Metrics

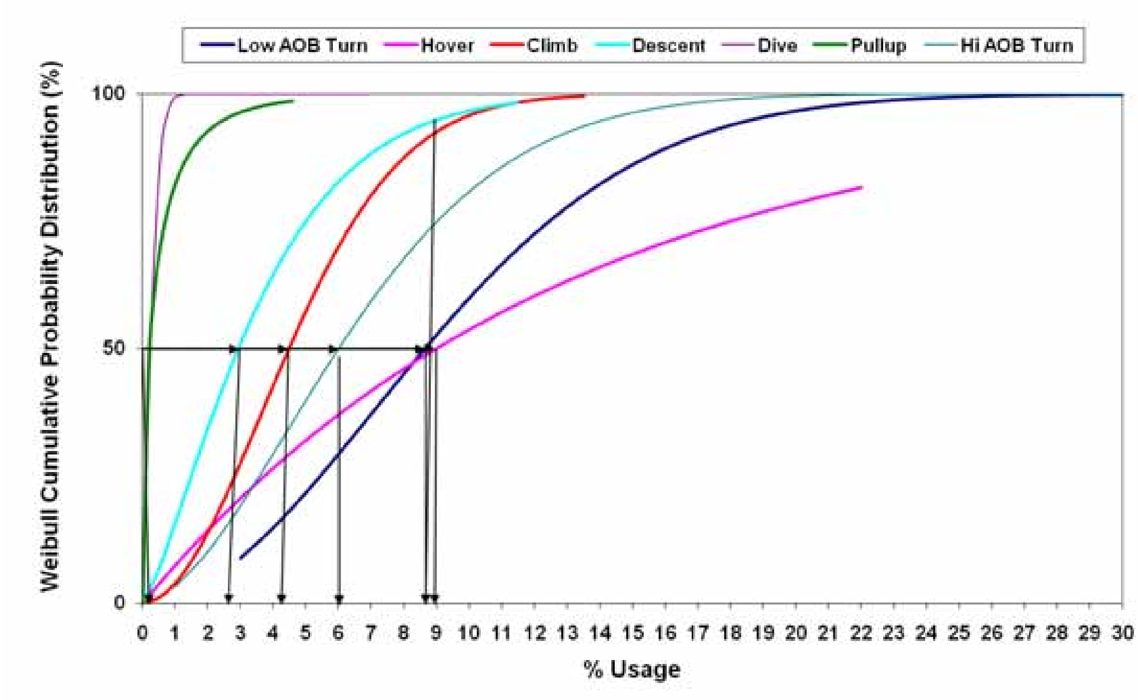

Figure 9.5-4 AH-1W 50 Percentile Usage Severity Spectrum

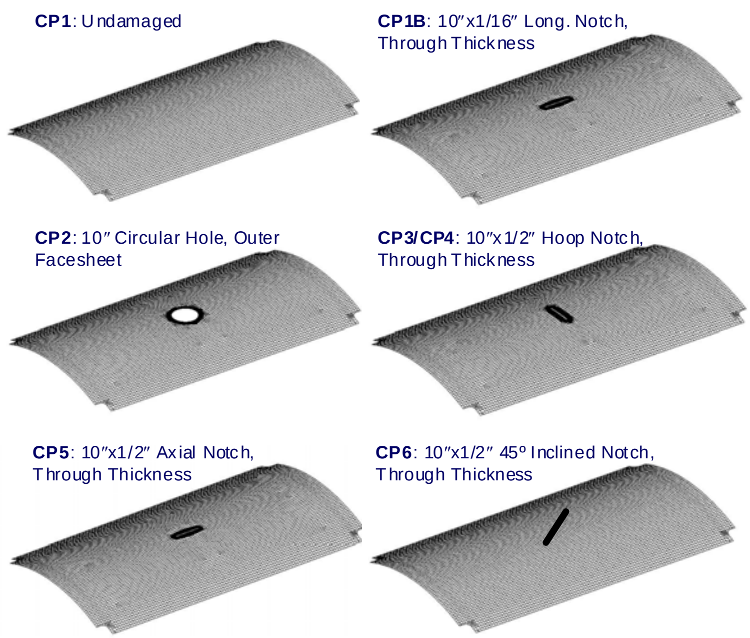

Figure 9.6-1 Damage Configurations Evaluated

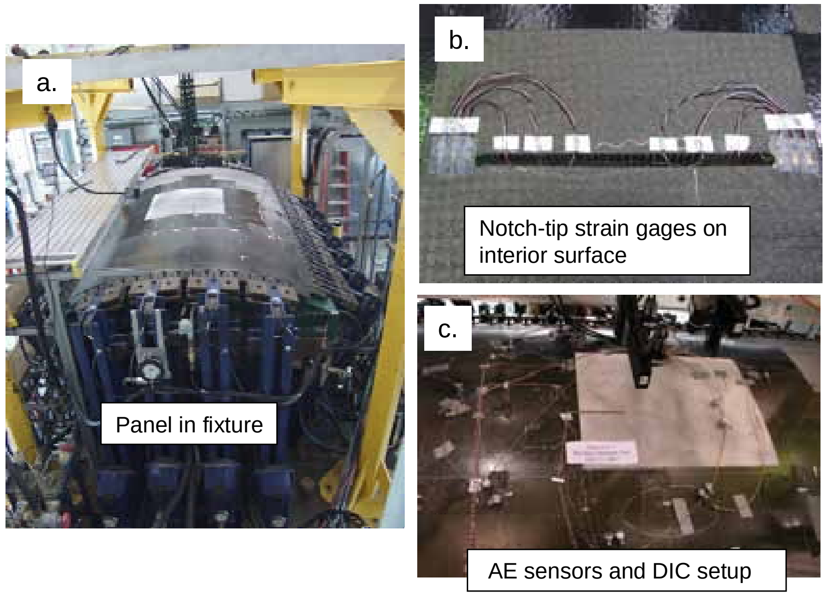

Figure 9.6-2a-c Test Setup: a. panel mounted in FASTER fixture, b. strain gages at the notch-tip on interior surface, and c. DIC pattern to measure strain on exterior surface and AE sensors to monitor damage growth.

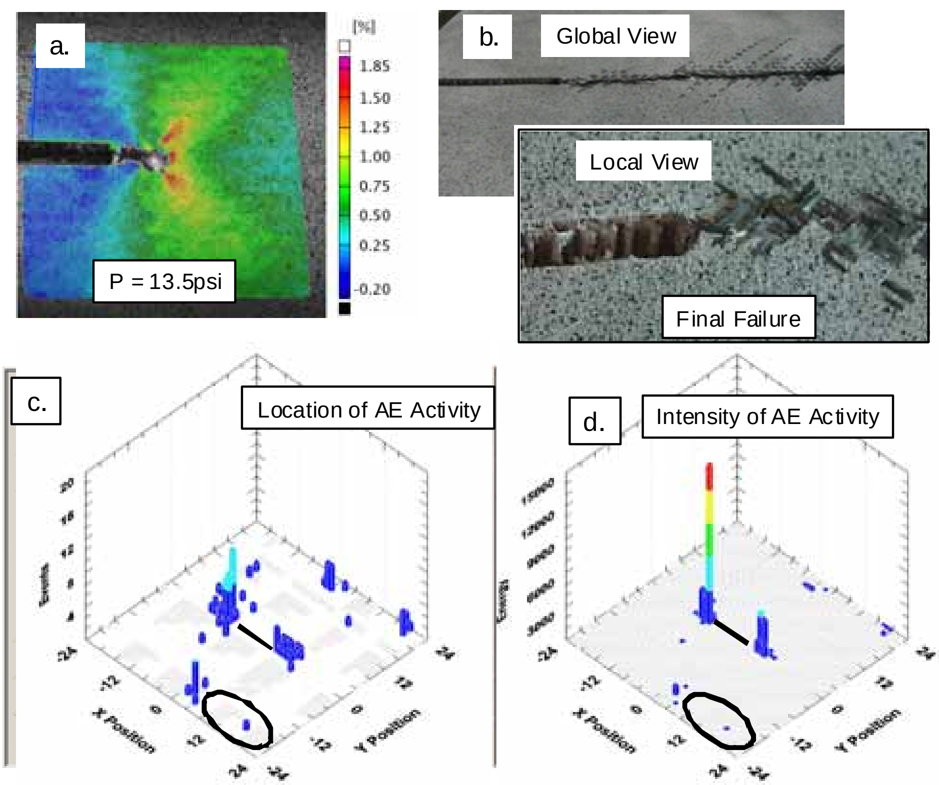

Figure 9.6-3a-d Test Results: a. hoop strain at notch tip just prior to catastrophic failure, b. global and local views of final failure, c. planar location of AE activities occurring mainly near the notch tips, and d. magnitude of the energy and location of AE.

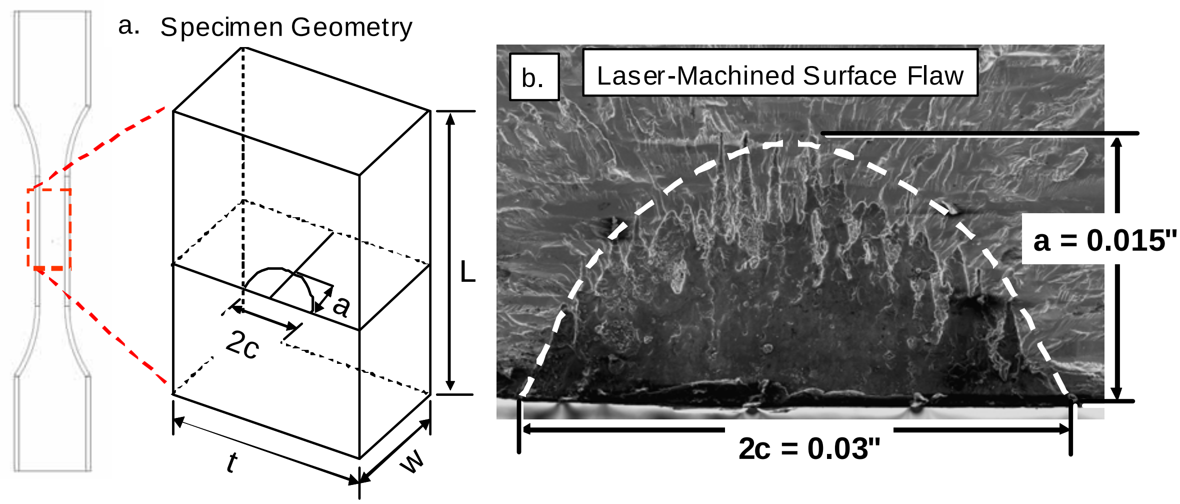

Figure 9.6-4a-b Specimen Configuration: a. Dog bone geometry with a semi-circular surface flaw and b. Surface of laser-machined notch

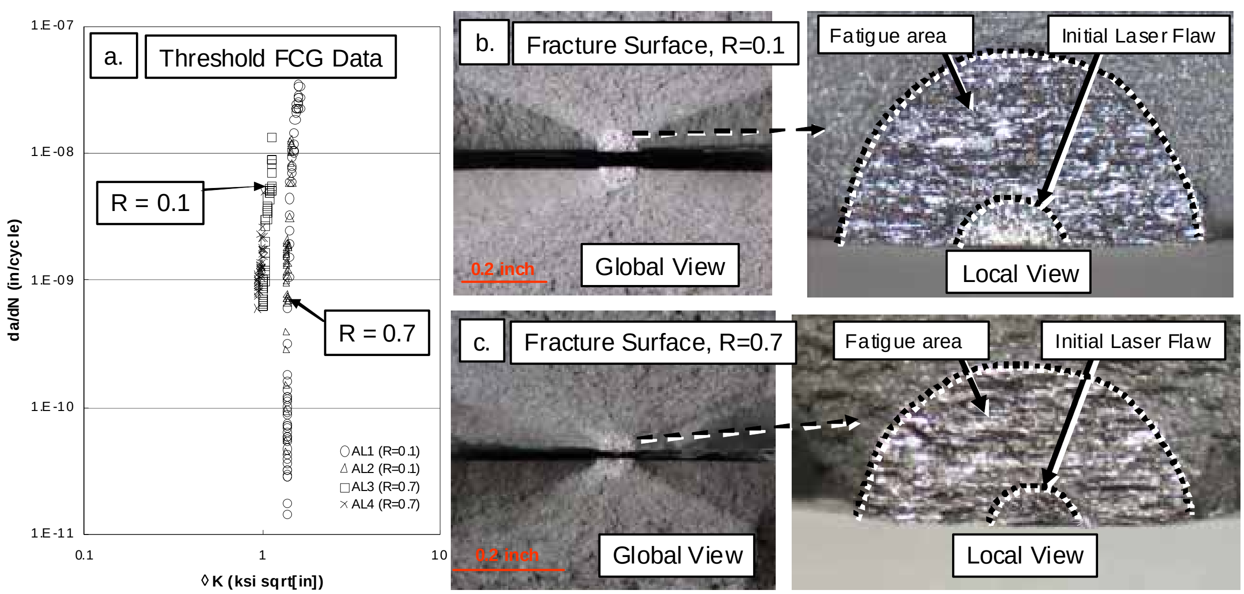

Figure 9.6-5a-c Results for As-Received 7075-T7351 Aluminum: a. Near-threshold FCG data, b. Fracture surface of specimen subjected to *R*=0.1, showing the initial laser flaw and fatigue area, and c. Fracture surface of specimen subjected to *R*=0.7, showing the initial laser flaw and fatigue area

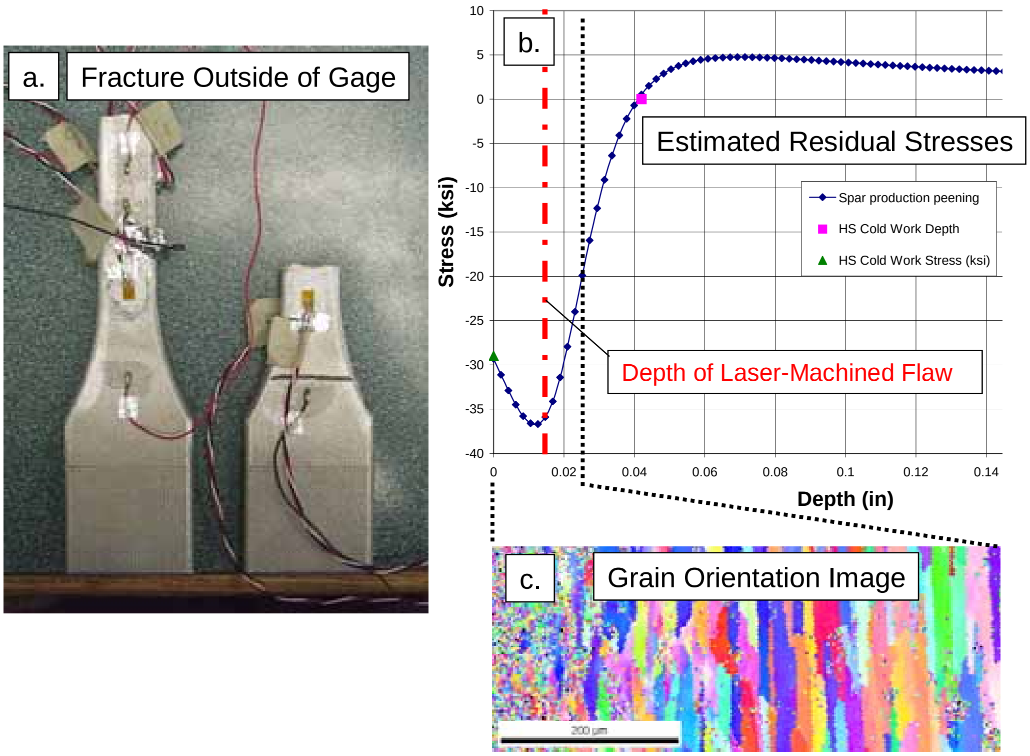

Figure 9.6-6a-c Results for Shot-peened 7075-T7351 Aluminum: a. Fracture outside of gage section, b. Estimated residual stress profile, showing laser-machined flaw under compression, and c. EBSD technique showing distortion and orientation of microstructure in the laser-machined flaw region

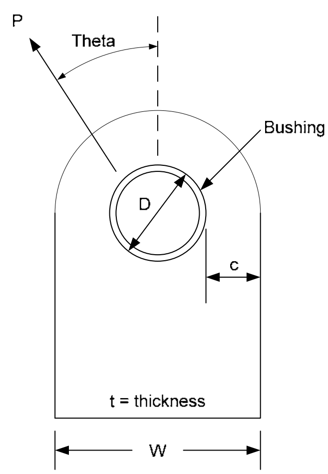

Figure 9.6-7 Basic Lug

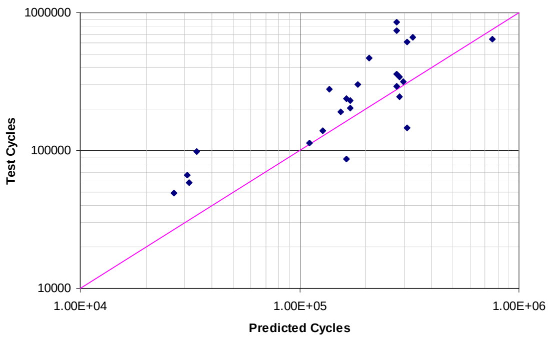

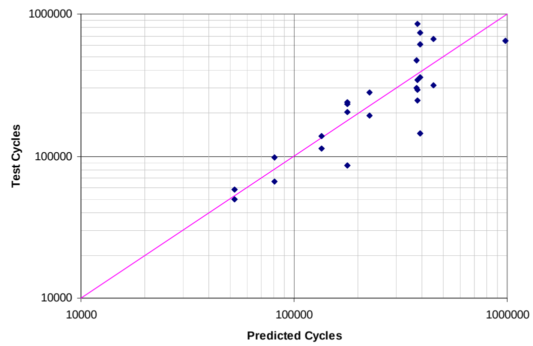

Figure 9.6-8 Aluminum Lug Data vs. Predicted Life (R = .06 and .50)
Left: Common Factors, Right: Higher Order Factors

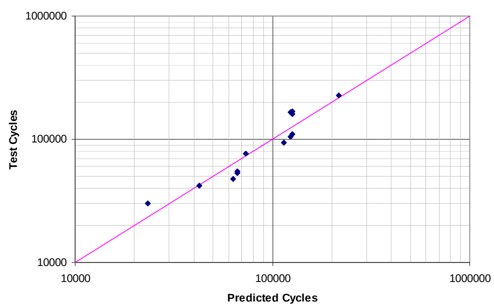

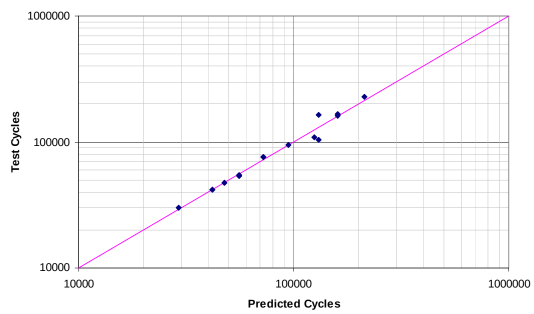

Figure 9.6-9 Titanium Lug Data vs. Predicted Life (R = .06 and .50)
Left: Common Factors, Right: Higher Order Factors

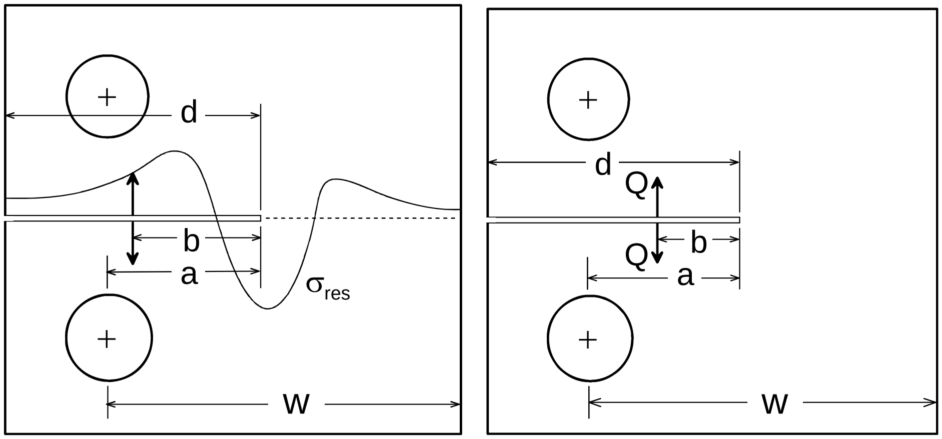

(a) Arbitrary residual-stress distribution (b) Concentrated forces acting on crack surfaces

Figure 9.6-10a-b Compact Test Specimen Subjected to Residual Stresses and Concentrated Forces.

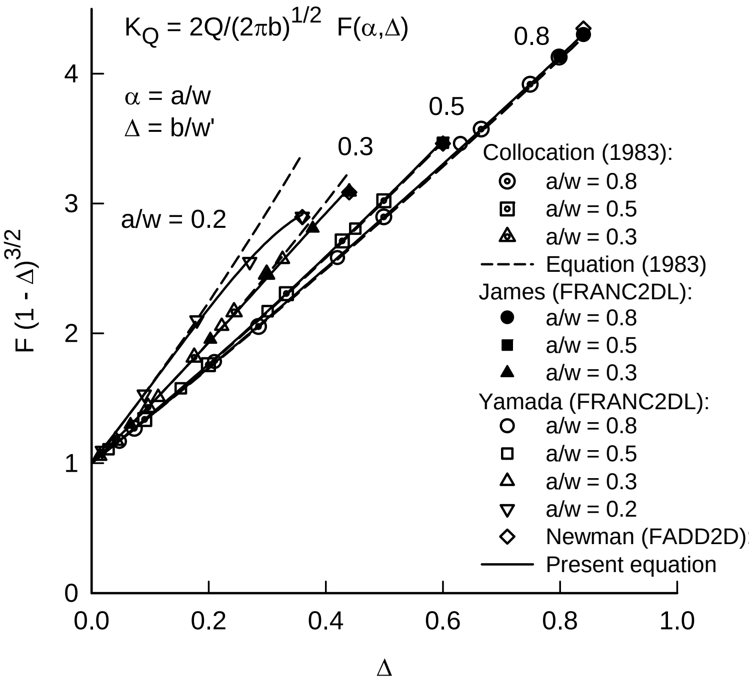

Figure 9.6-11 Comparison Among Normalized Boundary-correction Factors for Compact Specimen With Pair of Concentrated Forces Acting on Crack Surfaces.

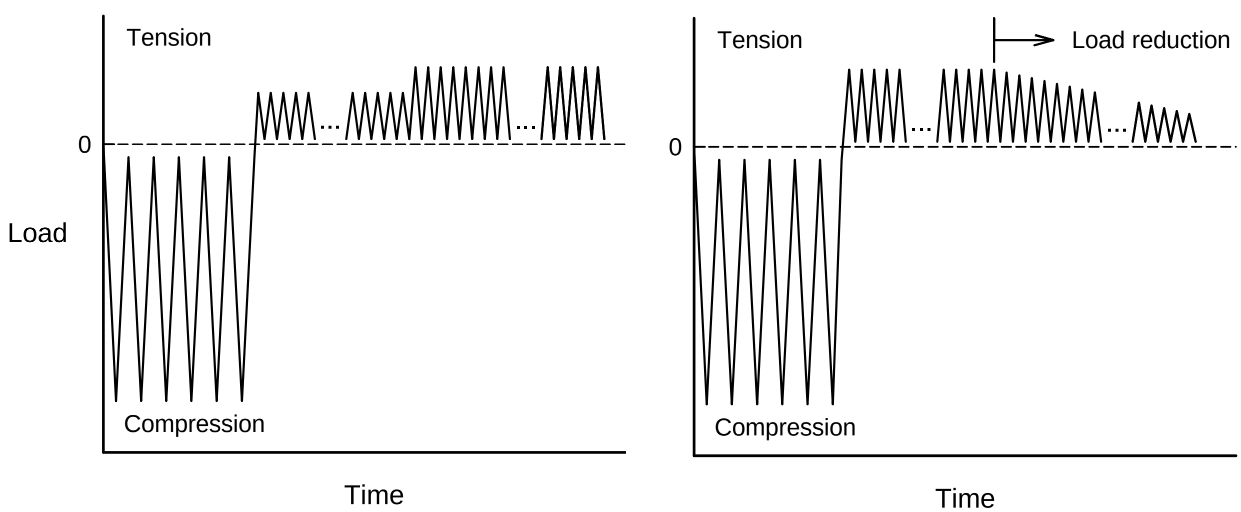

(a) CPCA loading

(b) CPLR loading

Figure 9.6-12a-b Types of Loading Applied to Fatigue-crack-Growth Specimens.

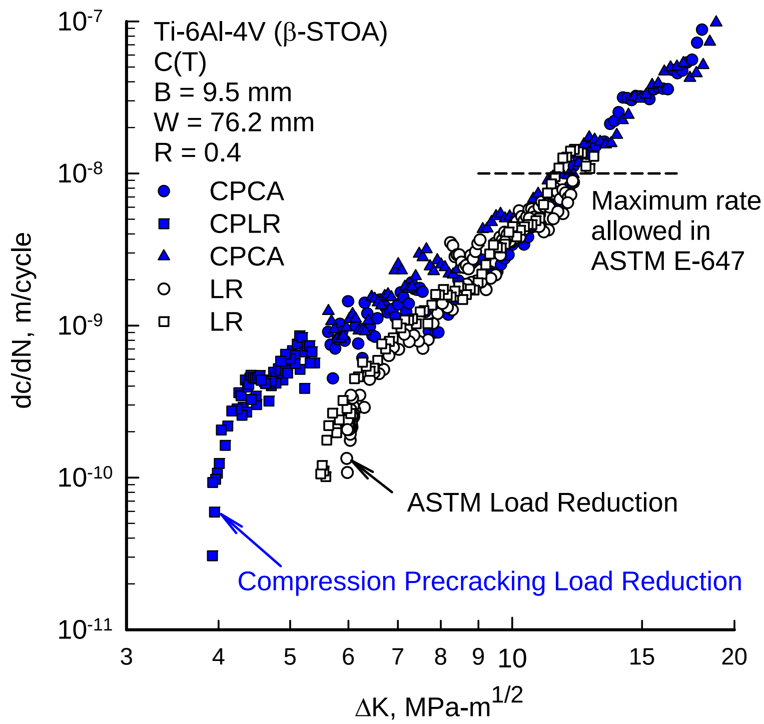

Figure 9.6-13 Crack-growth Rate Data on Ti-6Al-4V β-STOA Titanium Alloy at R = 0.4.

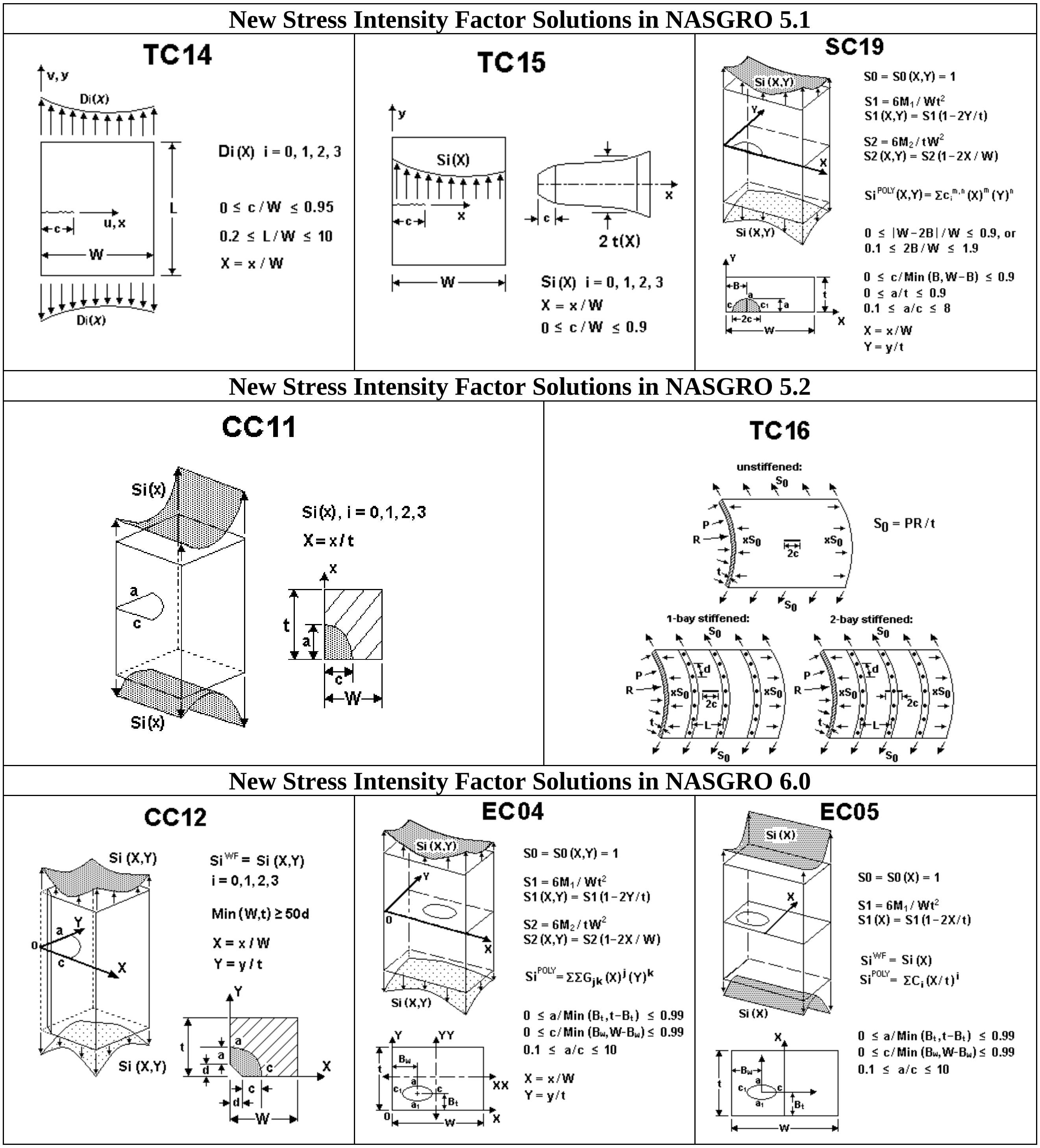

Figure 9.6-14 New Stress Intensity Factor Solutions in NASGRO Versions 5.1, 5.2, and 6.0

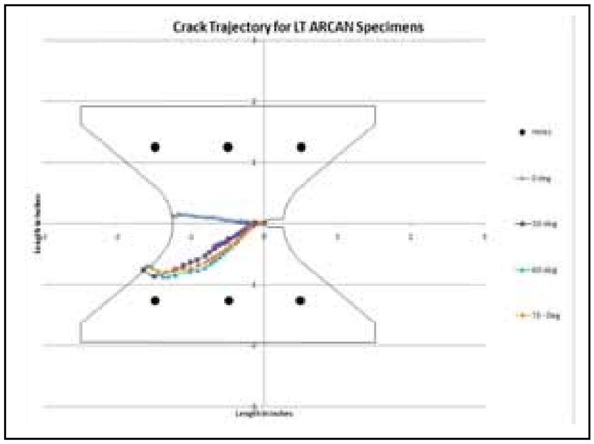

Figure 9.6-15 Crack Trajectory for Samples Loaded at 0, 30, 60 and 75 Degrees With the Same Initial $K_{eq.}$

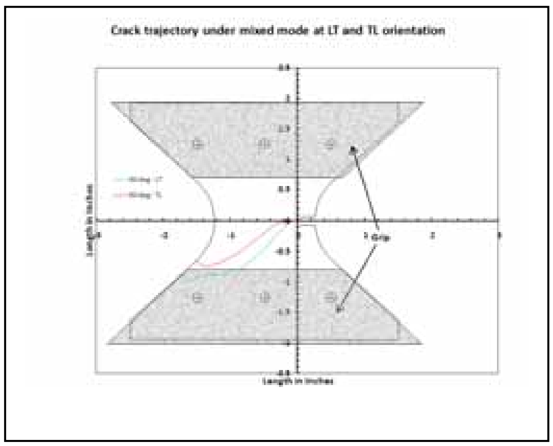

Figure 9.6-16 Crack Trajectory for Samples Loaded at 60 Degrees With LT and LT Material Orientation.

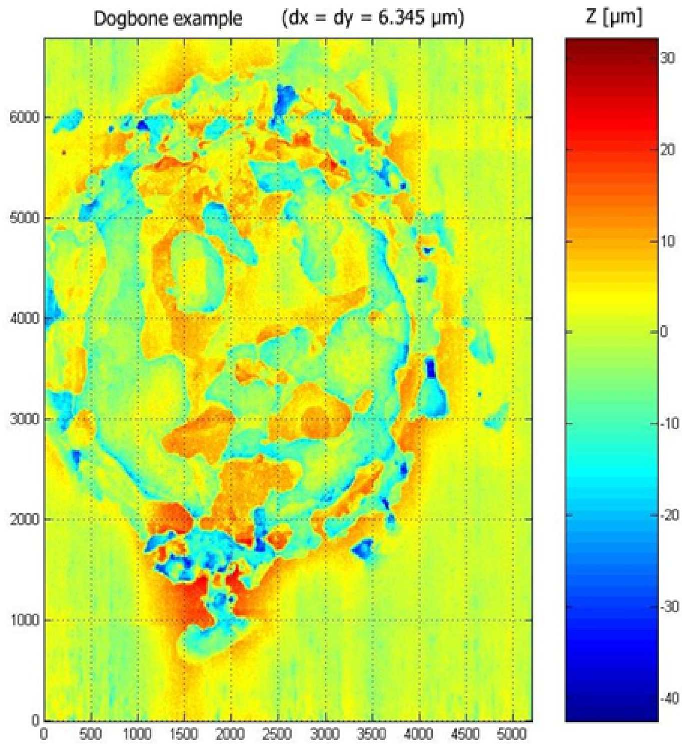

Figure 9.6-17 Surface Topography of Corroded Test Specimen From Laser Profilimetry

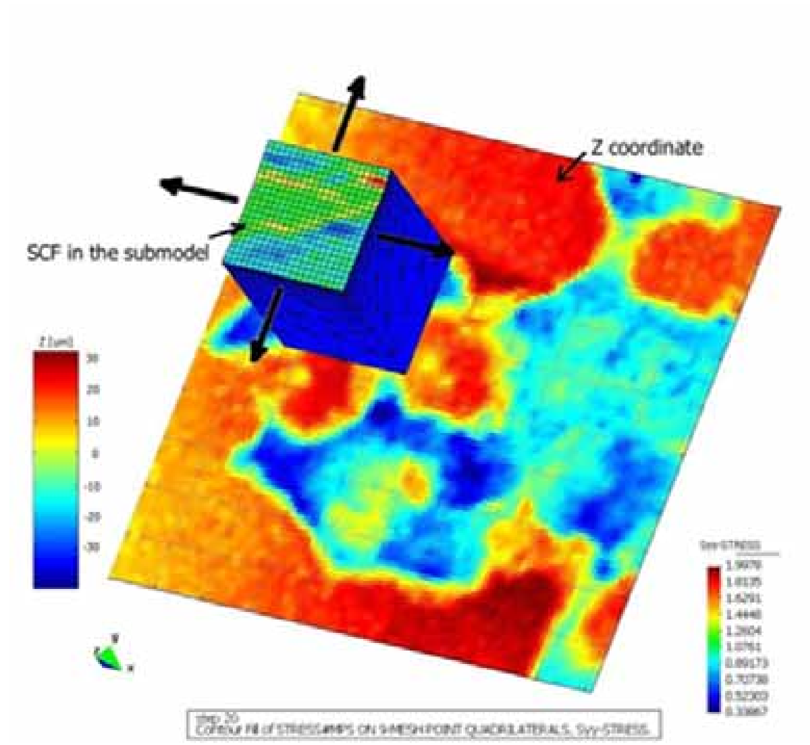

Figure 9.6-18 Spatial Distribution of SCF for Initial Defeatured Solution Stage

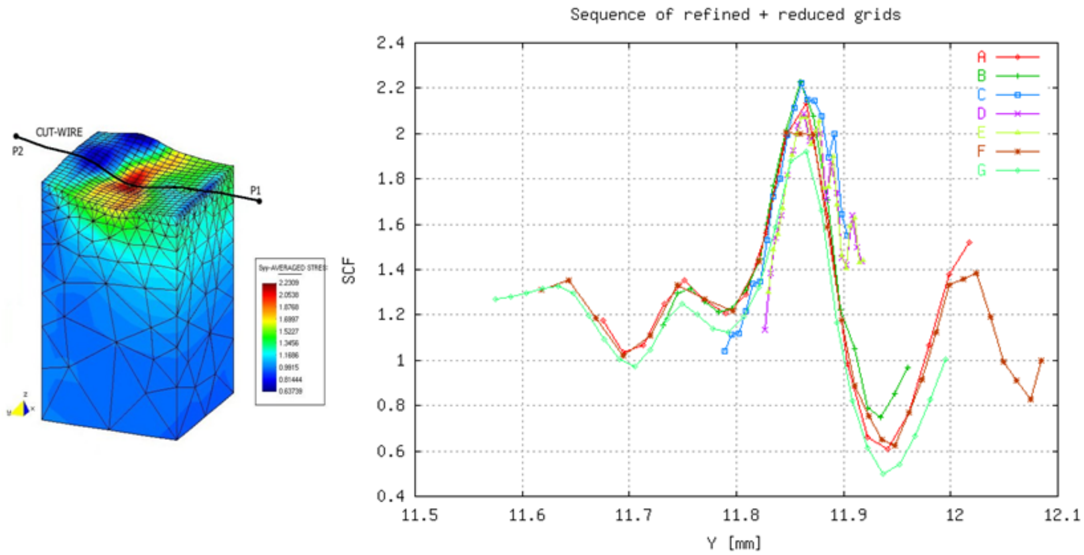

Figure 9.6-19 SCF Showing Impact of Different Levels of Mesh Refinement and Submodel Size (*the F, A, G, B, C, D, E progression indicate reducing element and submodel size*).

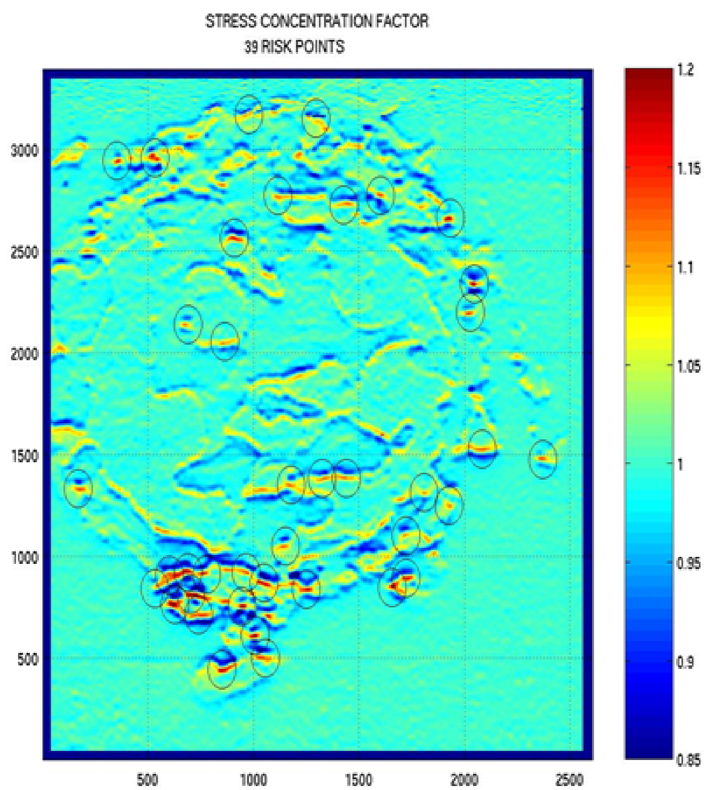

Figure 9.6-20 SCF at Identified Risk Points for Full Test Specimen (*low resolution stage*).

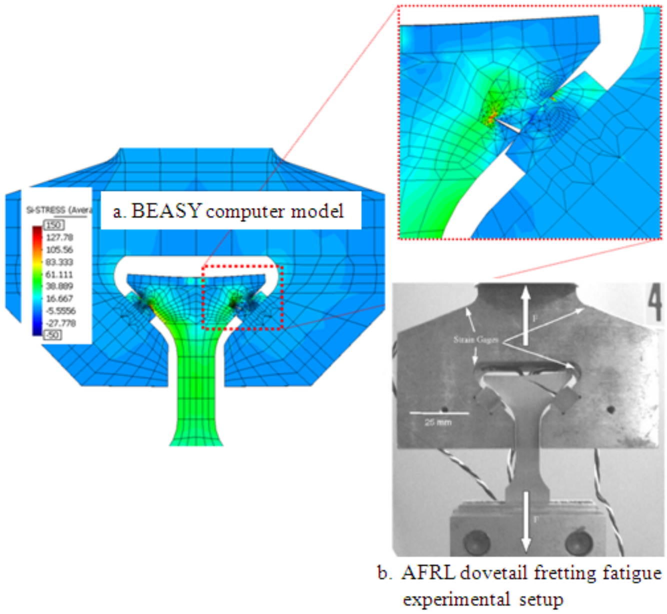

Figure 9.6-21 3D Crack Growth Model of AFRL Fretting Fatigue Test Specimen. (Details of the experimental procedure can be found in the work by Golden and Calcaterra [1])

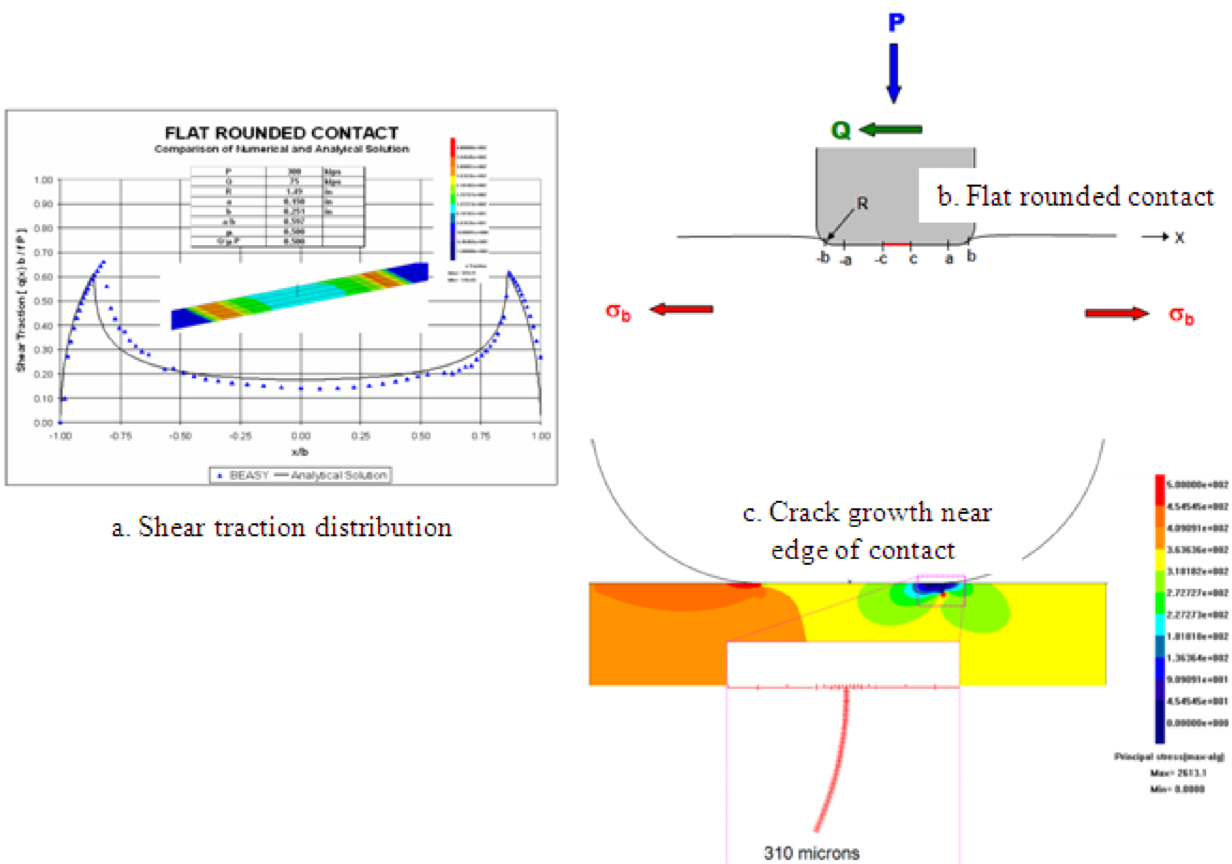

Figure 9.6-22a-c Flat Rounded Contact Showing Shear Traction Distribution and Crack Growth Near Edge of Contact.

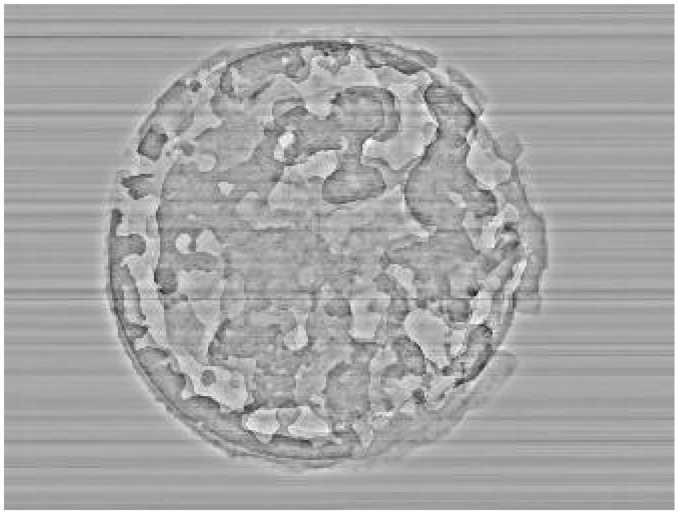

Figure 9.6-23 Example of a Stitched Topographic Image (41 mm x 41 mm) of a Corrosion Patch on an AF1410 Fatigue Test Plate

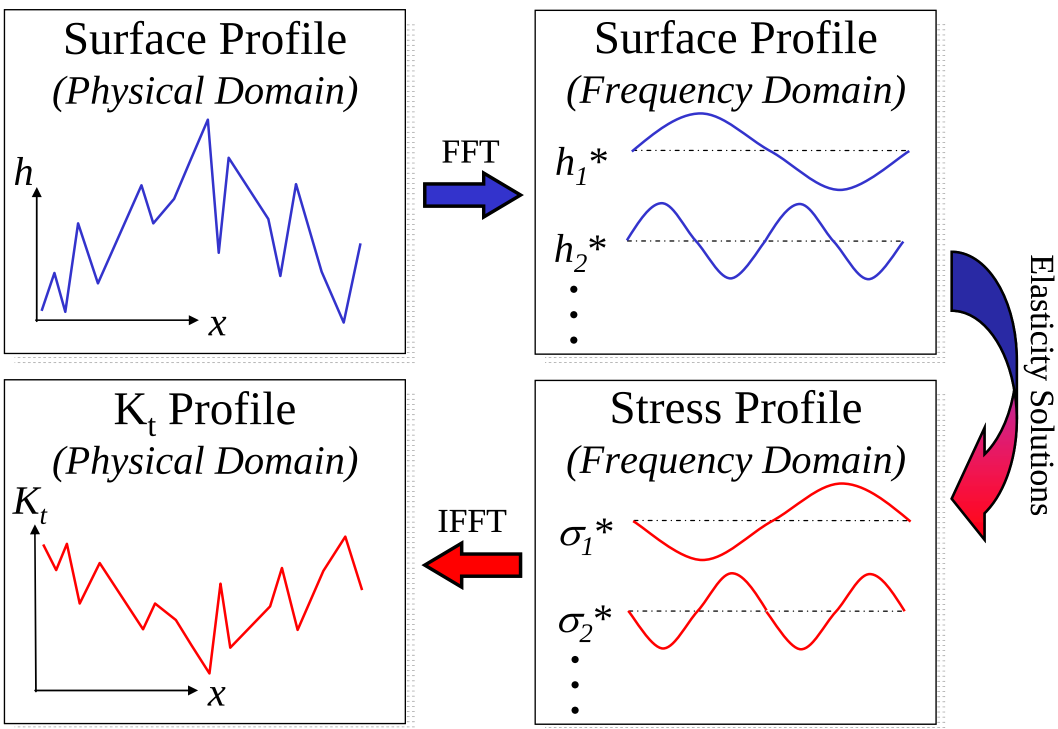

Figure 9.6-24 Elasticity Approach for Corroded Surface Modeling

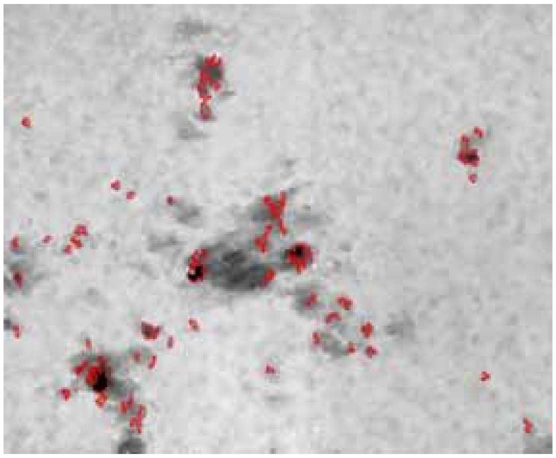

Figure 9.6-25 F/A-18C/D Arrestment Shank Corroded Surface Topology with Region of Interest Features Marked in Red

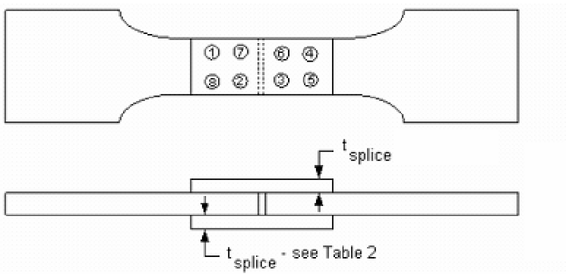

Figure 9.6-26 High Load Transfer Specimen

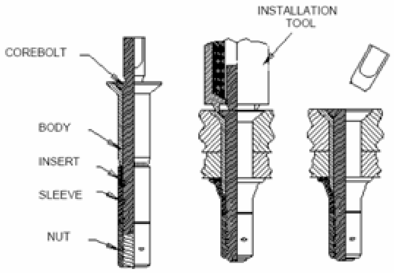

Figure 9.6-27 Ti OSI® Fastener

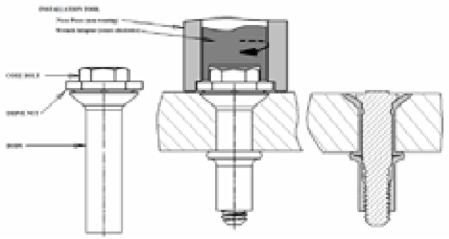

Figure 9.6-28 Monogram MLA® Fastener

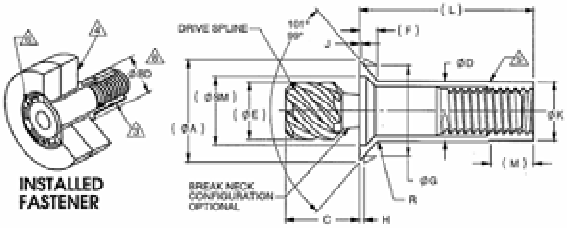

Figure 9.6-29 Ergo-Tech® Fastener

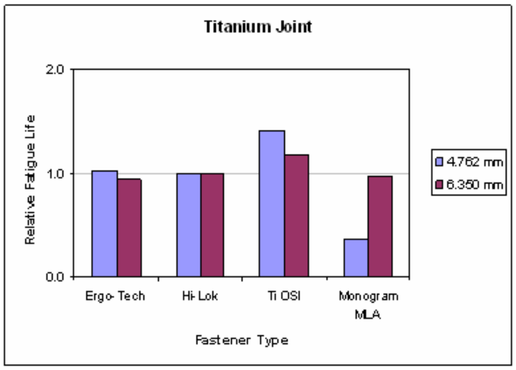

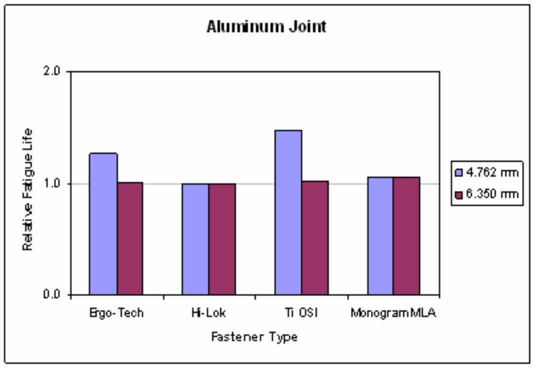

Figure 9.6-30 Titanium Joint Analysis Results

Figure 9.6-31 Aluminum Joint Analysis Results

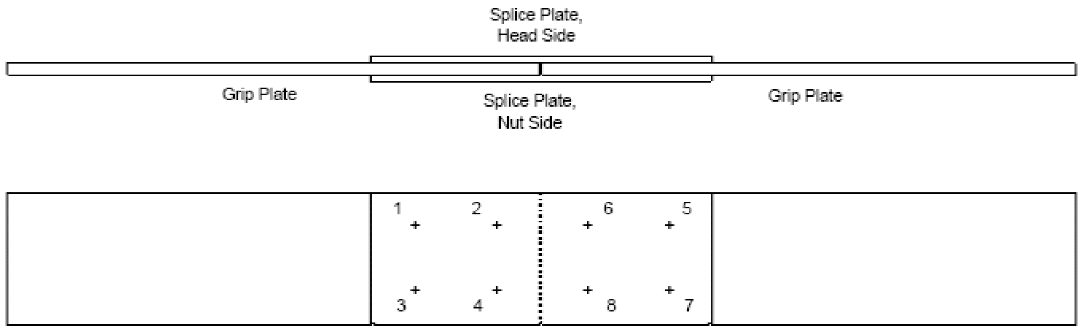

Figure 9.6-32 Double Shear Joint Specimen Used in Test Program

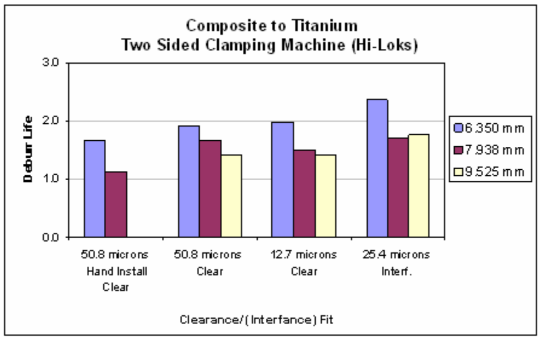

Figure 9.6-33 Ti (Hi-Lok) Two-Sided Clamping Machine

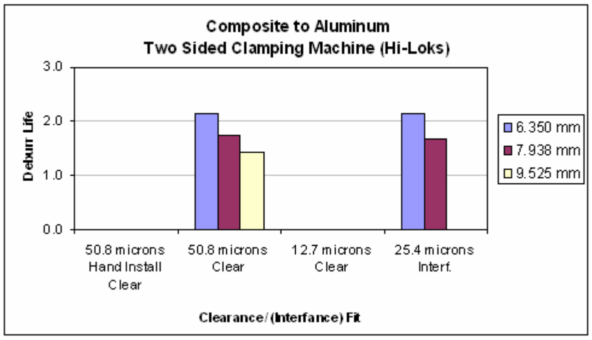

Figure 9.6-34 Al (Hi-Lok) Two-Sided Clamping Machine

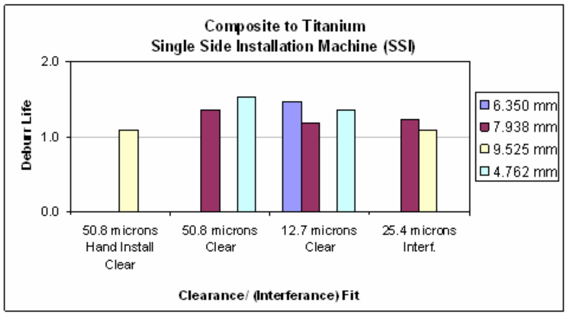

Figure 9.6-35 Ti (OSI) Single-Side Installation Machine

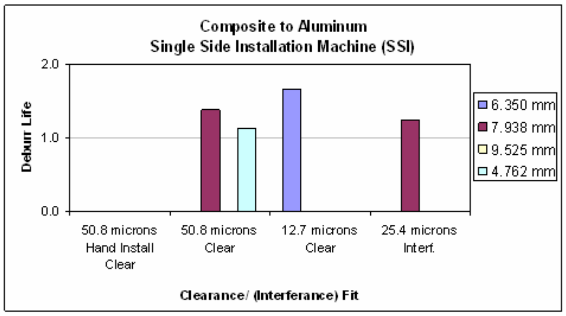

Figure 9.6-36   Al (OSI) Single-Side Installation Machine

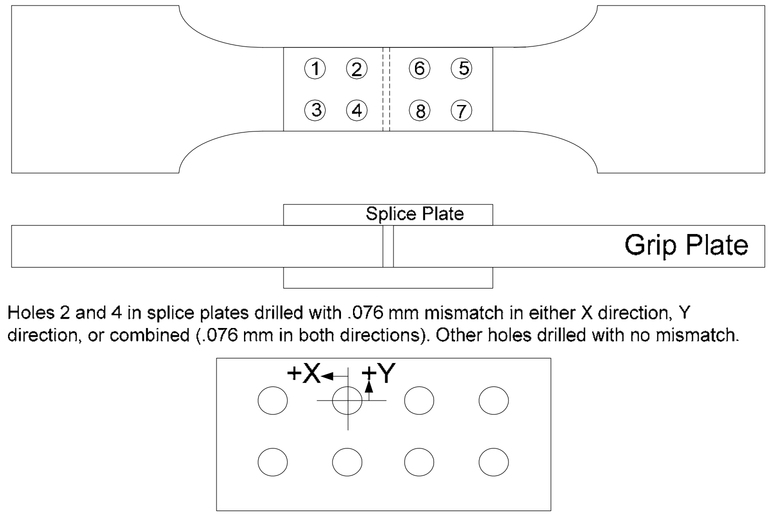

Figure 9.6-37 Development of Mismatch in Fatigue Specimens

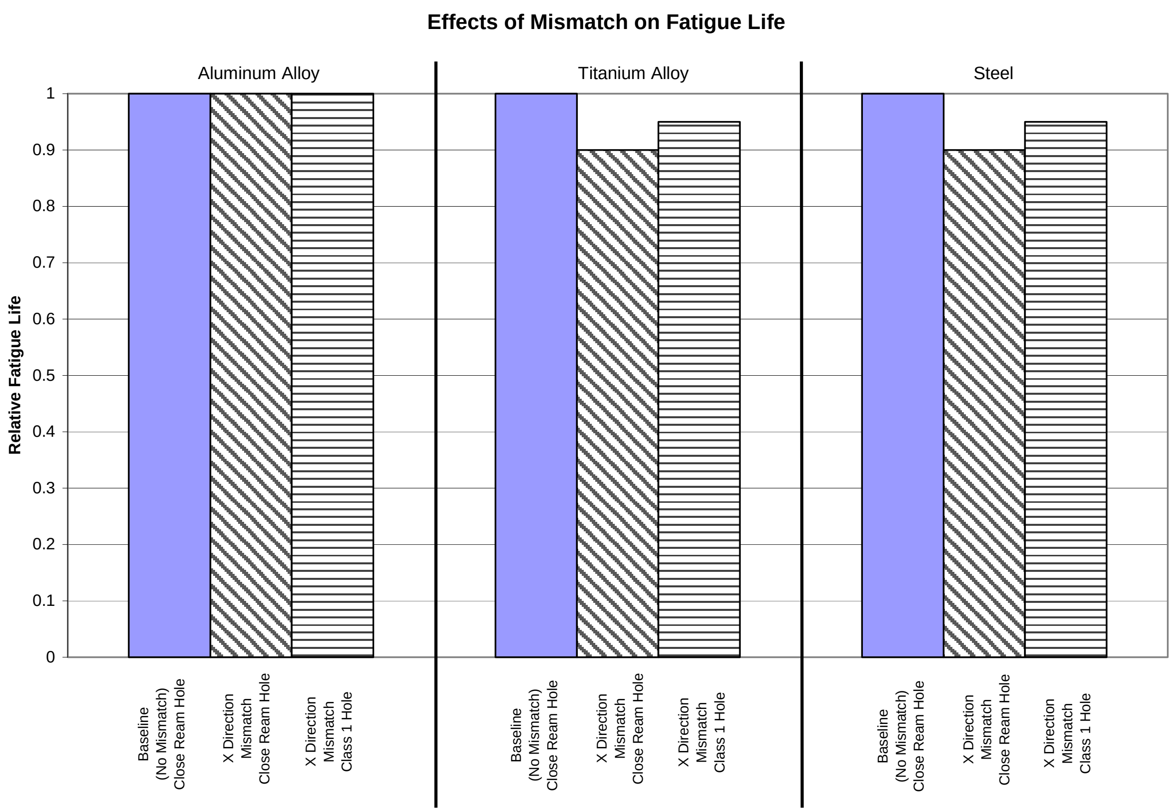

Figure 9.6-38 Relative Fatigue Life vs. Hole Fill

Figure 9.6-39 Scribe Line on a Kt Specimen

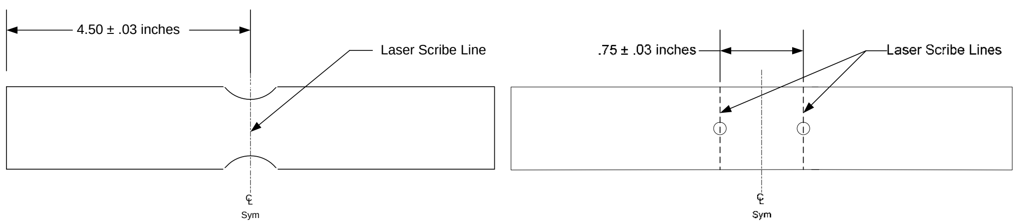

Figure 9.6-40 Kt and Open Hole Specimen Layout

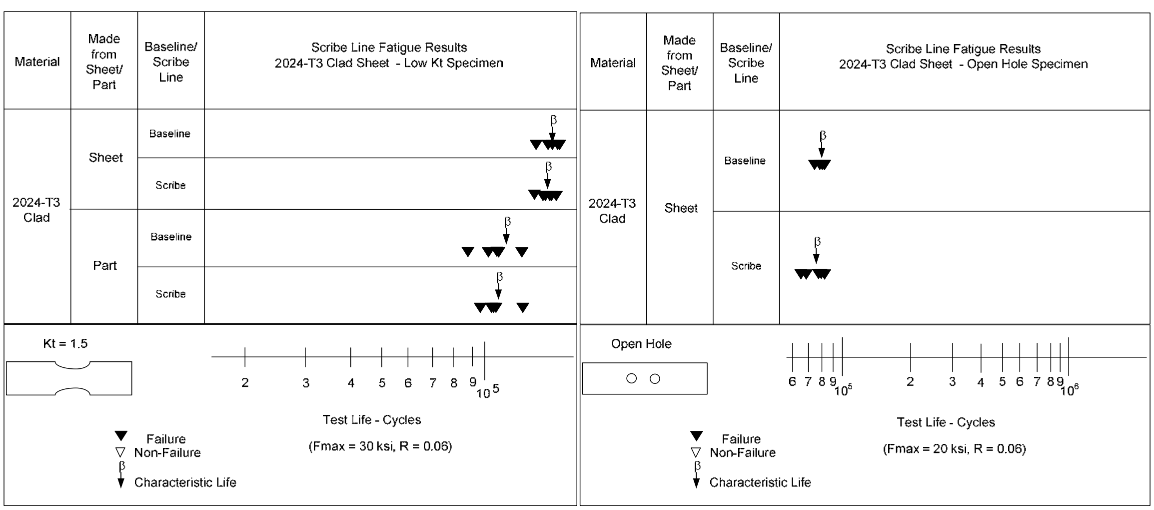

Figure 9.6-41 Kt and Open Hole Specimen Results

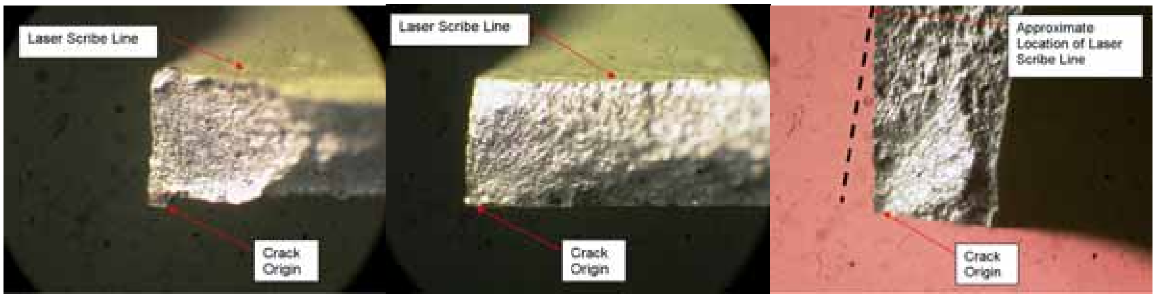

Figure 9.6-42 Crack Origins Far From the Laser Damage

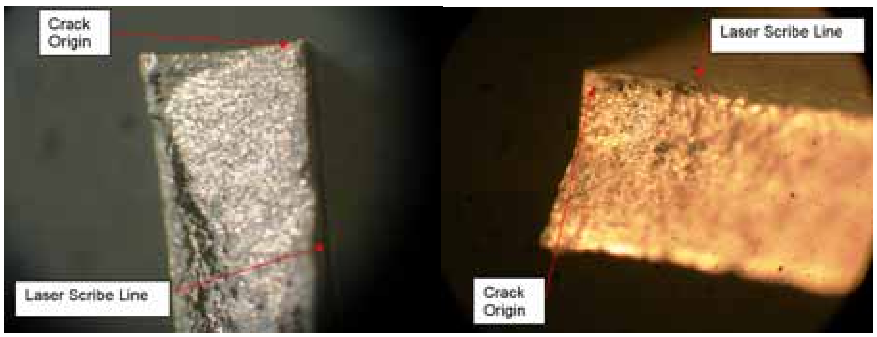

Figure 9.6-43 Crack Origins Near the Laser Damage

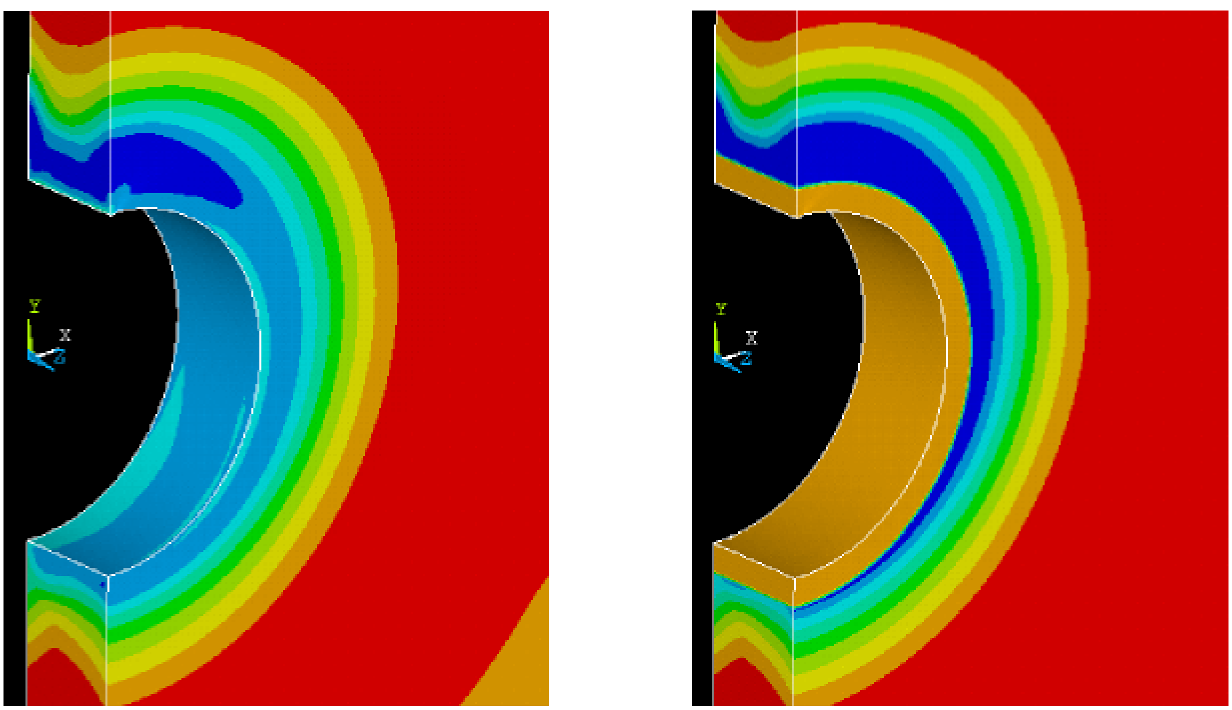

(a) Cold worked with split sleeve

(b) Reamed after cold worked with split sleeve

Figure 9.6-44a-b Hoop Residual Stress Contours From 3D Cold-work Simulations With Split Sleeve

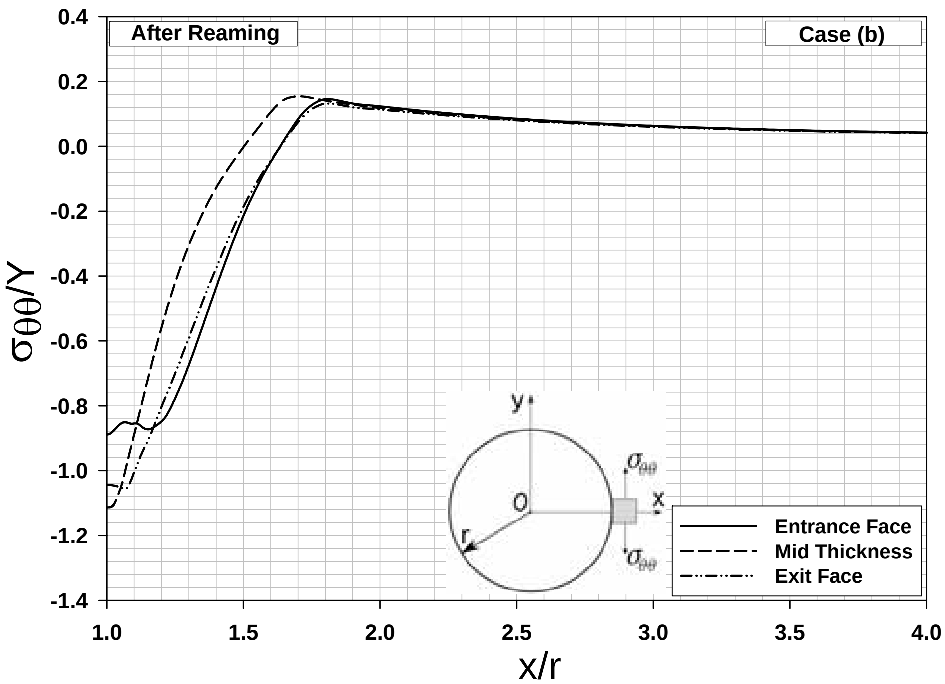

Figure 9.6-45 Normalized Hoop Residual Stress Curves After CW and Reaming at Plate Entrance, Mid-plane, and Exit Faces.

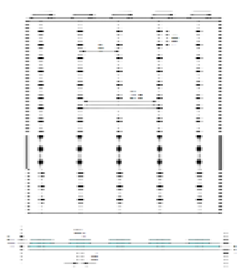

$$K_{Panel} = \beta(a)\sigma\sqrt{\pi a}$$

$$\mu = \frac{w_s t_s E_s}{w_s t_s E_s + btE}$$

Residual Strength:

$$S_{RS} = \frac{K_C}{\beta\sqrt{\pi a}}$$

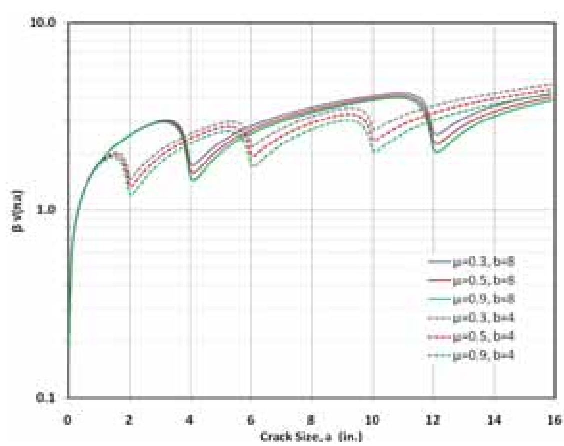

a) 2-bay Crack

b) $\beta\sqrt{\pi a}$ vs. Crack Size

Figure 9.7-1a-b Crack Geometry and β Correction Factor

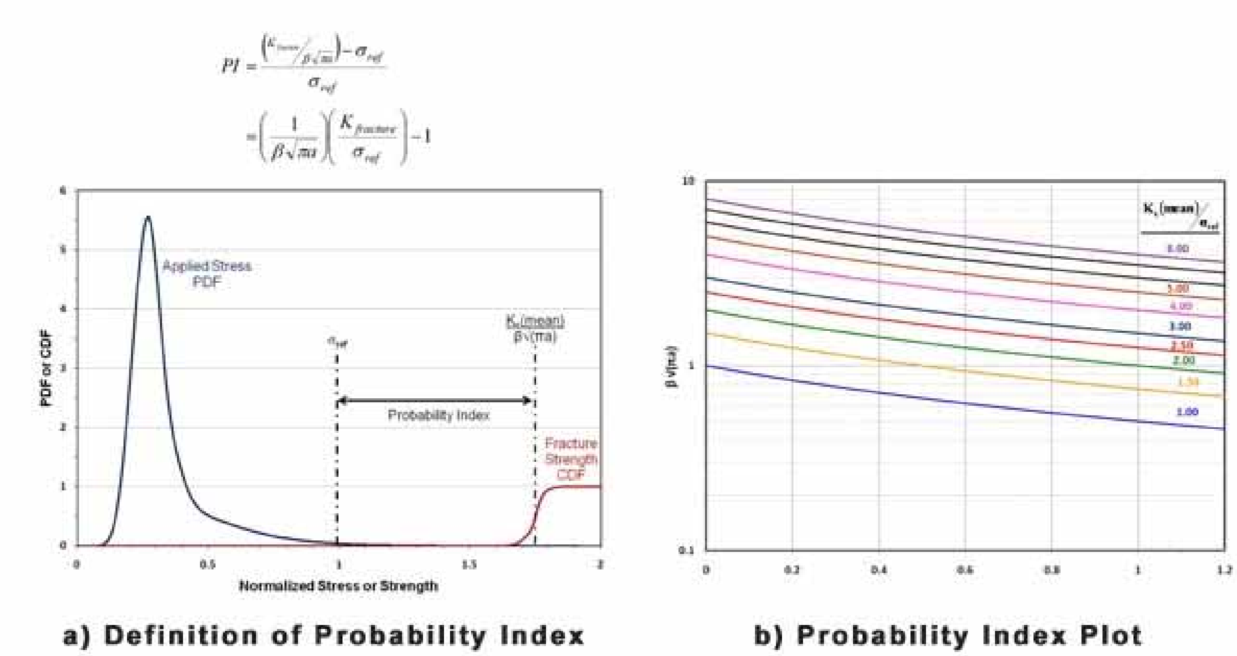

Figure 9.7-2a-b Determination of Probability Index

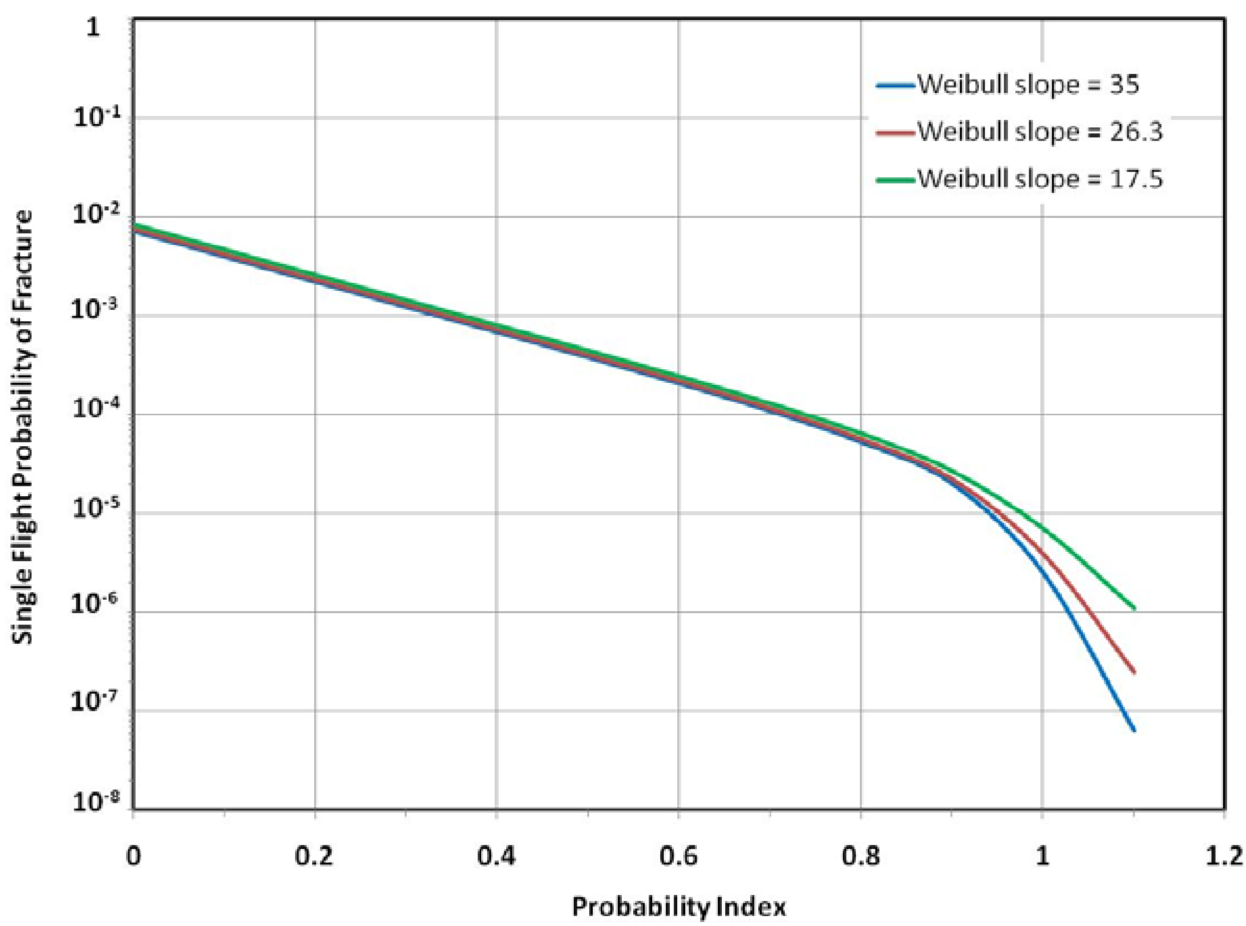

Figure 9.7-3 Probability of Fracture vs. Probability Index

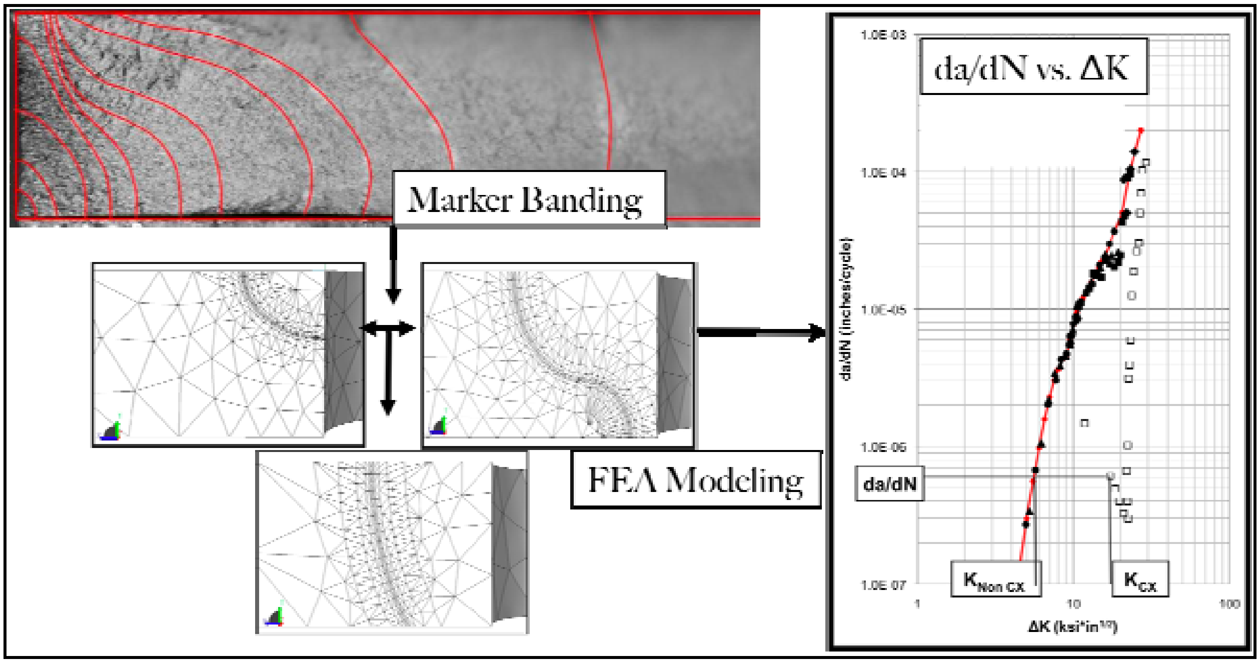

Figure 9.8-1 Research Process to Develop Stress Intensities for Baseline Non-Cold-Expanded and Cold-Expanded Specimens

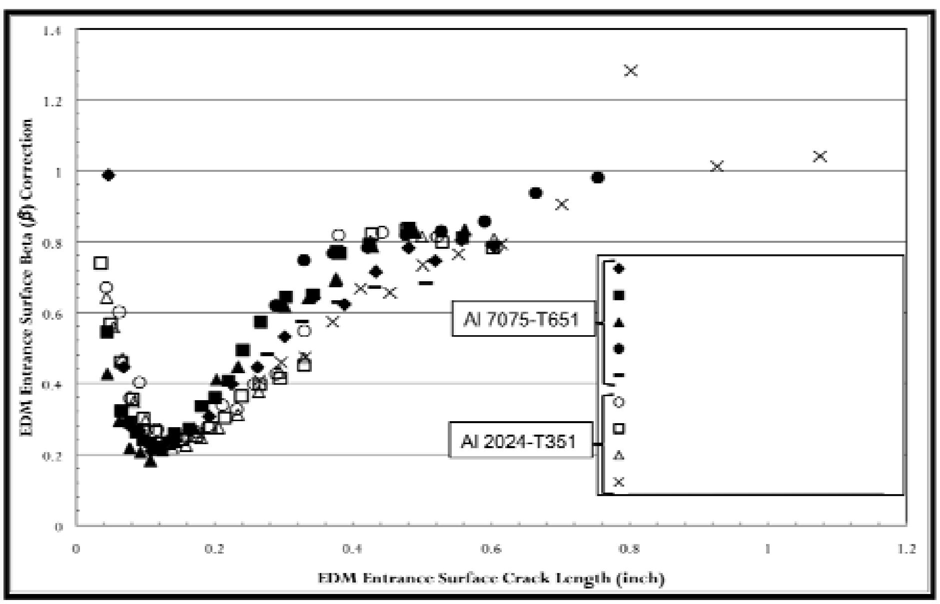

Figure 9.8-2 Plot of β Correction versus Crack Length for 2024 & 7075 Alloys

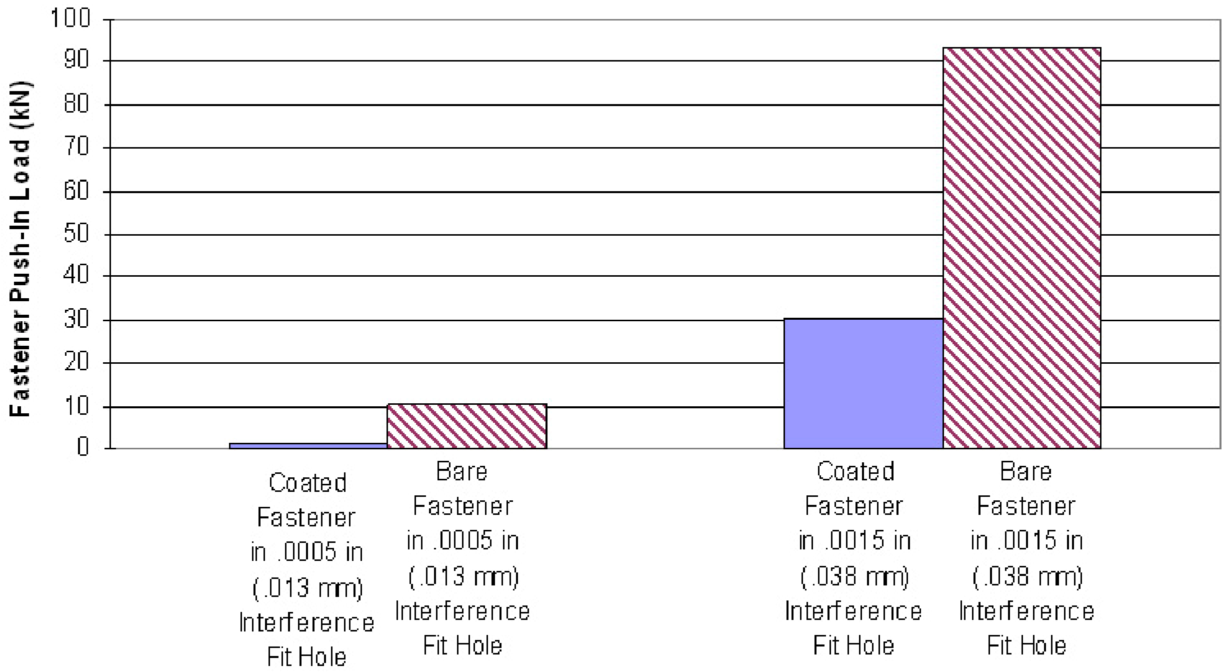

Figure 9.8-3 Fastener Push-in Load vs. Fastener Finish

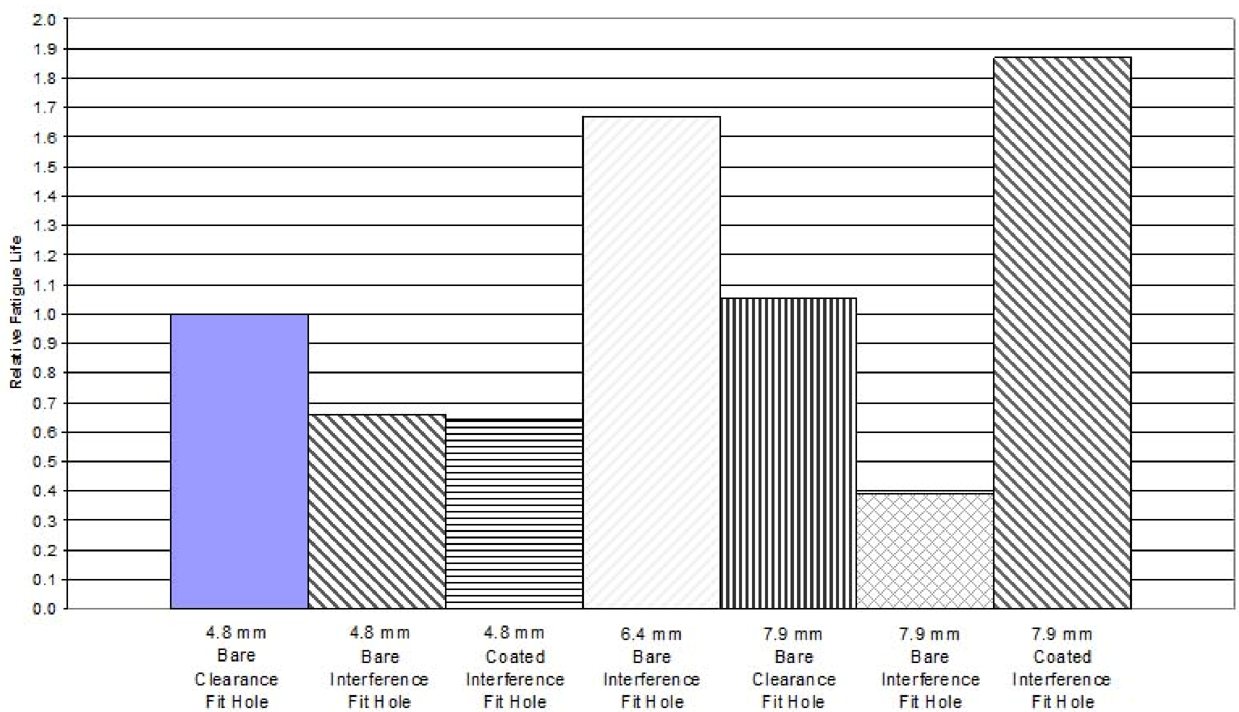

Figure 9.8-4 Relative Fatigue Life of High-Load Transfer Specimens

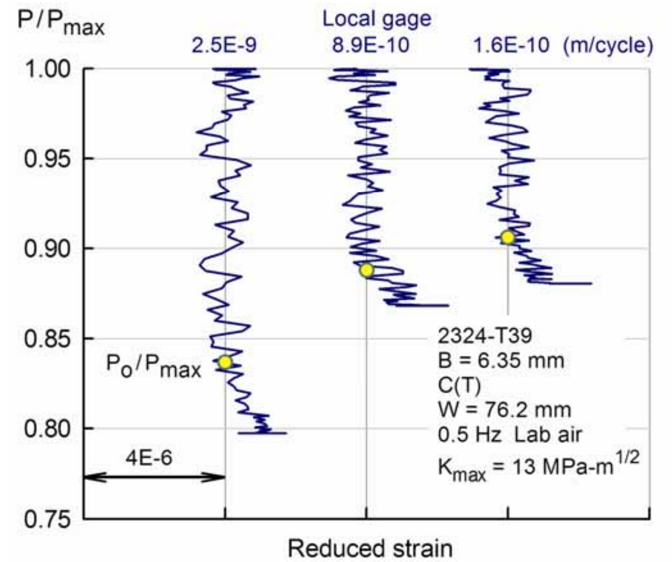

Figure 9.8-5 Determination of Crack-opening Loads for Constant K_{max} Test.

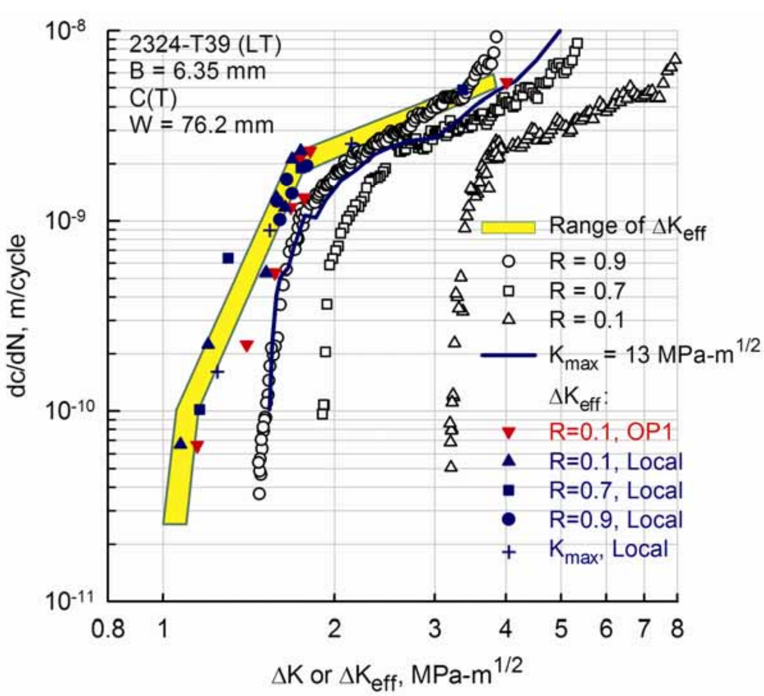

Figure 9.8-6 Effective Stress-intensity Factor Results on 2324 Alloy for Wide Range in Stress Ratios.

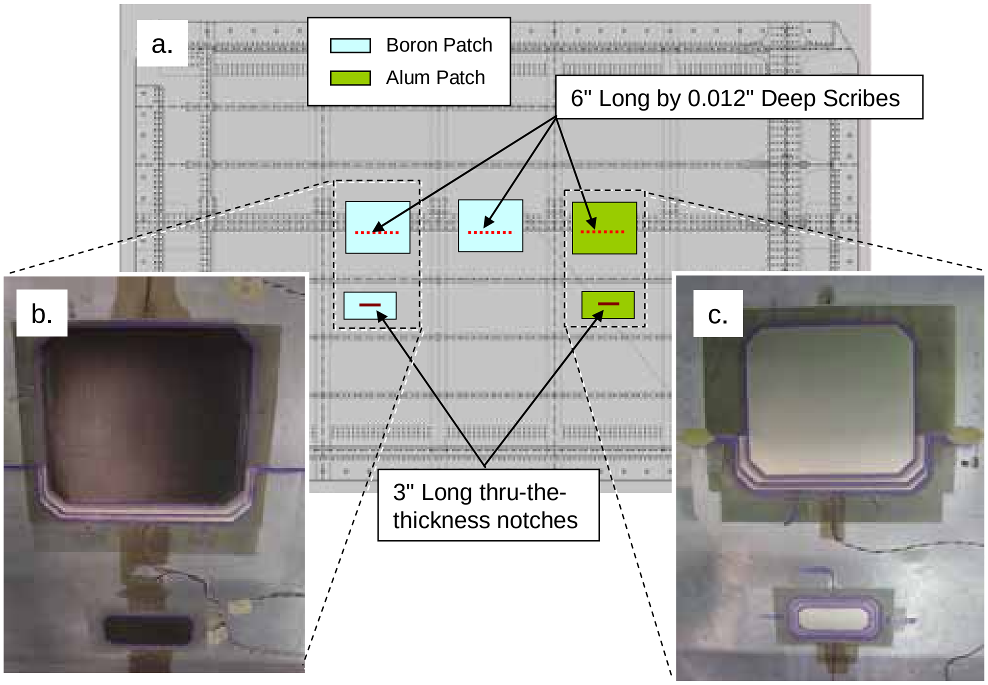

Figure 9.9-1a-c Test Article: a. Panel, damage and repair configurations, b. Boron/epoxy repair patches, and c. Aluminum repair patches.

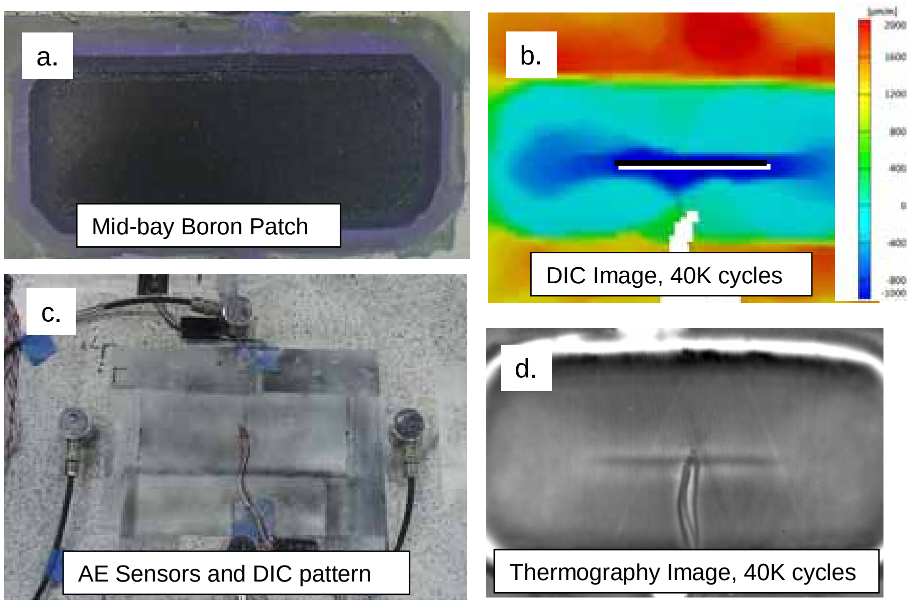

Figure 9.9-2a-d Test Set-up: a. Mid-bay boron patch, b. DIC image taken after 40,000 cycles, c. DIC pattern to measure strain on exterior surface and AE sensors to monitor damage growth, and d. Thermography image taken after 40,000 cycle to monitor crack growth and disbonding.

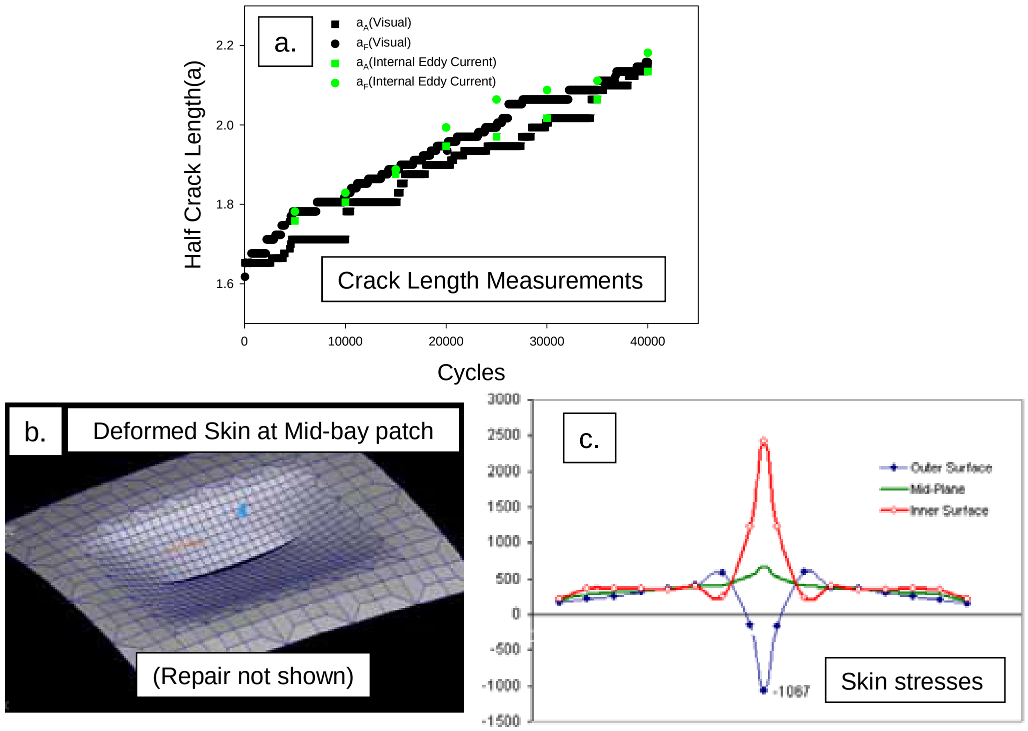

Figure 9.9-3a-c Test Results: a. Crack length measurements under mid-bay boron patch, b.FEA showing deformed mesh in the skin at the mid-bay region, and c. Stresses resulting from eccentricity of patch installation.

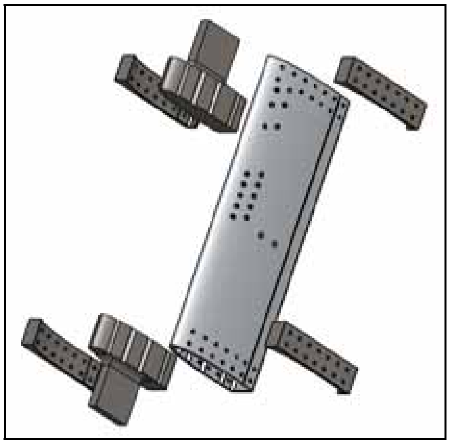

Figure 9.9-4 Fixture Concept

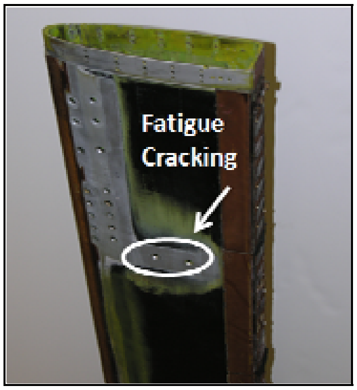

Figure 9.9-5 Main Rotor Beam

Figure 9.9-6a-c Examples of Airplanes Being Surveyed: a. Retired B737 at salvage yard, b. MD-88 in for heavy maintenance, and c. B737 with interior removed for heavy maintenance. Note window belt modification around the windows.

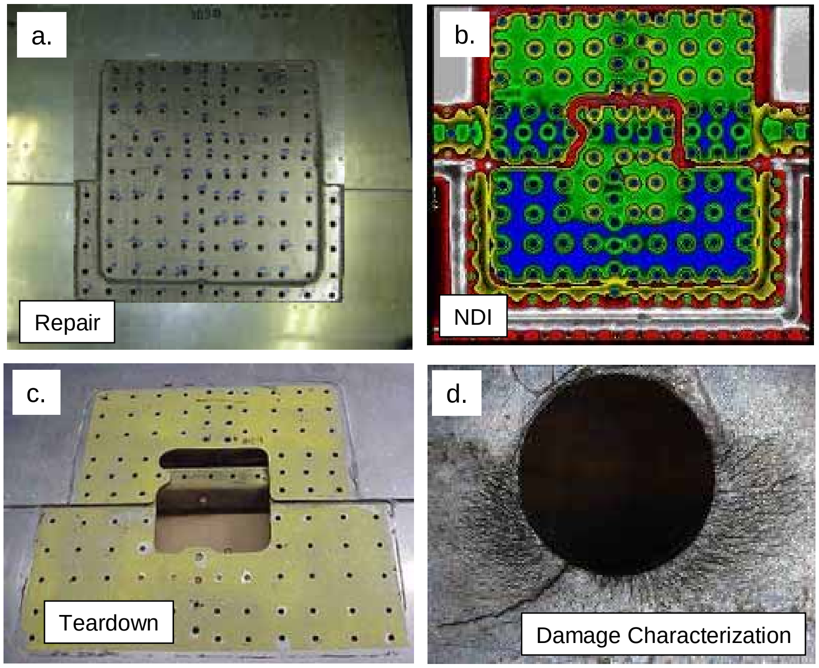

Figure 9.9-7a-d Teardown Procedure: a. Clean and catalog RAM, b. NDI for cracks, c. Disassembly and cleaning, and d. Measure crack size, shape and distribution.

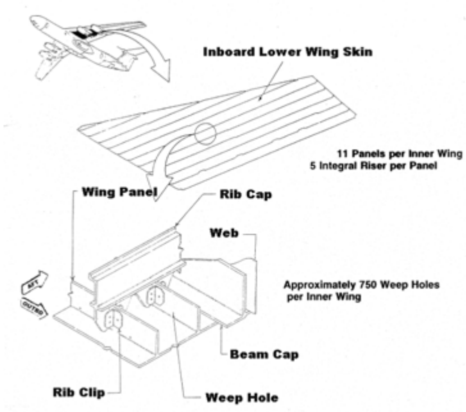

Figure 9.9-8 C-141 Structural Geometry in Weep Hole Repair Area

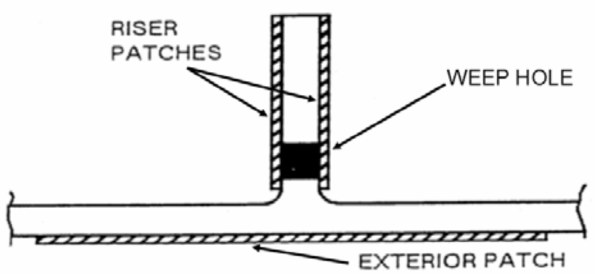

Figure 9.9-9 Schematic of Typical Weep Repair Using Three Boron/epoxy Patches

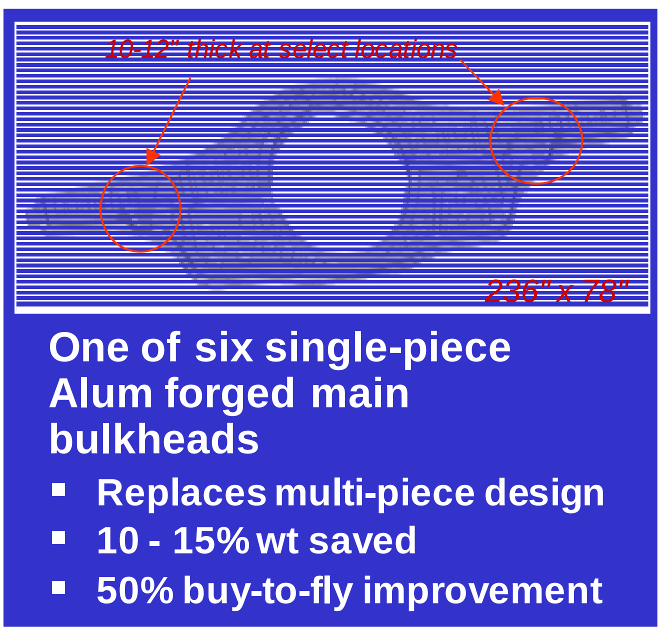

Figure 9.10-1 Unitized Bulkhead Structure

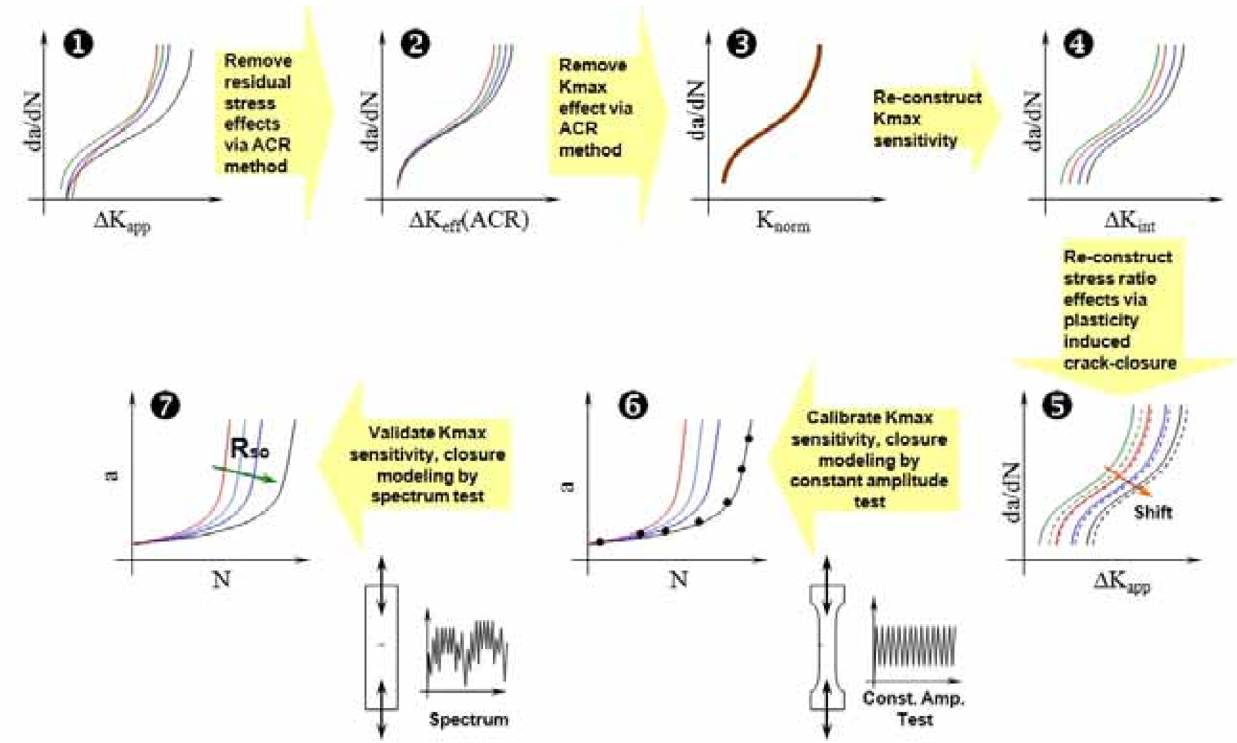

Figure 9.10-2 Fatigue Crack Growth Rate (FCGR) Data Reduction

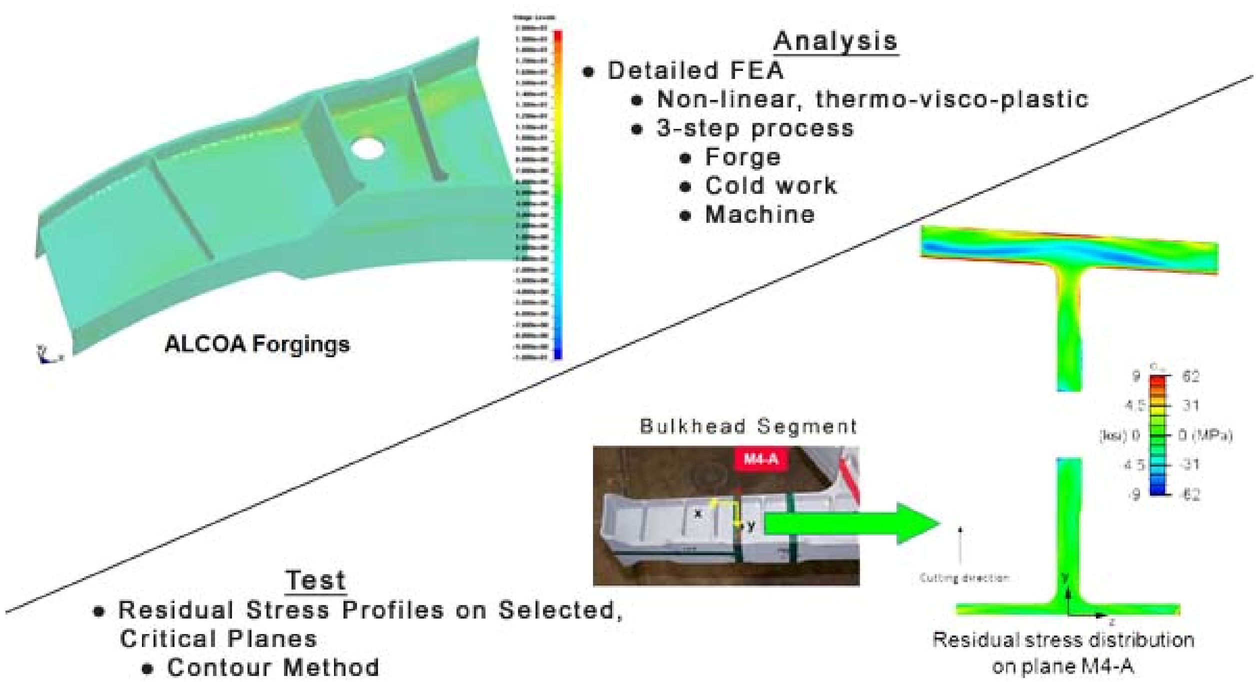

Figure 9.10-3 Quantification of Residual Stresses

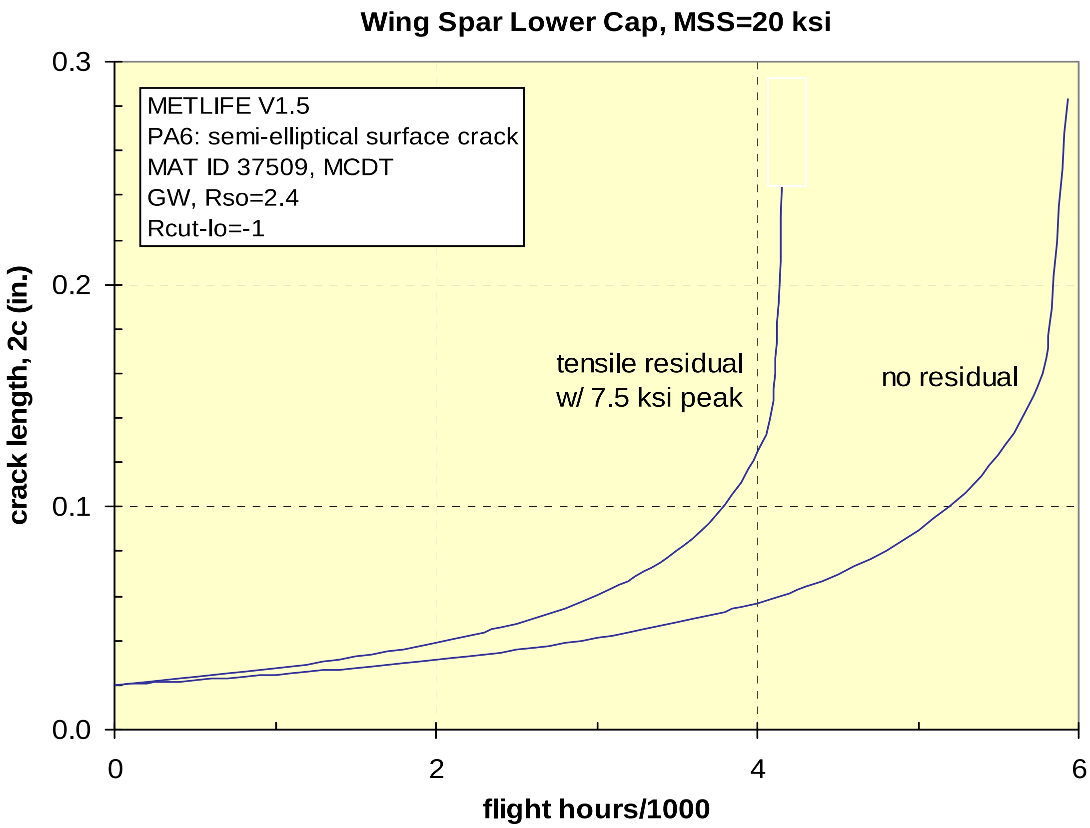

Figure 9.10-4 Fatigue Crack Growth Analysis

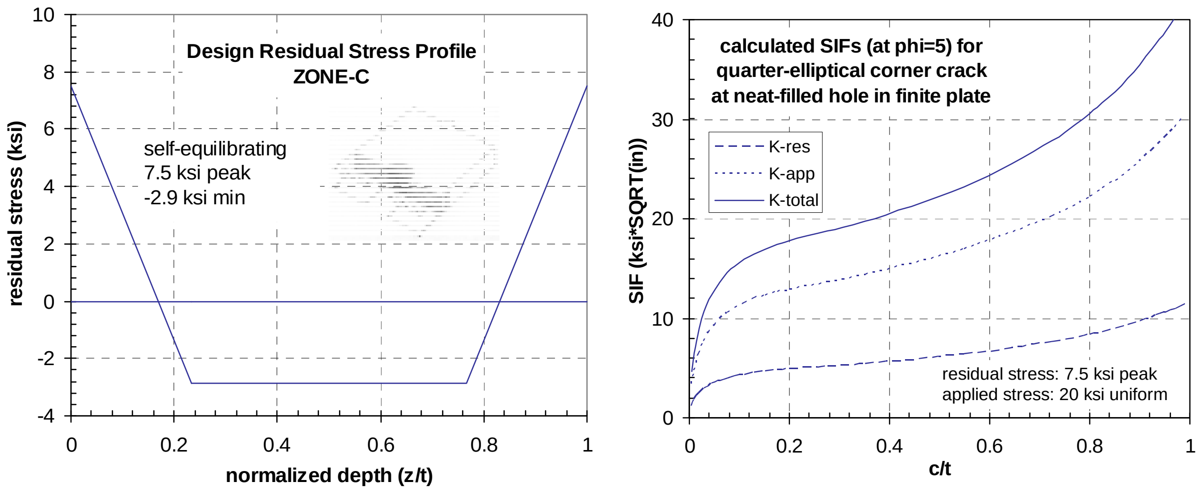

Figure 9.10-5 New Deisgn Analysis Approach

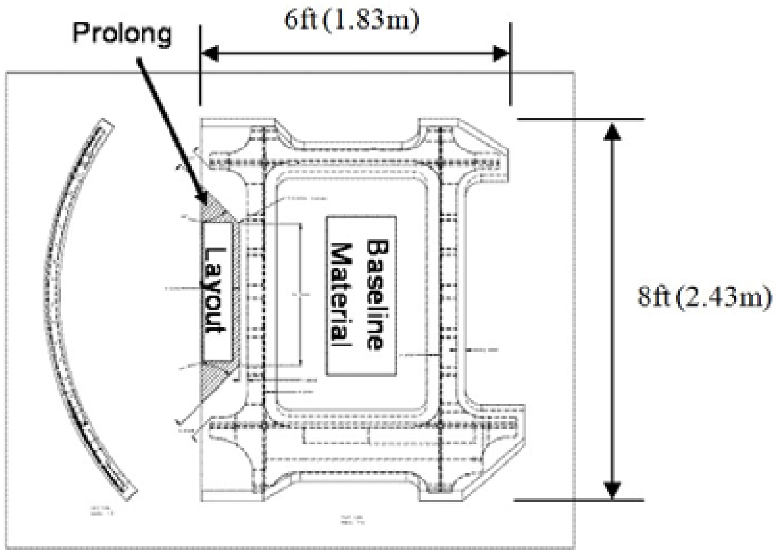

Figure 9.10-6 Door Surround Fixture

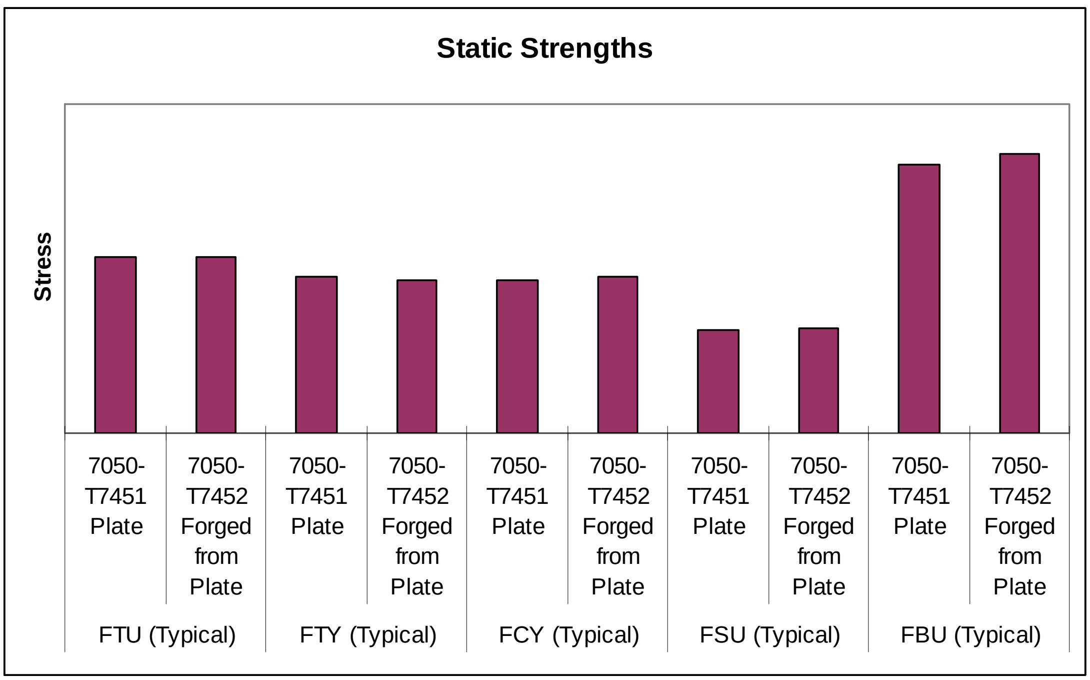

Figure 9.10-7 Static Test Results

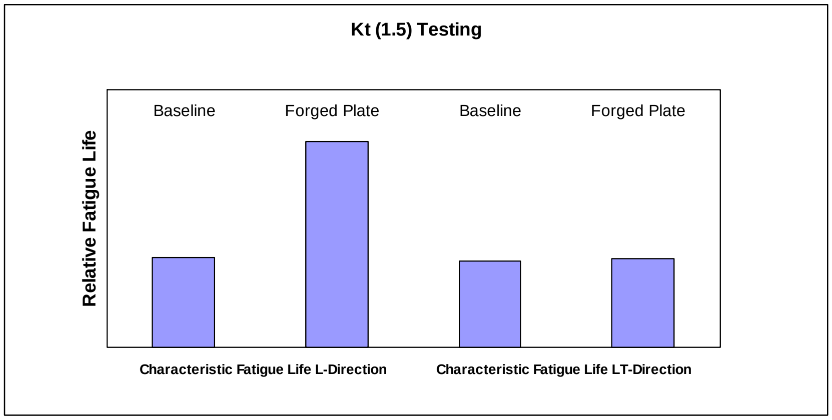

Figure 9.10-8 Kt Test Results

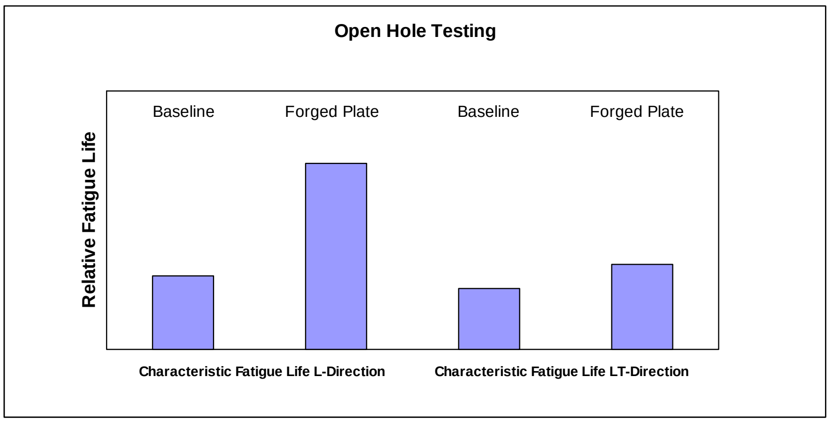

Figure 9.10-9 Open Hole Test Results

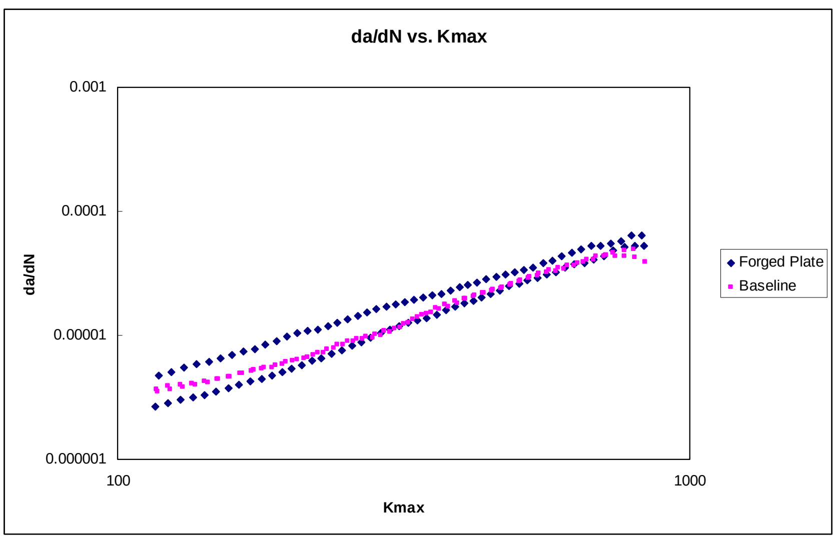

Figure 9.10-10 Crack Growth Results